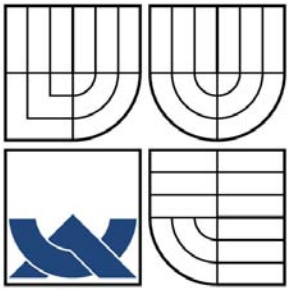

VYSOKÉ UČENÍ TECHNICKÉ V BRNĚ

BRNO UNIVERSITY OF TECHNOLOGY

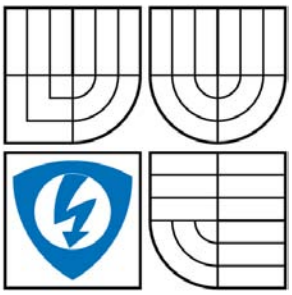

FAKULTA ELEKTROTECHNIKY A KOMUNIKAČNÍCH TECHNOLOGIÍ

ÚSTAV MIKROELEKTRONIKY

FACULTY OF ELECTRICAL ENGINEERING AND COMMUNICATION

DEPARTMENT OF MICROELECTRONICS

REMOTE OPERATED PROBE FOR DEEP-WATER CAVE EXPLORATION

DÁLKOVĚ ŘÍZENÁ SONDA PRO PRŮZKUM ZATOPENÝCH KRASOVÝCH OBLASTÍ

DIPLOMOVÁ PRÁCE

MASTER'S THESIS

AUTOR PRÁCE — Bc. DANIEL ŠIROKÝ

AUTHOR

VEDOUCÍ PRÁCE — Ing. PAVEL ŠTEFFAN, Ph.D.

SUPERVISOR

BRNO 2009

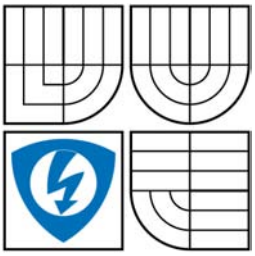

VYSOKÉ UČENÍ TECHNICKÉ V BRNĚ

Fakulta elektrotechniky a komunikačních technologií

Ústav mikroelektroniky

Diplomová práce

magisterský navazující studijní obor
Mikroelektronika

Student:	Bc. Daniel Široký	***ID:***	89226
Ročník:	2	***Akademický rok:***	2008/2009

NÁZEV TÉMATU:

Dálkově řízená sonda pro průzkum zatopených krasových oblastí

POKYNY PRO VYPRACOVÁNÍ:

Navrhněte a sestrojte zařízení, které umožňuje průzkum zatopených jeskynních a krasových prostor pomocí soustavy senzorů (měření hloubky, teploty a polohy zařízení) a dálkově ovládané CMOS kamery. Kamerové a telemetrické signály zobrazte v počítači. Vytvořte rozhraní pro dálkové řízení kamery.

DOPORUČENÁ LITERATURA:

Dle pokynů vedoucího práce

Termín zadání:	9.2.2009	***Termín odevzdání:***	29.5.2009

Vedoucí práce: Ing. Pavel Šteffan, Ph.D.

prof. Ing. Vladislav Musil, CSc.
Předseda oborové rady

Abstrakt:

Předkládaná diplomová práce se zabývá návrhem a konstrukcí podvodní sondy pro výzkum zatopených krasových oblastí. Hlavním cílem práce je konstrukce dálkově řízené sondy schopné ponoru do minimální hloubky 200 m. Sonda je vyrobena z odolného materiálu a je schopna vydržet tlak 3500 kPa. Základním vybavením sondy je dálkově řízena kamera umístěná na servomechanismu umožňující pohled do stran. Sonda je vybavena pokročilým systémem určení polohy, měření hloubky a externí teploty. Sonda je dále vybavena systémem ochrany vnitřní elektroniky v případě vniknutí vody nebo vysoké vnitřní teploty. Komunikaci sondy s hladinou zajišťuje kvalitní optický kabel. Pro pohodlné ovládání sondy byl naprogramován ovládací software zobrazující veškeré naměřené údaje a obraz z kamery.

Abstract:

The diploma thesis is focused on deep-water probe design and realization for cave exploration. Main aim is to build remote-operated probe that can dive into minimal depth of 200 m. The probe is made of durable material that can sustain pressure of 3500 kPa. The probe carries on-board remote-controlled digital camera mounted on two-axis servo mechanism providing two degrees of freedom. The probe is fitted with advanced position, depth and external temperature measurement systems. Leak and internal high temperature detection systems are also included. High-quality optical cable provides probe communication with surface. PC control software is programmed to display all acquired telemetry data and visual signal.

Klíčová slova:

Podvodní zařízení, dálkově řízená ponorka, vodní sonda, jeskynní průzkum, podvodní výzkum, hloubkový, design.

Keywords:

Underwater vehicle, remotely operated vehicle, water probe, cave exploration, submersible research, deep-water, design.

Bibliografická citace díla:

ŠIROKÝ, D. *Dálkově řízená sonda pro průzkum zatopených krasových oblastí -diplomová práce*. Brno, 2009. 93 s. Vedoucí diplomové práce Ing. Pavel Šteffan, Ph.D. FEKT VUT v Brně

Prohlášení autora o původnosti díla:

Prohlašuji, že jsem tuto vysokoškolskou kvalifikační práci vypracoval samostatně pod vedením vedoucího diplomové práce, s použitím odborné literatury a dalších informačních zdrojů, které jsou všechny citovány v práci a uvedeny v seznamu literatury. Jako autor uvedené diplomové práce dále prohlašuji, že v souvislosti s vytvořením této diplomové práce jsem neporušil autorská práva třetích osob, zejména jsem nezasáhl nedovoleným způsobem do cizích autorských práv osobnostních a jsem si plně vědom následků porušení ustanovení § 11 a následujících autorského zákona č. 121/2000 Sb., včetně možných trestněprávních důsledků vyplývajících z ustanovení § 152 trestního zákona č. 140/1961 Sb.

V Brně dne 29. 5. 2009

…….

Poděkování:

Děkuji vedoucímu diplomové práce Ing. Pavlovi Šteffanovi, Ph.D. za metodické a cíleně orientované vedení při plnění úkolů realizovaných v návaznosti na diplomovou práci. Dále děkuji spolupracující firmě LOLA Olomouc a majiteli této firmy Miroslavu Lukášovi za poskytnutou odbornou pomoc a rady.

CONTENTS

1 Introduction

Remotely operated vehicles (ROVs) are commonly used for under-water scientific research. They are made in varied modifications. Many of them are designed only for a depth of 250 meters or even less. On top of that, their purchase costs are extremely high (some of them start at a price 25000 EUR). A vast majority of small research organizations cannot afford such expenses and sometimes they would actually make do with a simplified remote operated probe.

I have always been interested in anything electrical that includes mechanical or robotic properties, but I got started designing and building a deep-water probe as a result of my caving and speleology research activity. I live near the Hranicka Abyss, situated in the Hranicky limestone karst, which is at this moment the deepest abyss in the Central Europe. However, nobody was able to measure or to confirm a real depth so far, either because of lack of money or proper technology. All these circumstances made me start thinking about construction of low-cost underwater probe that will use the latest technology and will be capable to dive into 200 meters or even more.

My aim is to propose and build remotely operated probe that will carry on-board two-axis remote controlled CMOS camera with additional lighting (illumination), will be able to trace its position (including orientation and depth measurement) using the latest technology including MEMS sensor systems. Remote controlling and communication should be provided with a high-speed data transmission system using optical cable. The probe should sustain minimal pressure of 20000 kPa (20 bars) or more in an extremely harsh environment. The probe with these parameters requires specific electrical and mechanical considerations in design. Since I have studied microelectronics, I focus more on electronic parts, but I also do mechanical design.

The main purpose of this diploma thesis is to show whether it is possible to build an operating deep-water probe that has also practical use and has a reasonable price. Total expenses should not exceed 2500 EUR.

2 Underwater vehicles

Remotely operated underwater vehicles (ROVs) are unoccupied, highly maneuverable underwater robots operated by a person aboard a surface. They are linked to the surface control device by a group of cables that carry electrical (or optical) signals back and forth between the operator and the vehicle. Most are equipped with at least a video camera and lights. Additional equipment is commonly added to expand the vehicle's capabilities. These may include a still camera, a manipulator or cutting arm, water samplers, and instruments that measure water clarity, light penetration, and temperature. First developed for industrial purposes, such as internal and external inspections of pipelines and the structural testing of offshore platforms, ROVs are now used for many applications, many of them scientific.

2.1 ROV categories

ROV systems come in three basic categories:

Observation class – Observation-class ROVs are normally a "flying eye" designed specifically for lighter usage with propulsion systems to deliver a camera and sensor package to a place where it can provide a meaningful picture or gather data. The newer observation-class ROV is able these systems to do more than just see. With its tooling package and many accessories, the observation-class ROV is able to deliver payload packages of instrumentation, intervention equipment, and underwater navigational aid, enabling them to perform as a full-function underwater vehicle.

Work class – Work-class systems generally have large frames (measured in multiple meters) with multi-function manipulators, hydraulic propulsion or actuation, and heavy equipment underwater needs movement.

Special use – Special-use ROV systems describe tethered underwater vehicles designed for specific purposes. An example of a special-use vehicle is a cable burial ROV system designed to plow the sea floor to bury telecommunications cable.

2.2 Ideal ROV

We should be familiar with the fact that vehicle geometry does not affect the motive performance of an ROV (over any appreciable tether length) nearly as much as the dimensions of the tether. Accordingly, the perfect ROV would have the following characteristics:

- Minimal tether diameter (for instance, a single strand of unshielded optical fiber)
- Power from the surface having unlimited endurance (as opposed to battery operated with limited power available)

- Very small in size (to work around and within structures)
- Have an extremely high data pipeline for sensor throughput.

ROV systems are trade-off a number of factors, including cost, size, deployment resources, and operational requirement. Tether designed can help create (or destroy) the perfect ROV.

2.3 Power source for the vehicle

Vehicles can be powered in any of the following categories: surface-powered, vehicle-powered or a hybrid system.

- **Surface-powered vehicles** must, by practicality, be tethered, since the power source is from the surface to the vehicle. The vehicle-based power storage is not defined within this power category. In other words, this type of vehicle does not contain on-board batteries.
- **Vehicle-powered vehicles** store all of their power-producing capacity on the vehicle in the form of battery, fuel cell, or other means of power storage needed for vehicle propulsion and operation
- **Hybrid system** involves a mixture of surface and submersible supplied power. Examples of the hybrid system include the battery-powered submersible with a surface-supplied charger (through a tether) for recharging during times of less-than-maximum power draw.

2.4 Communications linkage to the vehicle

The linkage to the vehicle can come in several forms or methods depending upon the distance and medium through which the communication must take place. Such linkages include:

- Hard-wire communication (either electrical or fiber)
- Acoustic communication (via underwater analog or digital modem)
- Optical communication (while on the surface)
- Radio frequency (RF) communication (while on or near the surface).

What is communicated between the vehicle and the operator can be of any of the following:

- **Telemetry** – The measurement and transmission of data or video through the vehicle via tether, RF, optical, acoustic, or other means.

- **Tele-presence** – The capability of an unmanned system to provide the human operator with some amount of sensory feedback similar to that which operator would receive if inside the vehicle
- **Control** – The upload or download of operational instruction
- **Records** – The upload or download of mission record and files.

ROVs receive their power, their data transmission or their control (or all three) directly from the surface through direct hard-wire communication (i.e. the tether). [1]

3 Sensors for underwater vehicles

A sensor system is necessary when a remotely operated probe is out of operator's sight. An electronic compass, gyroscopes, accelerometers and a depth sensor are normally used to provide telemetry data.

3.1 Electronic compass

The magnetic compass (MC) is a crucial navigation tool in many areas, even in times of the global positioning system (GPS). Replacing the "old" magnetic needle compass or the gyrocompass by an electronic solution offers advantages like having a solid-state component without moving parts and the ease of interfacing with other electronic systems.

For the magnetic field sensors within a compass system, the magnetoresistive (MR) technology is the preferable solution. Compared to flux-gate sensors, which could be found in most electronic compasses until now, the MR technology offers a much more cost effective solution, as it requires no coils to be wound and can be fabricated in an IC-like process. Due to their higher sensitivity, MR sensors are also superior to Hall elements in this application field.

To understand problems with MC, I will give a general introduction to electronic compass design with MR. Therefore, the basic characteristics of the earth´s magnetic field are explained and an overview of the building blocks of an electronic compass is given.

Earth´s magnetic field

The magnetic field of the earth is the physical quantity to be evaluated by a compass. Thus, an understanding of its basic properties is required, when designing a compass. **Fig. 3.1** gives an illustration of the field shape.

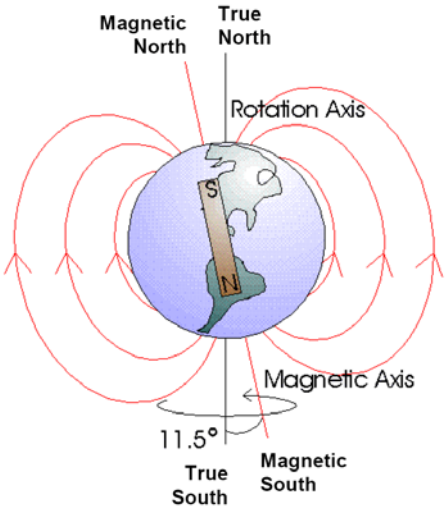

Fig. 3.1: Earth´s magnetic field [3]

The magnetic field strength on the earth varies with location and covers the range from about 20 to 50 A/m. An understanding of the earth´s field shape can be gained, if it is assumed to be generated by a bar magnet within the earth, as pointed out in **Fig. 3.1**. The magnetic field lines point from the earth´s south pole to its north pole. **Fig. 3.1** indicates, that this is opposite to the physical convention for the poles of a bar magnet (the background is a historical one, in that a bar magnet´s north pole has been defined as that pole, that points towards north in the earth´s magnetic field). The field lines are perpendicular to the earth surface at the poles and parallel at the equator. Thus, the earth field points downwards in the northern hemisphere and upwards in the southern hemisphere. An important fact is that the magnetic poles do not coincide with the geographical poles which are defined by the earth´s axis of rotation. The angle between the magnetic and the rotation axis is about 11.5 °. As a consequence, the magnetic field lines do not exactly point to geographic or "true" north.

Fig. 3.2 gives a 3-D representation of the earth field vector **He** at some point on the earth. This illustration allows to define the quantities which are of importance for a compass. Here, the x- and y-coordinates are parallel to the earth´s surface, whereas the z-coordinate points vertically downwards.

- **Azimuth α** is the angle between magnetic north and the heading direction. Magnetic north is the direction of **Heh**, the earth´s field component perpendicular to gravity. Throughout this paper, **Heh** will be referred to as "horizontal" component of the earth´s field. **Fig. 3.2** shows, that:

$$\alpha = \arctan\frac{Hey}{Hex} \tag{4.1}$$

  The azimuth is the reading quantity of a compass. Throughout this paper, a is counted clockwise from magnetic north, i.e. north is 360 ° or 0 °, east is 90 °, south is 180 °, west is 270 °.

- **Inclination or dip δ** is the angle between the earth´s field vector and the horizontal plane. As already pointed out, the inclination varies with the actual location on earth, being zero at the equator and approaching ±90 ° near the poles. If a compass is tilt, then inclination has to be considered. For tilt correction, we can use 2-axis accelerometer, inclinometer or electronically gimbaled compass.

- **Declination λ** is the angle between geographic or true north and magnetic north. Declination is dependent on the actual position on earth. It also has a long term drift. Declination can be to the east or to the west and can reach values of about ±25 °. The

azimuth measured by a compass has to be corrected by the declination in order to find the heading direction with respect to geographic north. See more in [3].

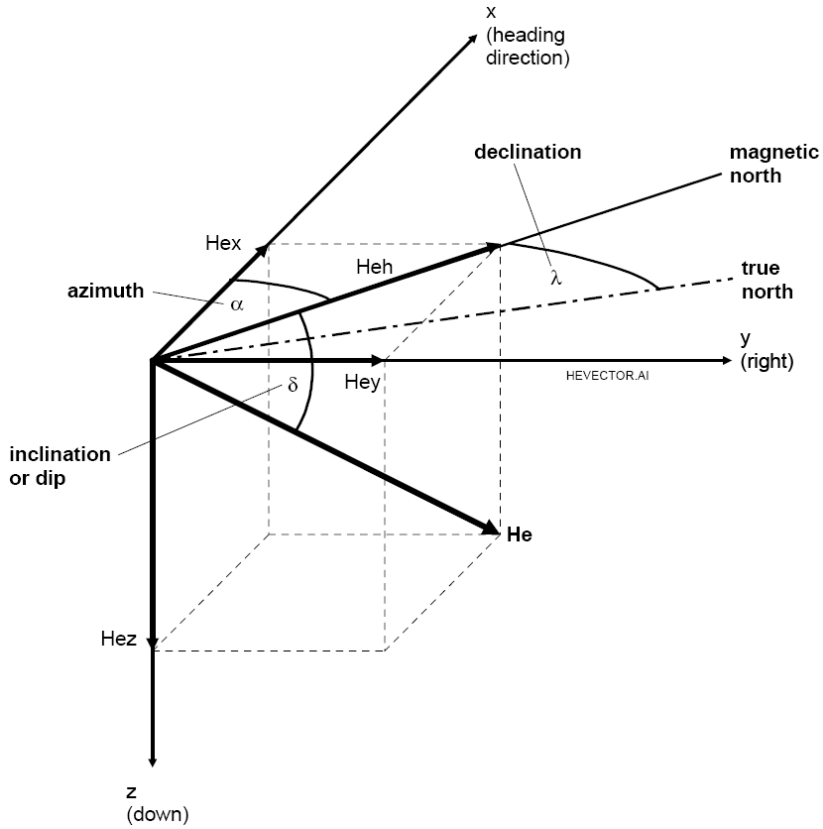

Fig. 3.2: Earth field vector [3]

Magnetoresistive effect

Magnetoresistive sensors make use of the magnetoresistive effect, the property of a current carrying magnetic material to change its resistivity in the presence of an external magnetic field. **Fig. 3.3** shows a strip of ferromagnetic material, called Permalloy (19 % Fe, 81 % Ni).

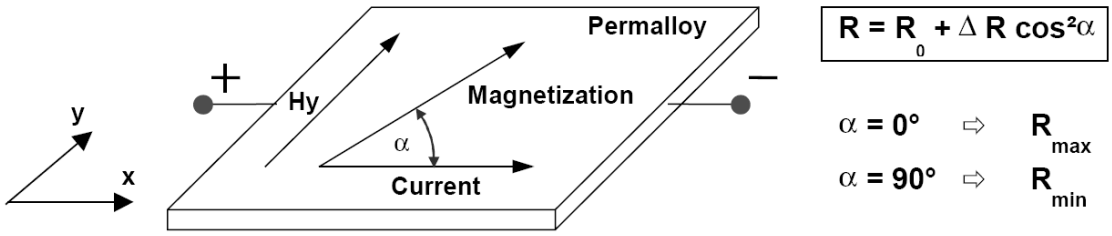

Fig. 3.3: The magnetoresistive effect in Permalloy [3]

During deposition of the Permalloy strip, a strong external magnetic field is applied parallel to the strip axis. By doing this, a preferred magnetization direction is defined within the strip. In absence of any external magnetic field, the magnetization always points into this

direction. In **Fig. 3.3**, this is assumed to be the x-direction, which is also the direction of current flow. An MR sensor now relies on two basic effects:

- The strip resistance R depends on the angle α between the direction of the current and the direction of the magnetization.
- The direction of magnetization and therefore α can be influenced by an external magnetic field H_y, where H_y is parallel to the strip plane and perpendicular to the preferred direction.

When no external magnetic field is present, the Permalloy has an internal magnetization vector parallel to the preferred direction, i.e. α = 0. In this case, the strip resistance R has its maximum value R_{max}. If now an external magnetic field H_y is applied, the internal magnetization vector of the Permalloy will rotate around an angle α. At high field strengths, the magnetization tends to align itself parallel to H_y and the rotation angle α approaches 90 °. In this case, the resistance reaches its minimum value R_{min}. The equation next to **Fig. 3.3** gives the functional dependence between R and α, where $R_0 = R_{min}$ and $\Delta R = (R_{max} - R_{min})$. Finally, the function of R versus H_y is as follows:

$$R = R_0 + \Delta R \cdot \left(1 - \left(\frac{H_y}{H_0} \right)^2 \right) \tag{4.2}$$

where H_0 is a parameter, which depends on material and geometry of the strip. **Equation 4.2** is defined for field strength magnitudes of $H_y \leq H_0$. For $H_y > H_0$, R equals R_0. R_0 and ΔR are also material parameters. For Permalloy, ΔR is in the range of 2 to 3 % of R_0. See more in [3].

3.2 Accelerometer

An accelerometer is a sensing element that measures acceleration; acceleration is the rate of change of velocity with respect to time. It is a vector that has magnitude and direction. Accelerometers measure in units of g – a g is the acceleration measurement for gravity which is equal to 9.81 m/s². Accelerometers have developed from a simple water tube with an air bubble that showed the direction of the acceleration to an integrated circuit that can be placed on a circuit board. Accelerometers can measure vibrations, shocks, tilt, impacts and motion of an object.

3.2.1 Types of accelerometers

There are a number of types of accelerometers. What differentiates the types is the sensing element and the principles of their operation.

Capacitive accelerometers sense a change in electrical capacitance, with respect to acceleration. The accelerometer senses the capacitance change between a static condition and the dynamic state.

Piezoelectric accelerometers use materials such as crystals, which generate electric potential from an applied stress. This is known as the piezoelectric effect. As stress is applied, such as acceleration, an electrical charge is created.

Piezoresistive accelerometers (strain gauge accelerometers) work by measuring the electrical resistance of a material when mechanical stress is applied.

Hall Effect accelerometers measure voltage variations stemming from a change in the magnetic field around the accelerometer.

Magnetoresistive accelerometers work by measuring changes in resistance due to a magnetic field. The structure and function is similar to a Hall Effect accelerometer except that instead of measuring voltage, the magnetoresistive accelerometer measures resistance.

Heat transfer accelerometers measure internal changes in heat transfer due to acceleration. A single heat source is centered in a substrate and suspended across a cavity. Thermoresistors are spaced equally on all four sides of the suspended heat source. Under zero acceleration the heat gradient will be symmetrical. Acceleration in any direction causes the heat gradient to become asymmetrical due to convection heat transfer.

MEMS accelerometers use MEMS (Micro-Electro Mechanical System) technology that is based on a number of tools and methodologies which are used to form small structures with dimensions in the micrometer scale. This technology is now being utilized to manufacture state of the art MEMS-Based Accelerometers (the structure examples are shown in **Fig. 3.4**).

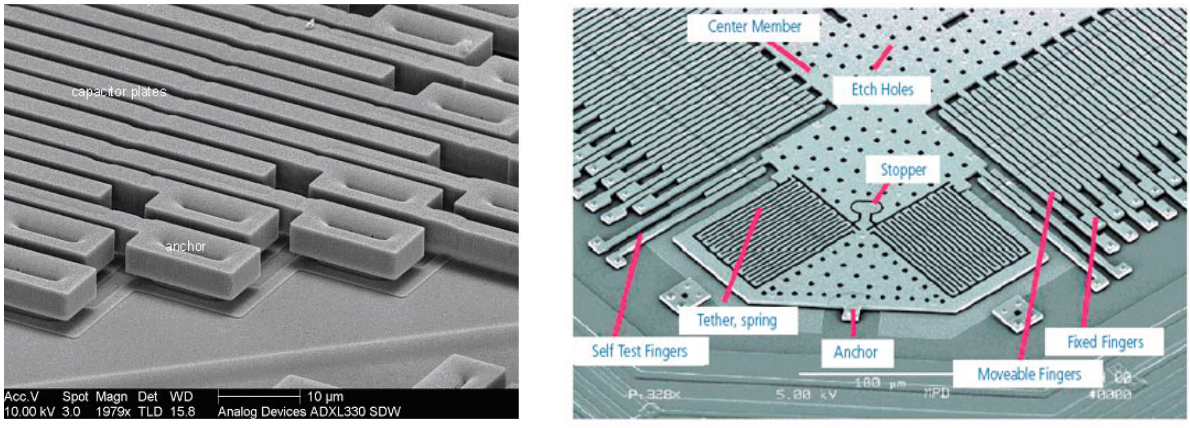

a) b)

Fig. 3.4: MEMS-based accelerometers: a) detail of capacitor plates, b) layout example [6]

Future Accelerometer Advancements

In the next decade, nanotechnology will create new applications and dramatically reshape this area of technology. See more in [6].

3.2.2 Selecting an accelerometer

When selecting an accelerometer for an application the first factors to consider are:

- **Dynamic Range:** Dynamic range is the maximum amplitude that the accelerometer can measure before distorting or clipping the output signal. Dynamic range is typically specified in g's
- **Sensitivity:** Sensitivity is the scale factor of a sensor or system, measured in terms of change in output signal per change in input measured. Sensitivity references the accelerometer's ability to detect motion. Accelerometer sensitivity is typically specified in millivolt per (mV/g).
- **Frequency response:** Frequency response is the frequency range for which the sensor will detect motion and report a true output. Frequency response is typically specified as a range measured in Hertz (Hz).
- **Sensitive axis:** Accelerometers are designed to detect inputs in reference to an axis; single-axis accelerometers can only detect inputs along one plane. Tri-axis accelerometers can detect inputs in any plane and are required for most applications.
- **Size and Mass:** Size and mass of an accelerometer can change the characteristics of the object being tested. The mass of the accelerometers should be significantly smaller than the mass of the system to be monitored.

3.3 Gyroscopes

In order to discuss MEMS gyroscopes we must first understand gyroscopes in general and what role they play in science. Technically, a gyroscope is any device that can measure angular velocity. As early as the 1700's, spinning devices were being used for sea navigation in foggy conditions. The more traditional spinning gyroscope was invented in the early 1800's, and the French scientist Jean Bernard Leon Foucault coined the term gyroscope in 1852. In the late 1800's and early 1900's gyroscopes were patented for use on ships. Around 1916, the gyroscope found use in aircraft where it is still commonly used today. Throughout the 20th century improvements were made on the spinning gyroscope. In the 1960's, optical gyroscopes using lasers were first introduced and soon found commercial success in aeronautics and military applications. In the last ten to fifteen years, MEMS gyroscopes have

been introduced and advancements have been made to create mass-produced successful products with several advantages over traditional macro-scale devices.

Gyroscopes function differently depending on their type. Traditional spinning gyroscopes work on the basis that a spinning object that is tilted perpendicularly to the direction of the spin will have a precession. The precession keeps the device oriented in a vertical direction so the angle relative to the reference surface can be measured. Optical gyroscopes are most commonly ring laser gyroscopes. These devices send two lasers around a circular path in opposite directions. If the path spins, a phase shift can be detected since the speed of light always remain constant. Usually the rings are triangles or rectangles with mirrors at each corner. Optical gyroscopes are a great improvement to the spinning mass gyroscopes because there is no wear, greater reliability and smaller size and weight. See more in [8].

3.3.1 MEMS gyroscopes

Almost all reported micromachined gyroscopes use vibrating mechanical elements (proof-mass) to sense rotation. They have no rotating parts that require bearings, and hence they can be easily miniaturized and batch fabricated using micromachining techniques. All vibratory gyroscopes are based on the transfer of energy between two vibration modes of a structure caused by Coriolis acceleration. Coriolis acceleration, named after the French scientist and engineer G. G. de Coriolis (1792–1843), is an apparent acceleration that arises in a rotating reference frame and is proportional to the rate of rotation.

3.3.2 Types of MEMS gyroscopes

Tuning fork gyroscopes contain a pair of masses that are driven to oscillate with equal amplitude but in opposite directions. When rotated, the Coriolis force creates an orthogonal vibration that can be sensed by a variety of mechanisms. The gyro in **Fig. 3.5a** uses comb-type structures to drive the tuning fork into resonance, and rotation about either in-plane axis results in the moving masses to lift, a change that can be detected with capacitive electrodes under the mass.

Vibrating-Wheel Gyroscopes have a wheel that is driven to vibrate about its axis of symmetry, and rotation about either in-plane axis results in the wheel's tilting, a change that can be detected with capacitive electrodes under the wheel. It is possible to sense two axes of rotation with a single vibrating wheel. A surface micromachined polysilicon vibrating wheel gyro is shown in **Fig. 3.5b**.

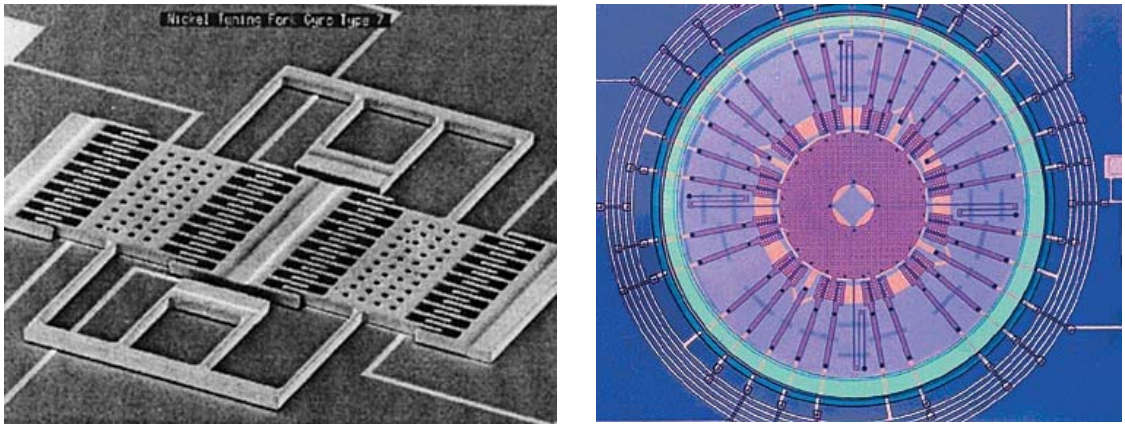

a) b)

Fig. 3.5: MEMS-based gyroscopes: a) Tuning fork, b) Vibrating-Wheel gyroscope [9]

Wine Glass Resonator Gyroscopes. A third type of gyro is the wine glass resonator. Fabricated from fused silica, this device is also known as a hemispherical resonant gyro. In a wine glass gyro, the resonant ring is driven to resonance and the positions of the nodal points indicate the rotation angle. The input and output modes are nominally degenerate, but due to imperfect machining some tuning is required. [9]

3.3.3 Selecting a gyroscope

The rotation is usually measured in reference to one of three axes: yaw, pitch, or roll. **Fig. 3.6a** shows each axis of sensitivity relative to a package mounted on a flat surface. Choosing a different mounting for a gyroscope with a single axis of sensitivity allows it to measure other axes, as shown in **Fig. 3.6b**. Here, the gyro is mounted on its side so that its yaw axis becomes the roll axis.

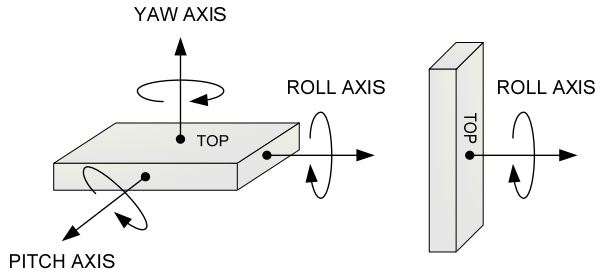

Fig. 3.6a, b: Three axes of movement (that can be measured with gyroscope) [10]

For example, a yaw axis gyro mounted on a turntable rotating at 33.3 rpm would measure a rotation of 360 ° × 33.3 rpm divided by 60 s, or 200 °/s. It would output a voltage proportional to the angular rate, or the sensitivity, as measured in millivolts per degree per second. The full-scale range determines the amount of angular rate that can be measured, so in the example of the turntable, a gyro would need to have a full-scale range of at least 200 °/s.

There is typically a tradeoff between full-scale range and sensitivity. For instance, ADXRS300 gyroscope produced by Analog Devices has a full-scale range of 300 °/s and a sensitivity of 5 mV/°/s, whereas the ADXRS150 has a more limited full-scale range of 150 °/s, but a greater sensitivity of 12.5 mV/°/s. [10]

3.4 Humidity and Inside temperature sensor

Humidity, barometer and inside temperature measurements provide monitoring of internal environmental conditions in the probe.

3.4.1 Humidity basic terminology

In order to choose a proper humidity sensor I have to be familiar with basic terminology.

Humidity refers to the water vapor content in air or other gases. Humidity measurements can be stated in a variety of terms and units. The three commonly used terms are absolute humidity, dew point, and relative humidity (RH).

Absolute Humidity is the ratio of the mass of water vapor to the volume of air or gas. It is commonly expressed in grams per cubic meter or grains per cubic foot (1 grain = 1/7000 lb.). It can be calculated from known RH, temperature, or wet bulb, or it can be measured directly.

Dew Point, expressed in °C or °F, is the temperature and pressure at which a gas begins to condense into a liquid.

Relative Humidity, abbreviated as RH, refers to the ratio (stated as a percent) of the moisture content of air compared to the saturated moisture level at the same temperature and pressure.

3.4.2 Types of humidity sensors

The most commonly used humidity sensors are:

Resistive Humidity Sensors

Resistive humidity sensors measure the change in electrical impedance of a hygroscopic medium such as a conductive polymer, salt, or treated substrate.

Thermal Conductivity Humidity Sensors

These sensors measure the absolute humidity by quantifying the difference between the thermal conductivity of dry air and that of air containing water vapor.

Capacitive Humidity Sensors

Capacitive relative humidity (RH) sensors consist of a substrate on which a thin film of polymer or metal oxide is deposited between two conductive electrodes. The sensing surface is coated with a porous metal electrode to protect it from contamination and exposure to

condensation. The substrate is typically glass, ceramic, or silicon. The incremental change in the dielectric constant of a capacitive humidity sensor is nearly directly proportional to the relative humidity of the surrounding environment. The change in capacitance is typically 0.2 – 5 pF for a 1 % RH change, while the bulk capacitance is between 100 and 500 pF at 50 % RH at 25 °C. Capacitive sensors are characterized by low temperature coefficient, ability to function at high temperatures (up to 200 °C), full recovery from condensation, and reasonable resistance to chemical vapors. The response time ranges from 30 to 60 s for a 63 % RH step change.

3.4.3 Selecting a humidity sensor

The most important specifications to keep in mind when selecting a humidity sensor are:

- Accuracy
- Repeatability
- Interchangeability
- Long-term stability
- Ability to recover from condensation
- Resistance to chemical and physical contaminants
- Size
- Cost effectiveness

Additional significant long-term factors are the costs associated with sensor replacement, field and in-house calibrations, and the complexity and reliability of the signal conditioning and data acquisition (DA) circuitry. [12]

3.5 Depth measurement

Fluid systems, pressure and pressure measurements are extremely complex. In this chapter, I will define and explain the basic concepts of fluid mechanics that are necessary for proper understanding of the fluid pressure measurement.

3.5.1 Pressure and pressure measurement

Fluid pressure can be defined as the measure of force per-unit-area exerted by a fluid, acting perpendicularly to any surface it contacts (a fluid can be either a gas or a liquid, fluid and liquid are not synonymous). The standard SI unit for pressure measurement is the Pascal (Pa) which is equivalent to one Newton per square meter (N/m^2) or the KiloPascal (kPa) where 1 kPa = 1000 Pa. In the English system, pressure is usually expressed in pounds per

square inch (psi). Pressure can be expressed in many different units including in terms of a height of a column of liquid. **Table 3.1** lists commonly used units of pressure measurement and the conversion between the units. Pressure measurements can be divided into three different categories: absolute pressure, gage pressure and differential pressure.

Table 3.1: Conversion table for common units of pressure

	kPa	mm Hg	millibar	in H_2O	PSI
1 atm	101.325	760.000	1013.25	406.795	14.6960
1 kPa	1.000	7.50062	10.000	4.01475	0.145038
1 mm Hg	0.133322	1.000	1.33322	0.535257	0.0193368
1 millibar	0.1000	0.750062	1.000	0.401475	0.0145038
1 in H_2O	0.249081	1.86826	2.49081	1.000	0.0361
1 PSI	6.89473	51.7148	68.9473	27.6807	1.000
1 mm H_2O	0.009806	0.07355	9.8 x 10-8	0.03937	0.0014223

Absolute pressure refers to the absolute value of the force per-unit-area exerted on a surface by a fluid. Therefore the absolute pressure is the difference between the pressure at a given point in a fluid and the absolute zero of pressure or a perfect vacuum.

Gage pressure is the measurement of the difference between the absolute pressure and the local atmospheric pressure. Local atmospheric pressure can vary depending on ambient temperature, altitude and local weather conditions. The U.S. standard atmospheric pressure at sea level and 59 °F (20 °C) is 14.696 pounds per square inch absolute (psia) or 101.325 kPa absolute (abs). When referring to pressure measurement, it is critical to specify what reference the pressure is related to. In the English system of units, measurement relating the pressure to a reference is accomplished by specifying pressure in terms of pounds per square inch absolute (psia) or pounds per square inch gage (psig). For other units of measure it is important to specify gage or absolute. The abbreviation ‘abs’ refers to an absolute measurement. A gage pressure by convention is always positive. A ‘negative’ gage pressure is defined as vacuum. Vacuum is the measurement of the amount by which the local atmospheric pressure exceeds the absolute pressure. A perfect vacuum is zero absolute pressure. Figure 1 shows the relationship between absolute, gage pressure and vacuum.

Sealed pressure sensor is the same as the gauge pressure sensor except that it is previously calibrated by manufacturers to measure pressure relative to sea level pressure (14.7 PSI).

Differential pressure is simply the measurement of one unknown pressure with reference to another unknown pressure. The pressure measured is the difference between the two unknown pressures. This type of pressure measurement is commonly used to measure the pressure drop in a fluid system. Since a differential pressure is a measure of one pressure referenced to

another, it is not necessary to specify a pressure reference. For the English system of units this could simply be psi and for the SI system it could be kPa.

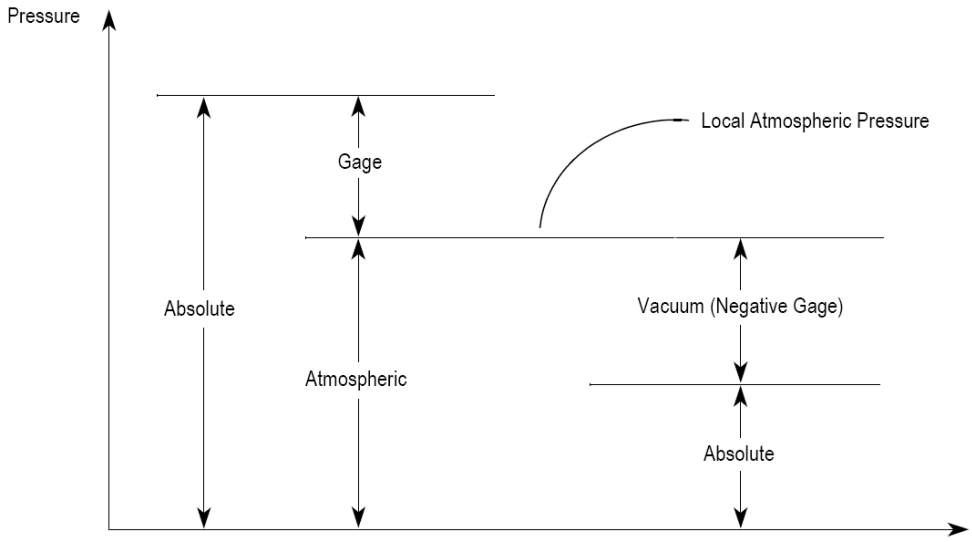

Fig. 3.7: Pressure term relationships [15]

In addition to these types of pressure measurement, there are different types of fluid systems and fluid pressures. There are two types of fluid systems; static systems and dynamic systems. As the names imply, a static system is the one in which the fluid is at rest and a dynamic system is the one in which the fluid is moving. The probe measures the static pressure.

3.5.2 Static pressure systems

The pressure measured in a static system is static pressure. In the pressure system shown in **Fig. 3.8** a uniform static fluid is continuously distributed with the pressure varying only with vertical distance. The pressure is the same at all points along the same horizontal plane in the fluid and is independent of the shape of the container. The pressure increases with depth in the fluid and acts equally in all directions. The increase in pressure at a deeper depth is essentially the effect of the weight of the fluid above that depth. **Fig. 3.9** shows two containers with the same fluid exposed to the same external pressure - *P*. At any equal depth within either tank the pressure will be the same. The pressure is dependent only on depth and has nothing to do with the shape of the container. If the working fluid is a gas, the pressure increase in the fluid due to the height of the fluid is in most cases negligible since the density and therefore the weight of the fluid is much smaller than the pressure being applied to the system. However, this may not remain true if the system is large enough or the pressures low enough. One example considers how atmospheric pressure changes with altitude. At sea level the standard U.S. atmospheric pressure is 14.696 psia (101.325 kPa). At an altitude of

10000 ft (3048 m) above sea level the standard U.S. atmospheric pressure is 10.106 psia (69.698 kPa) and at 30000 ft (9144 m), the standard U.S. atmospheric pressure is 4.365 psia (30.101 kPa). The pressure in a static liquid can be easily calculated if the density of the liquid is known. [15]

The absolute pressure at a depth H in a liquid is defined as:

$$P_{abs} = P + H \cdot \rho \cdot g \tag{4.3}$$

Where:

P_{abs} is the absolute pressure at depth H.

P is the external pressure at the top of the liquid. For most open systems this will be atmospheric pressure.

ρ is the density of the fluid.

g is the acceleration due to gravity (g = 9.81 m/s^2).

H is the depth at which the pressure is desired.

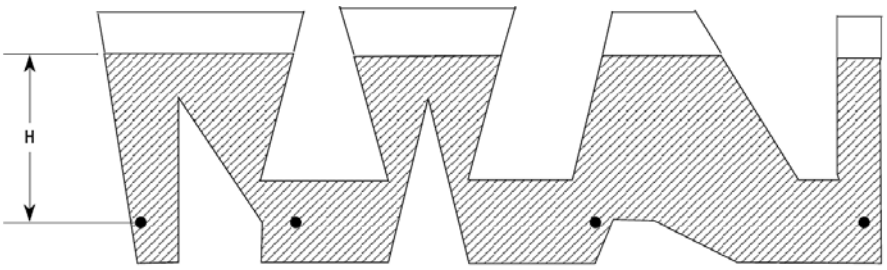

Fig. 3.8: Continuous fluid system [15]

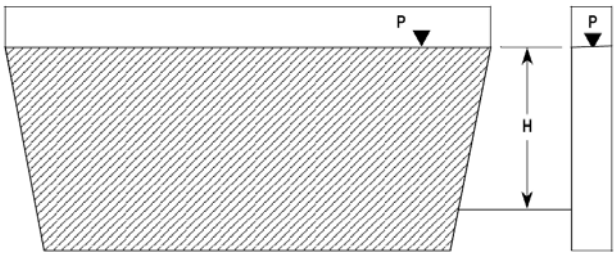

Fig. 3.9: Pressure measurement at a depth in a liquid [15]

3.5.3 Types of pressure sensors

Potentiometric Pressure Sensors

Potentiometric pressure sensors use a Bourdon tube, capsule, or bellows to drive a wiper arm on a resistive element. For reliable operation the wiper must bear on the element with some force, which leads to repeatability and hysteresis errors.

Inductive Pressure Sensors

Several configurations based on varying inductance or inductive coupling are used in pressure sensors. They all require AC excitation of the coil(s) and, if a DC output is desired, subsequent demodulation and filtering. The linear variable differential transformer (LVDT) types have a fairly low frequency response due to the necessity of driving the moving core of the differential transformer. The LVDT uses the moving core to vary the inductive coupling between the transformer primary and secondary.

Capacitive Pressure Sensors

Capacitive pressure sensors typically use a thin diaphragm as one plate of a capacitor. Applied pressure causes the diaphragm to deflect and the capacitance to change. This change may or may not be linear and is typically on the order of several picofarads out of a total capacitance of 50 - 100 pF. The change in capacitance may be used to control the frequency of an oscillator or to vary the coupling of an AC signal through a network. The electronics for signal conditioning should be located close to the sensing element to prevent errors due to stray capacitance.

Piezoelectric Pressure Sensors

Piezoelectric elements are bi-directional transducers capable of converting stress into an electric potential and vice versa. They consist of metallized quartz or ceramic materials. One important factor to remember is that this is a dynamic effect, providing an output only when the input is changing. This means that these sensors can be used only for varying pressures. The piezoelectric element has a high-impedance output and care must be taken to avoid loading the output by the interface electronics. Some piezoelectric pressure sensors include an internal amplifier to provide an easy electrical interface.

Strain Gauge Pressure Sensors

Strain gauge sensors originally used a metal diaphragm with strain gauges bonded to it. A strain gauge measures the strain in a material subjected to applied stress. Metallic strain gauges depend only on dimensional changes to produce a change in resistance. A stress applied to the strip causes it to become slightly longer, narrower, and thinner, resulting in a resistance change. Semiconductor strain gauges are widely used, both bonded and integrated into a silicon diaphragm, because the response to applied stress is an order of magnitude larger than for a metallic strain gauge. When the crystal lattice structure of silicon is deformed by applied stress, the resistance changes. This is called the piezoresistive effect. [16]

Piezoresistive Integrated Semiconductor

IC processing is used to form the piezoresistors on the surface of a silicon wafer (see **Fig. 3.10a**). There are four piezoresistors within the diaphragm area on the sensor. Two are subjected to tangential stress and two to radial stress when the diaphragm is deflected (see **Fig. 3.10b**).

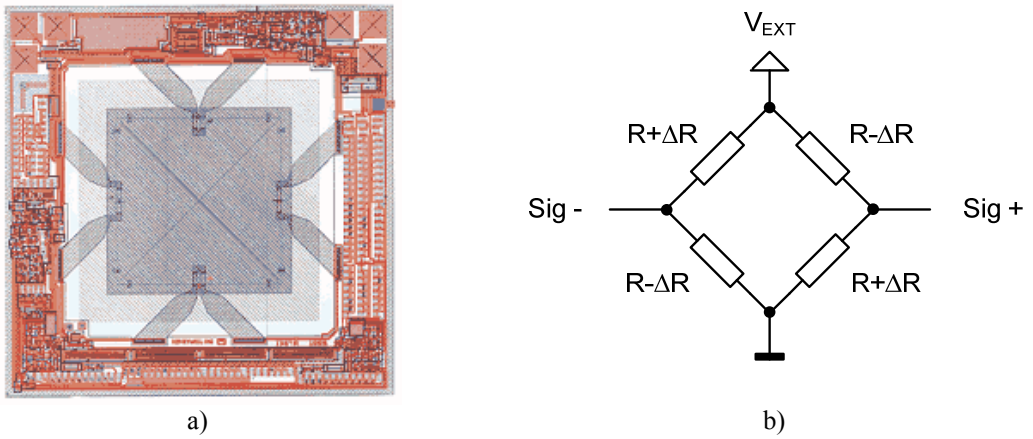

Fig. 3.10: Piezoresistive sensor: a) IC processing, b) Wheatstone bridge sensor [16]

3.6 Current sensing

Current sensing is not actually a part of a sensor system that provides telemetry data but is very important in a probe power management system. The exact information about a draining battery current and a remaining capacity is crucial. Basically, there are two types of current measurements and many ways how to perform that measurement and obtain desired current information. Most common applications use current sensing resistor in high-side or to low-side connection. The principle of this technique is described further in the text.

3.6.1 High side current sensing using resistor

High side current sensing techniques connect the current sensor element between the supply and the load. Current is measured by looking at the voltage drop across a resistor placed between the supply and the load.

The traditional approach for high-side current measurements has been the use of a differential amplifier, which is employed as a gain amplifier and a level shifter from the high side to ground.

Advantages

- Current sensor connected directly to the power source and can detect any downstream failure and trigger appropriate corrective action

- Will not create an extra ground disturbance that comes with a low side current sensing design

Disadvantages

- Requires very careful resistor matching in order to obtain an acceptable common-mode rejection ratio (CMMR). A 1 % deviation lowers it to 46 dB.
- Must withstand very high, and often dynamic, common-mode voltages (often outside the limits of the supply rails of the amplifiers used).

When to Choose High Side Current Sensing

- When low side sensing is not an option due to the added ground disturbance. A high percentage of applications cannot tolerate the ground disturbance and must turn to high side sensing.
- Enables diagnostic systems to detect shorts to ground.
- When cost is saved by eliminating wiring (allows for the load to be grounded remotely).

3.6.2 Low side current sensing using resistor

Low side current sensing techniques connect the current sensor element between the load and ground. Current is measured by looking at the voltage drop across a resistor placed between the load and ground.

Advantages

- Straightforward, easy, and rarely requires more than an op-amp to implement
- Inexpensive and precise.

Disadvantages

- Adds undesirable resistance in the ground path
- May require an additional wire to the load that could otherwise be omitted

When to Choose Low Side Current Sensing

- When it is possible.
- Choosing low side current sensing is almost always the best option if your application can tolerate the extra disturbance in the ground path. [20]

3.6.3 *Current sensing using Hall-effect sensor*

Hall-effect sensor can provide non-intrusive current sensing method. Hall-effect sensors may be implemented in high volume with relatively low cost for many applications. There are two techniques for sensing current using Hall-effect devices. According to the Hall effect, a magnetic field passing through a semiconductor resistor will generate a differential voltage proportional to the field.

In an open loop topology, the Hall element output is simply amplified and the output is read as a voltage that represents the measured current through a scaling factor as depicted in **Fig. 3.11a**.

In a closed loop topology, the output of the Hall element drives a secondary coil that will generate a magnetic field to cancel the primary current field. The secondary current, scaled proportional to the primary current by the secondary coil ratio, can then be measured as voltage across a sense resistor (**Fig. 3.11b**). [21]

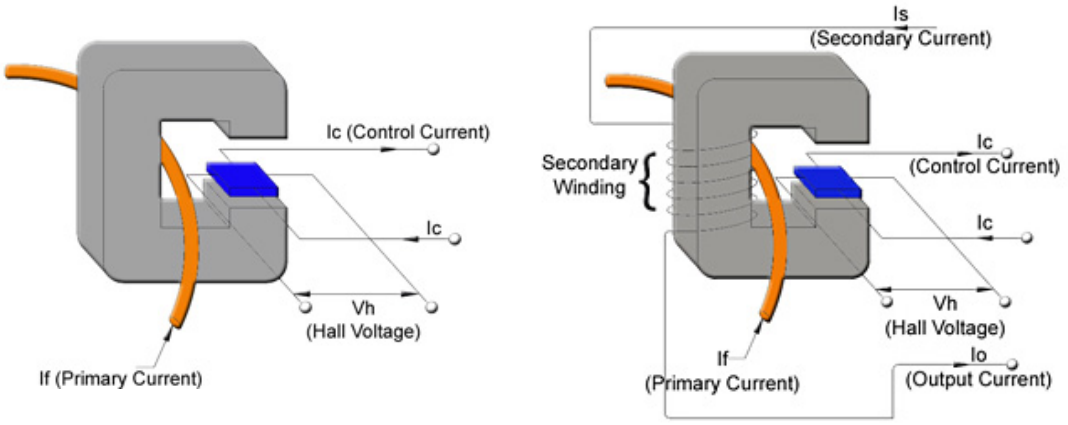

a) b)

Fig. 3.11: Hall effect principle: a) Open loop topology, b) Close loop topology [21]

4 Deep-water probe realization

A whole concept of my deep-water probe is based on remote-operated vehicle (ROV). Submersible ROVs are normally classified into categories based on their size, weight, ability or power. Some common ratings are e.g. micro, mini, general, light workclass, light workclass and trenching/burial. Since my deep-water probe is intended for special applications and since this is my first design, I have decided to build mini ROV without thrusters.

For starters, I list down some features that I desire in my probe design. I would like to achieve following parameters:

- minimal dimensions (round shape, max. 500 x 250 mm)
- minimal submersion depth – 200 meters
- weight up to 8 kg
- durable probe shell
- available construction material
- affordable price
- long probe lifespan

These features are required to provide better user interface and handling with the device. One person may be able to transport the complete ROV system out with them to an application site, deploy it and complete the job without outside help. This is one of the advantages of my deep-water probe.

4.1 Electrical design

The entire system consists of several major electrical parts that include a microcontroller unit (MCU), an inertial measurement unit (IMU), additional sensors, servos, a power supply unit with two DC/DC modules, a high-power LED module, a CMOS camera and a terminal server, an Ethernet switch and converters for communication. A block diagram is shown in **Fig. 4.1**.

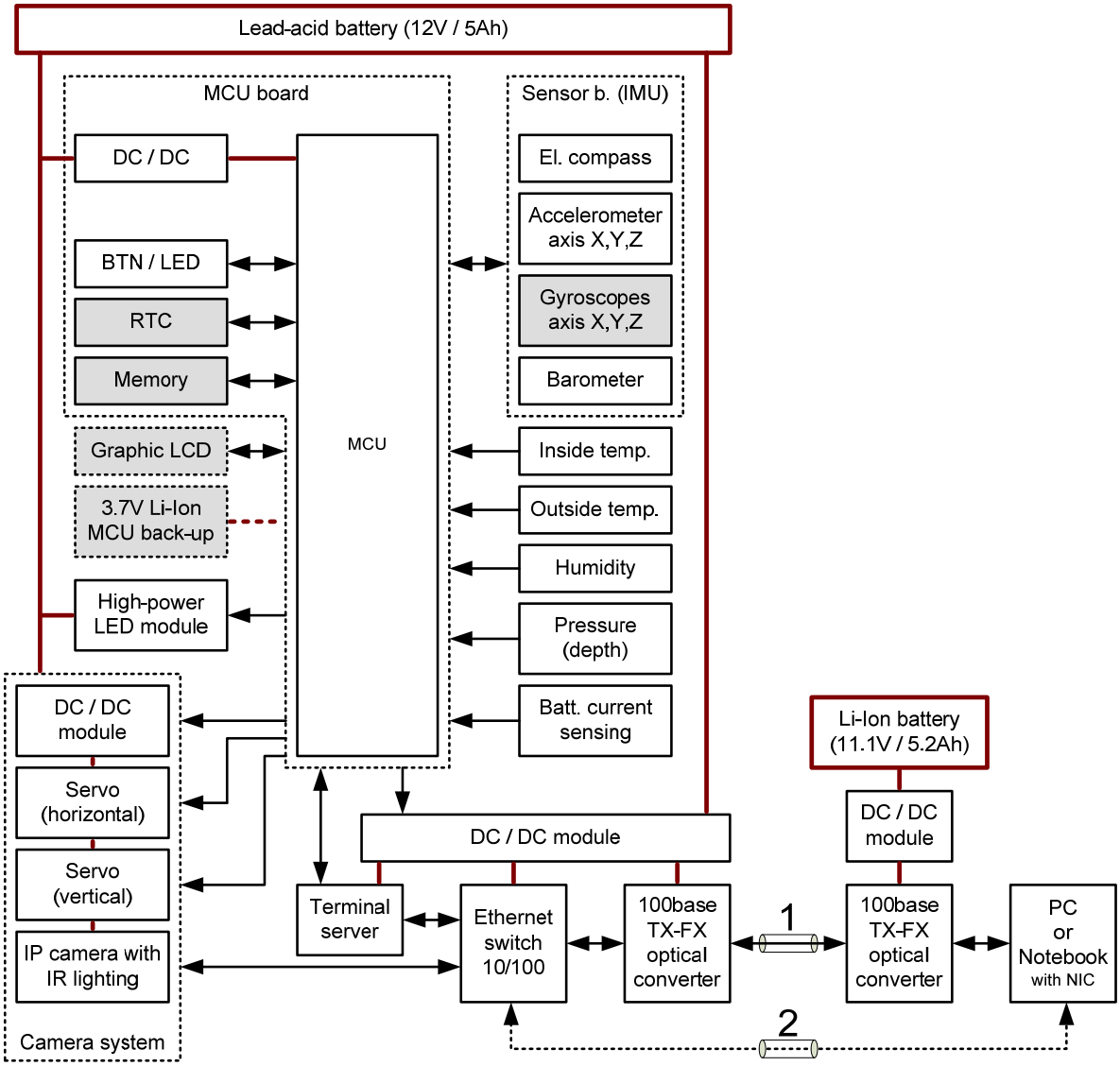

Fig. 4.1: Block diagram of the entire probe system

Fig. 4.2 shows main electronic systems assembled and fixed to the internal support system.

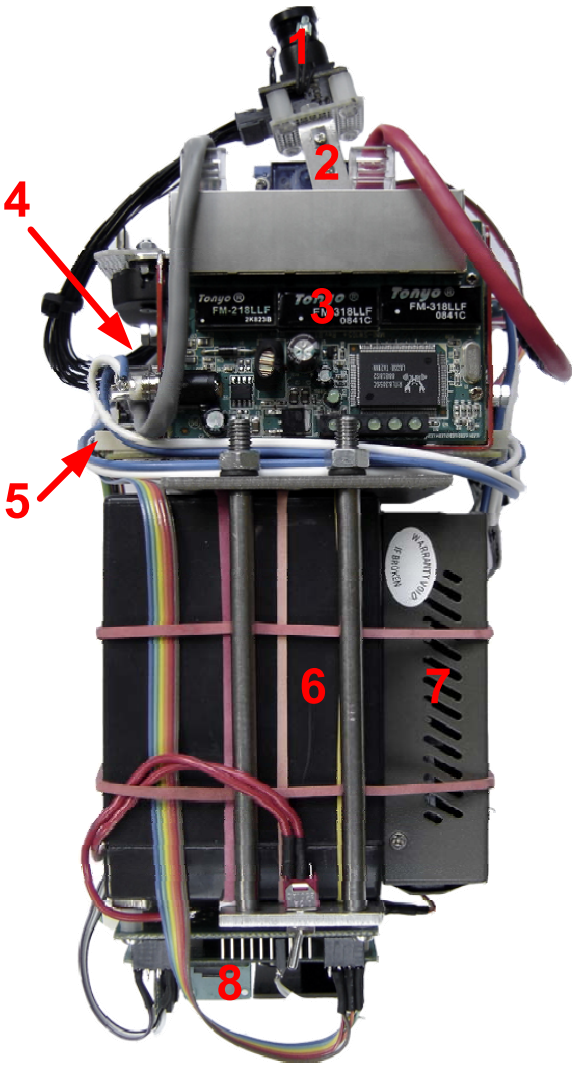

Fig. 4.2: Probe electronic systems overview

Table 4.1: Probe electronic systems overview description for **Fig. 4.2**

1	Camera lens	5	Power-supply board
2	Servo mechanism	6	Battery
3	Ethernet switch	7	Optical converter
4	Terminal server	8	MCU and sensor board

4.2 Mechanical design

The probe shell is made of hard anodized aluminum and has a regular cylinder shape, 330 mm in high and 140 mm in diameter. A top cover is also made from hard anodized aluminum, thickness of 20 mm. A bottom cover is a transparent plastic material that can sustain high pressures, also thickness of 20 mm. Top and bottom covers are fixed with stainless hinges with locks. Every mechanical joint is sealed using the special technical glue.

There are two O-rings at the top and bottom covers to provide a proper sealing. Optical or electrical cables are sealed with rubber bushings.

An internal self-supporting structure is made from non-corroding steel and carries most of the internal devices. Every other additional part (ether internal or external) is made of non-corroding steel. The entire probe is hooked to a carrying cable.

Fig. 4.3: Probe chassis overview

Table 4.2: Probe chassis overview description for **Fig. 4.3**

1	Optical cable	6	Lug (for carrying cable)
2	Cable bushing	7	Locks
3	High pressure sensor (depth measurement)	8	Probe chassis
4	Dome for temperature sensor (external temp.)	9	Bottom cover
5	Top cover		

5 MCU board

MCU is the heart of the probe. MCU processes every sensor data, takes control of external periphery devices like DC/DC modules, the high-power LED module and the communication with the remote PC. MCU also controls camera servo movements and their positions. Together with Inertial measurement unit (IMU), MCU can serve as an inertial navigation system and can also work as a probe stabilization system. This function is reserved for a future control system extension. Therefore, a LCD extension port, RTC, an EEPROM memory and a back-up Li-Ion battery have been already integrated to the designed.

The MCU board, with dimension 68 x 72 mm, is designed as a two-layer FR4 printed circuit board (PCB) with poured Cu on both sides for better ground shielding. **Fig. 5.1** shows assembled MCU board with a description below. The electrical diagram and the PCB layout are enclosed in the appendix.

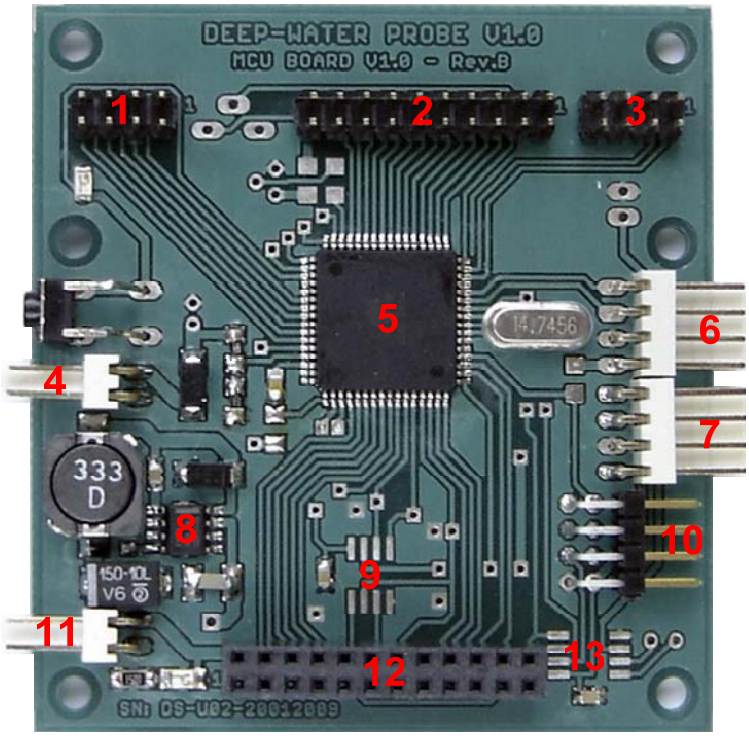

Fig. 5.1: MCU board

Table 5.1: MCU board description for **Fig. 5.1**

1	ADC/JTAG connector	8	DC/DC converter
2	EXPANSION connector	9	EEPROM memory (for future expansion)
3	EXT connector for Power-supply board controlling	10	ISP connector
4	Battery input (6 - 24 V)	11	5 V / 1.5 A output
5	MCU - Atmel ATmega128	12	SENSOR connector
6, 7	UART connectors	13	RTC (for future expansion)

5.1 Microcontroller Atmel ATmega128

The entire probe system is controlled with one microcontroller only. On top of that, MCU will serve as an inertial navigation unit and will provide a digital mapping and stabilization of the probe. Therefore, computing performance must be as high as possible. I chose ATmega128 that is a low-power CMOS 8-bit microcontroller based on the AVR enhanced RISC architecture. By executing powerful instructions in a single clock cycle, the ATmega128 achieves throughputs approaching 1 MIPS per MHz allowing the system designer to optimize power consumption versus processing speed.

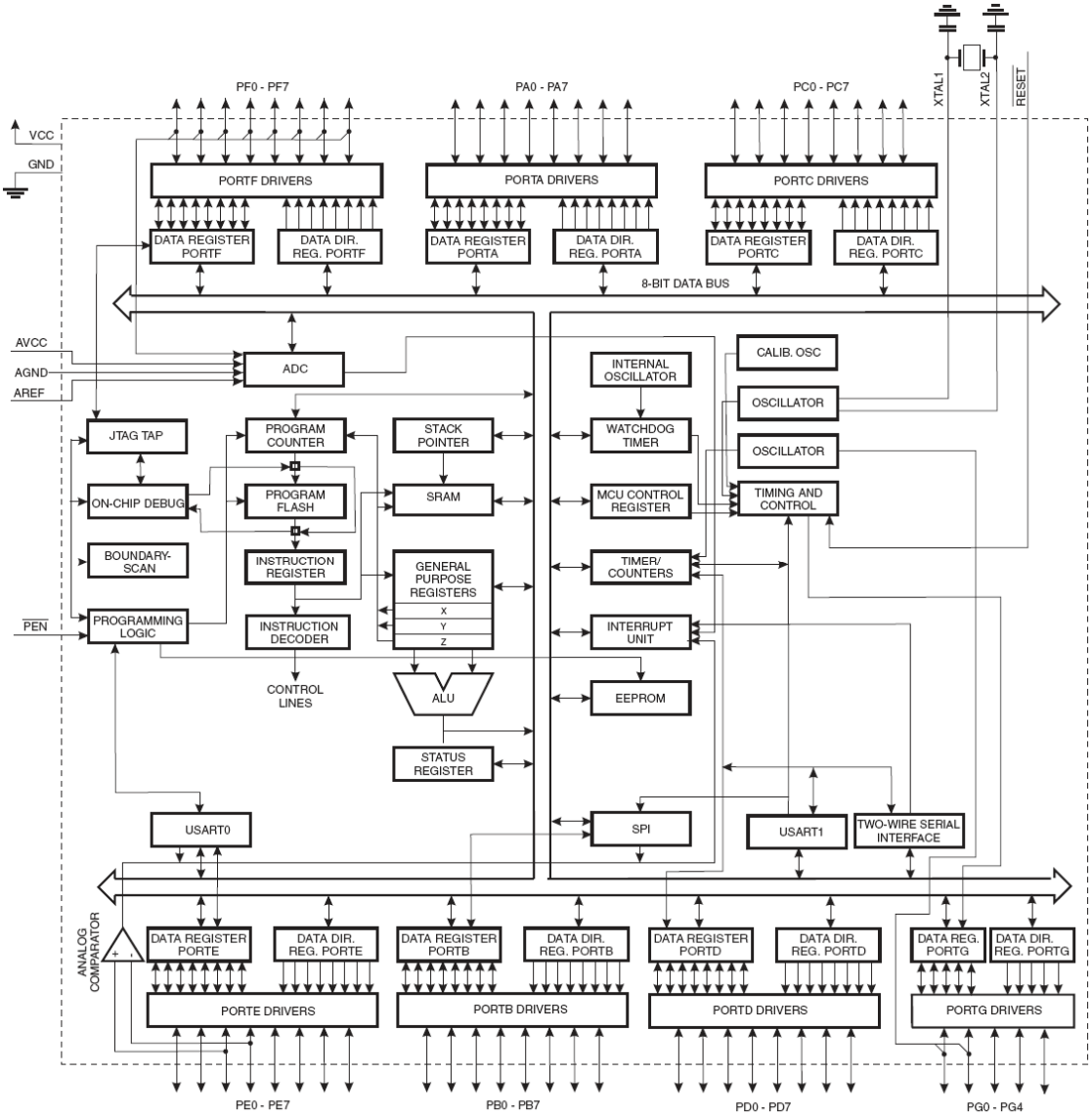

Fig. 5.2: Atmel ATmega128 internal block diagram [23]

The ATmega128 (**Fig. 5.2**) provides the following features: 128K bytes of In-System Programmable Flash with Read-While-Write capabilities, 4K bytes EEPROM, 4K bytes

SRAM, 53 general purpose I/O lines, 32 general purpose working registers, Real Time Counter (RTC), four flexible Timer/Counters with compare modes and PWM, 2 USARTs, a byte oriented Two-wire Serial Interface, an 8-channel, 10-bit ADC with optional differential input stage with programmable gain, programmable Watchdog Timer with Internal Oscillator, an SPI serial port, JTAG test interface, also used for accessing the On-chip Debug system and programming and six software selectable power saving modes. [23]

The external 14.7456 MHz crystal was used to provide more then 14 MIPS and flawless UART communication.

5.2 EEPROM memory

In the case of data transfer malfunction, there is 1 Mbit EEPROM memory to store data during failed communication with the remote PC. This could help prevent valuable data to be lost. An additional memory can also serve for inertial navigation system or for digital mapping.

The MCU board is ready to be fitted with Microchip 25AA1024 which is a 1024 kbit serial EEPROM memory with byte-level and pagelevel serial EEPROM functions. The memory is accessed via a simple Serial Peripheral Interface (SPI) compatible serial bus. The bus signals required are a clock input (SCK) plus separate data in (SI) and data out (SO) lines. Access to the device is controlled by a Chip Select (CS) input. Communication to the device can be paused via the hold pin (HOLD). While the device is paused, transitions on its inputs will be ignored, with the exception of Chip Select, allowing the host to service higher priority interrupts. [24]

5.3 Real-time clock (RTC)

The real-time clock provides precise information about current time and date. This device helps inertial navigation system to be more accurate. If we know time and date from IMU (that include accelerometer, gyroscope and electronic compass outputs), we can integrate them twice with respect to the time and we obtain current position of the probe in the space (if we know the previous position).

The DS1307 serial real-time clock (RTC) is a low-power, full binary-coded decimal (BCD) clock/calendar plus 56 bytes of NV SRAM. Address and data are transferred serially through an I^2C, bidirectional bus. The clock/calendar provides seconds, minutes, hours, day, date, month, and year information. The end of the month date is automatically adjusted for months with fewer than 31 days, including corrections for leap year. The clock operates in either the 24-hour or 12- hour format with AM/PM indicator. The DS1307 has a built-in

power-sense circuit that detects power failures and automatically switches to the backup supply. Timekeeping operation continues while the part operates from the backup supply.

The DS1307 uses an external 32.768 kHz crystal. The accuracy of the clock is dependent upon the accuracy of the crystal and the accuracy of the match between the capacitive load of the oscillator circuit and the capacitive load for which the crystal was trimmed. Additional error will be added by crystal frequency drift caused by temperature shifts. External circuit noise coupled into the oscillator circuit may result in the clock running fast.

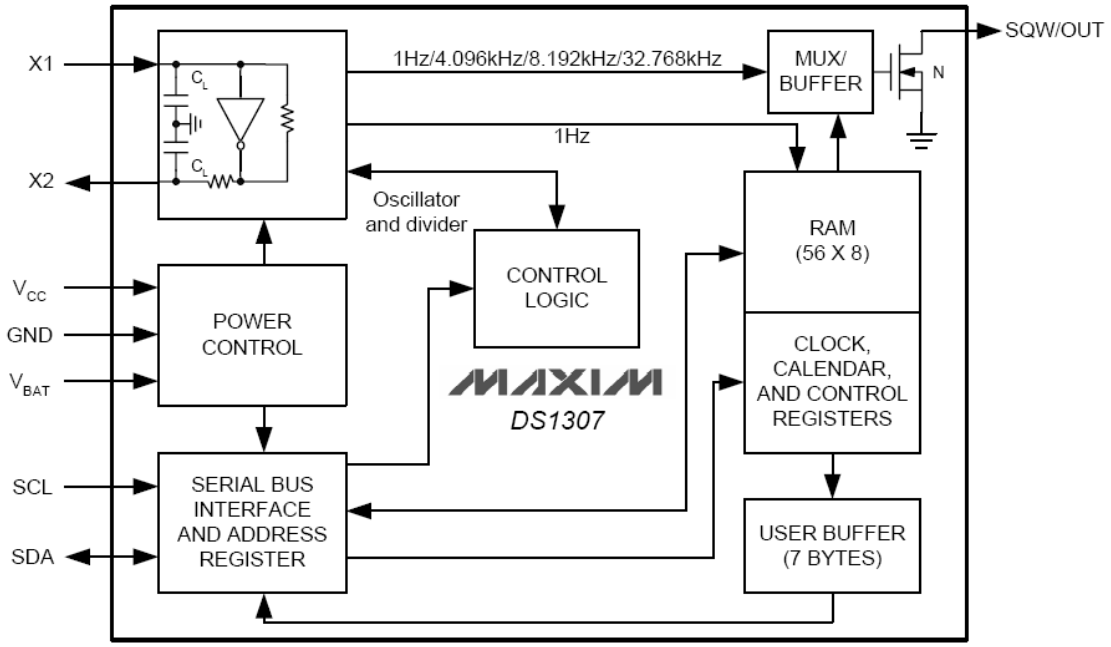

Fig. 5.3: RTC block diagram [25]

When VCC falls below VBAT, the device switches into a low-current battery-backup mode. Upon power-up, the device switches from battery to VCC when VCC is greater than VBAT +0.2 V and recognizes inputs when VCC is greater than 1.25 x VBAT. The block diagram in the **Fig. 5.3** shows the main elements of the serial RTC. A backup supply battery could be any standard 3 V Lithium cell or other energy source. A lithium battery with 48 mAh or greater will back up the DS1307 for more than 10 years in the absence of power at +25 °C. [25]

5.4 MCU board power-supply

The MCU board is powered by its own DC-DC converter driven by the TPS5420 produced by Texas Instruments. The TPS5420 is a high-output-current PWM step-down converter with an integrated low resistance high side N-channel MOSFET. The chip runs at fixed 500 kHz switching frequency and provides up to 2 A continuous current output with

high efficiency up to 95 %. The system is protected by over-current limitation, over-voltage protection and thermal shutdown. The MCU board is also equipped with a connector that could be used for either the MCU external power-supply source or as a multi-purpose 5 V output with 1.5 A current limit.

6 Sensor system

The probe is supplied with a full package of control and instrumentation sensors. For starters, there is an inside and an outside temperature measurement. A pressure sensor measures a real depth. Inertial measurement unit (IMU), which includes three-axis accelerometer, three gyroscopes placed in axis X, Y, Z and electronic compass, tracks position and can stabilize the probe. The probe is also equipped with the leak detection system. A very sensitive barometer and a humidity sensor can be monitored to ensure that there are no system leaks. The power-supply system is also under surveillance due to the voltage and the currency measurement. All of the sensors together with MCU provide the real-time measurement. In this chapter, I describe all used sensors, their principles and functions. Some of them are situated on the **Sensor board** and some are connected directly to the **MCU board** via **Expansion connector** or **ADC connector**.

The sensor board, with dimension 68 x 53 mm, is designed as a two-layer FR4 printed circuit board (PCB) with poured Cu on both sides for better ground shielding. The board is mounted on the MCU board and is connected via 20-pin connector made by SAMTEC. **Fig. 6.1** shows assembled sensor board with a description below. The electrical diagram and the PCB layout are enclosed in the appendix.

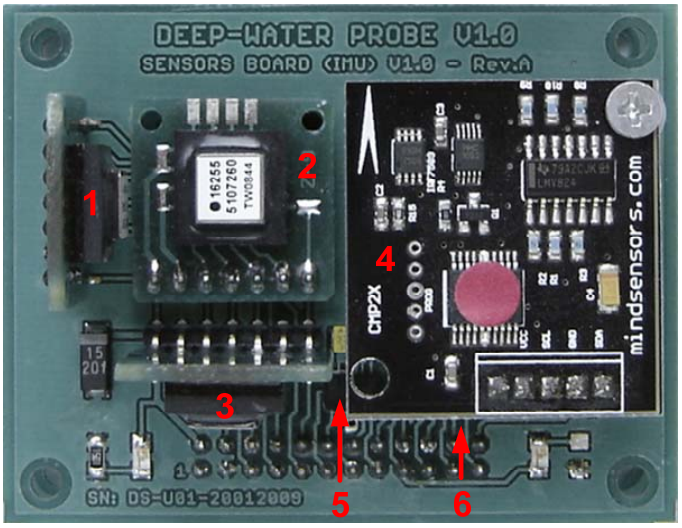

Fig. 6.1: Sensor board

Table 6.1: Sensor board description for **Fig. 6.1**

1, 2, 3	Gyro X, Z, Y
4	Electronic compass
5	3-axis accelerometer
6	Barometer (soldered under the electronic compass)

6.1 Electronic compass

Most of today applications use magnetoresistive (MR) sensors to measure magnetic field. In my diploma thesis, I used CMP2X module from mindsensors.com (described further) that contains MR sensor HMC1052 produced by Honeywell. Following a description of Honeywell´s magnetoresistive sensors for compass applications, the design of each building block is covered in detail.

6.1.1 HMC1052 magnetoresistive sensor

The Honeywell HMC1052 is high performance magnetoresistive sensor designs on a single chip. The advantage is two-axis sensing, ultra small size and low cost in miniature surface mount package.

This magneto-resistive sensor is configured as a 4-element Wheatstone bridge to convert magnetic fields to differential output voltages (**Fig. 6.2**). Capable of sensing fields down to 120 micro-gauss, this sensor offers a compact, high sensitivity (1.0 mV/V/gauss) and highly reliable solution for low field magnetic sensing.

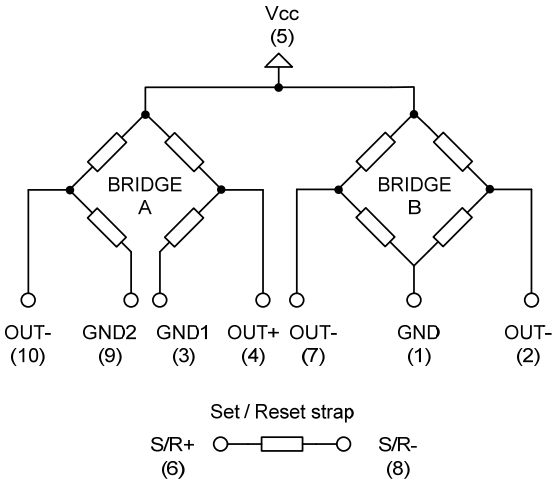

Fig. 6.2: HMC1052 internal configuration [4]

With power supply applied to a bridge, the sensor converts any incident magnetic field in the sensitive axis direction to a differential voltage output. In addition to the bridge circuit, the sensor has two on-chip magnetically coupled straps; the offset strap and the set/reset strap.

The offset strap allows for several modes of operation when a direct current is driven through it. These modes are:

1) Subtraction (bucking) of an unwanted external magnetic field,

2) Clearing the bridge offset voltage,

3) Closed loop field cancellation, and

4) Autocalibration of bridge gain.

The set/reset strap can be pulsed with high currents for the following benefits:

1) Enable the sensor to perform high sensitivity measurements,

2) Flip the polarity of the bridge output voltage, and

3) Periodically used to improve linearity and temperature effects.

6.1.2 CMP2X module

CMP2X is a digital compass sensor, which can be used in I^2C mode to detect deviation from magnetic north pole (heading). It appears as 24xxseries EPROM, with a different I^2C address. I have chosen the most important sections providing basic information about using this module. See more in [2]

Connection

Connector Pins are shown in **Fig. 6.3**.

Pin number	Function
1	SDA (Serial Data)
2	GND
3	SCL (Serial Clock)
4	+5V (VCC)
5	Interruption

Pin: 5 4 3 2 1

Fig. 6.3: CMP2X Pin description

I^2C operation

Used pins: SDA (1), GND (2), SCL (3), +5 V (4)

Heading Calculation calibration and setup commands:

Table 6.2: Heading Calculation calibration and setup commands

Commands		**Action**
AS CII	**Hex**	
A	0x41	Toggle AutoTrig mode
B	0x42	Compassing Mode: Result in Byte (0-360 mapped to 0-255)
I	0x49	Com passing Mode: Result in Integer (0-360 mapped to 0-36000)
F	0x46	Compassing Mode: Result in Float (0-360 mapped to 0-360.00)
E	0x45	Compassing Mode: Set Sampling frequency to 50 Hz (Europe std.)
U	0x55	Com passing Mode: Set Sampling frequency to 60 Hz (USA std.)
C	0x43	Begin Calibration mode
D	0x44	Calibration Done

Calibration

CMP2X is capable of calibrating in-situ and can supply high resolution heading information. To calibrate CMP2X, issue *Calibration command* and turn around at least twice while taking 20 seconds or more per turn. Issuing *Calibration Done* command ends the calibration mode and resumes normal operation. All the calibration constants are stored in internal nonvolatile memory. They are retained while power is off.

Current consumption

Average measured current profile is as follows:

Table 6.3: Current consumption

Operation	Current Consumption	Duration
AutoTrig ON	12 mA	Continuous
Heading calculation	12 mA	200 miliseconds
Standby	3 mA	-

The sensor module will automatically go to standby mode after a heading determination, whilst waiting for a new command on the I^2C bus.

Factory Default Address is 0xE0. CMP2X uses fixed I^2C bus address of 0xE0 and it is not selectable. However, Mindsensors can provide different addresses on demand.

To determine if CMP2X has finished the heading calculations, we can take advantage of the fact that the CMP2X will not respond to any I^2C activity whilst ranging. Therefore, if we try to read from the CMP2X (we use the software revision number at location 0) then we will get 255 (0xFF) whilst ranging. This is because the I^2C data line (SDA) is pulled high if no thing is driving it. As soon as the heading is determined, the CMP2X will again respond to the I^2C bus. We should keep reading the register until we receive the F/W revision number from CMP2X. We can then read the heading data. Our controller can perform other tasks while the CMP2X is determining heading. We can also use INT pin on CMP2X to connect to our processors interrupt line. INT pin on CMP2X is an open-drain pin with weak pull-up and when the heading is determined, CMP2X gives a low pulse of 180 μS for generating the interrupt to host.

6.2 MMA7455L digital accelerometer

Concerning all of the selecting factors mentioned in **Chapter 3.2**, I chose a 3-axis digital accelerometer made by Freescale Semiconductor. The MMA7455L is a digital output

(I^2C/SPI), low power, low profile capacitive micromachined accelerometer featuring signal conditioning, a low pass filter, temperature compensation, self-test, configurable to detect 0 g through interrupt pins (INT1 or INT2), and pulse detect for quick motion detection (**Fig. 6.4**). 0 g offset and sensitivity are factory set and require no external devices. The 0 g offset can be customer calibrated using assigned 0 g registers and g-Select which allows for command selection for 3 acceleration ranges (2 g / 4 g / 8 g). The MMA7455L includes a standby mode that makes it ideal for handheld battery powered electronics.

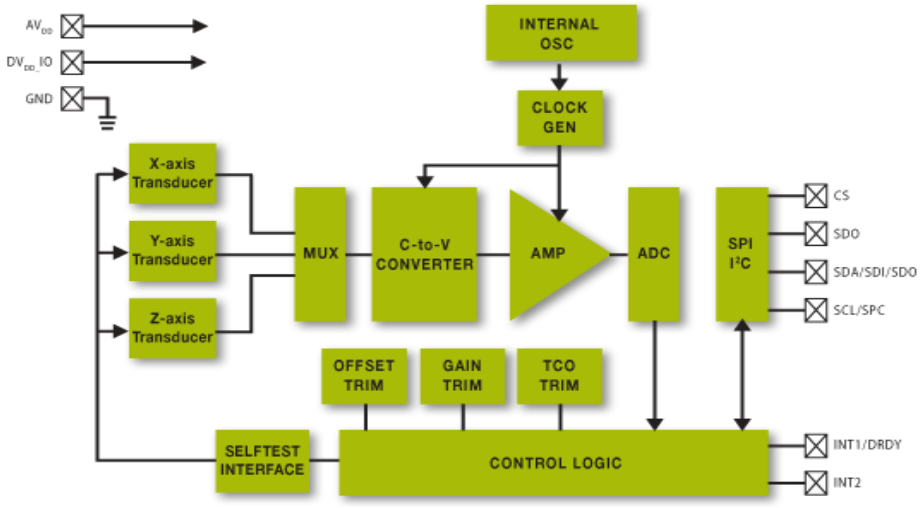

Fig. 6.4: MMA7455L block diagram [7]

Principle of operation

The Freescale accelerometer is a surface-micromachined integrated-circuit accelerometer. The device consists of a surface micromachined capacitive sensing cell (g-cell) and a signal conditioning ASIC contained in a single package. The sensing element is sealed hermetically at the wafer level using a bulk micromachined cap wafer. The g-cell is a mechanical structure formed from semiconductor materials (polysilicon) using semiconductor processes (masking and etching). It can be modeled as a set of beams attached to a movable central mass that move between fixed beams. The movable beams can be deflected from their rest position by subjecting the system to the acceleration (**Fig. 6.5**). As the beams attached to the central mass move, the distance from them to the fixed beams on one side will increase by the same amount as the distance to the fixed beams on the other side decreases. The change in distance is a measure of acceleration. The g-cell beams form two back-to-back capacitors (**Fig. 6.5**). As the center beam moves with acceleration, the distance between the beams changes and each capacitor's value will change, ($C = A\varepsilon/D$). Where A is the area of the beam, ε is the dielectric constant, and D is the distance between the beams. The ASIC uses switched capacitor techniques to measure the g-cell capacitors and extract the acceleration data from

the difference between the two capacitors. The ASIC also signal conditions and filters (switched capacitor) the signal, providing a digital output that is proportional to acceleration. See more in [7].

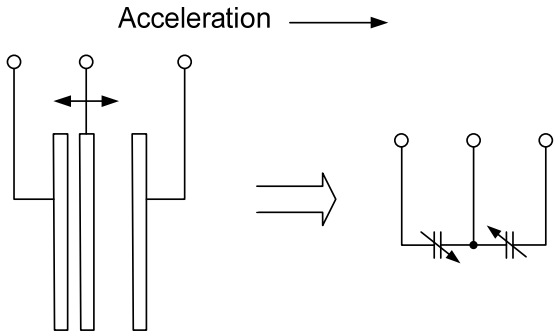

Fig. 6.5: Simplified transducer physical model

Self-Test feature

The sensor provides a self-test feature that allows the verification of the mechanical and electrical integrity of the accelerometer at any time before or after installation. This feature is critical in applications where system integrity must be ensured over the life of the product. When the self-test function is initiated through the mode control register ($16), accessing the "self-test" bit, an electrostatic force is applied to each axis to cause it to deflect. The Z-axis is trimmed to deflect 1 g. This procedure assures that both the mechanical (g-cell) and electronic sections of the accelerometer are functioning.

g-Select feature

The g-Select feature enables the selection between 3 acceleration ranges for measurement. Depending on the values in the Mode control register ($16), the MMA7455L's internal gain will be changed allowing it to function with a 2 g, 4 g or 8 g measurement sensitivity. The sensitivity can be changed during the operation by modifying the two GLVL bits located in the mode control register.

Standby Mode

This digital output 3-axis accelerometer provides a standby mode that is ideal for battery operated products. When standby mode is active, the device outputs are turned off, providing significant reduction of operating current. When the device is in standby mode the current will be reduced to 2.5 μA typical. In standby mode the device can read and write to the registers with the I^2C/ SPI available, but no new measurements can be taken in this mode as all current consuming parts are off. The mode of the device is controlled through the mode control register by accessing the two mode bits.

Measurement Mode

During measurement mode, continuous measurements on all three axes are enabled. The g-range for 2 g, 4 g, or 8 g is selectable with 8-bit data and the g-range of 8 g is selectable with 10-bit data. The sample rate during measurement mode is 125 Hz with 62.5 BW filter selected. The sample rate is 250 Hz with the 125 Hz filter selected. Therefore, when a conversion is complete (signaled by the DRDY flag), the next measurement will be ready. When measurements on all three axes are completed, a logic high level is output to the DRDY pin, indicating "measurement data is ready." The DRDY status can be monitored by the DRDY bit in Status Register (Address: $09). The DRDY pin is kept high until one of the three Output Value Registers are read. If the next measurement data is written before the previous data is read, the DOVR bit in the Status Register will be set. Also note that in measurement mode, level detection mode and pulse detection mode are not available. By default all three axes are enabled. X and/or Y and/or Z can be disabled. There is a choice between detecting an absolute signal or a positive or negative only signal on the enabled axes. There is also a choice between doing a detection for motion where X or Y or Z > Threshold vs. doing a detection for freefall where X & Y & Z < Threshold.

Digital Interface

The MMA7455L has both an I^2C and SPI digital output available for a communication interface. CS pin is used for selecting the mode of communication. When CS is low, SPI communication is selected. When CS is high, I^2C communication is selected. I have decided to use SPI communication in this project.

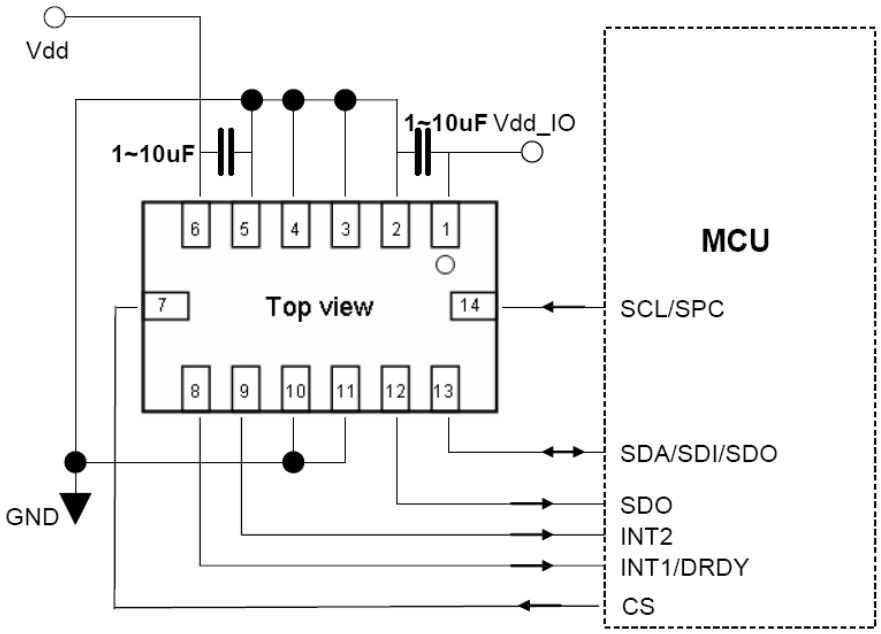

Fig. 6.6: SPI Connection to MCU [7]

SPI Slave Interface

The MMA7455L also uses serial peripheral interface communication as a digital communication. The SPI communication is primarily used for synchronous serial communication between a master device and one or more slave devices. **Fig. 6.6** shows an example of how to configure one master with one MMA745xL device. The MMA7455L is always operated as a slave device. Typically, the master device would be a microcontroller which would drive the clock (SPC) and chip select (CS) signals. [7]

The SPI interface consists of two control lines and two data lines: CS, SPC, SDI, and SDO. The CS, also known as Chip Select, is the slave device enable which is controlled by the SPI master. CS is driven low at the start of a transmission. CS is then driven high at the end of a transmission. SPC is the Serial Port Clock which is also controlled by the SPI master. SDI and SDO are the Serial Port Data Input and the Serial Port Data Output. The SDI and SDO data lines are driven at the falling edge of the SPC and should be captured at the rising edge of the SPC.

Read and write register commands are completed in 16 clock pulses or in multiples of 8, in the case of a multiple byte read/write.

6.3 ADIS16255 digital gyroscope

Concerning all of the selecting factors mentioned above, I have chosen a programmable low power gyroscope ADIS16255 that is complete angular rate measurement systems available in a single compact package enabled by Analog Devices, Inc. iSensor™ integration. By enhancing Analog Devices iMEMS® sensor technology with an embedded signal processing solution, the ADIS16255 provide factory-calibrated and tunable digital sensor data in a convenient format that can be accessed using a simple SPI serial interface. The SPI interface provides access to measurements for the gyroscope, temperature, power supply, and one auxiliary analog input.

The main advantage of the device I would like to highlight is that the device range can be digitally selected from three different settings: ±80 °/sec, ±160 °/sec, and ±320 °/sec. Setting 320 °/sec range, we are getting 0.07326 °/sec/LSB sensitivity. Unique characteristics of the end system are accommodated easily through several built-in features, including a single-command auto-zero recalibration function, as well as configurable sample rate and frequency response. Additional features can be used to further reduce system complexity, including configurable alarm function, auxiliary 12-bit ADC and DAC, two configurable digital I/O ports and digital self-test function. System power dissipation can be optimized via the ADIS16255 power management features, including an interrupt-driven wake-up.

Theory of operation

The core angular rate sensor integrated inside ADIS16255 is based on the Analog Devices iMEMS technology. This sensor operates on the principle of a resonator gyroscope (**Fig. 6.7**). Two polysilicon sensing structures each contain a dither frame electrostatically driven to resonance. This provides the necessary velocity element to produce a Coriolis force during rotation. At two of the outer extremes of each frame, orthogonal to the dither motion, are movable fingers placed between fixed fingers to form a capacitive pickoff structure that senses Coriolis motion. At a given angular rate and Coriolis acceleration, there will be a corresponding capacitance between the beams attached to the vibrating mass and those attached to the substrate. The resulting signal is fed to a series of gain and demodulation stages that produce the electrical rate signal output. The electronics can resolve change in capacitance as small as 12×10^{-21} F from beam deflections as small as 0.00016 Å.

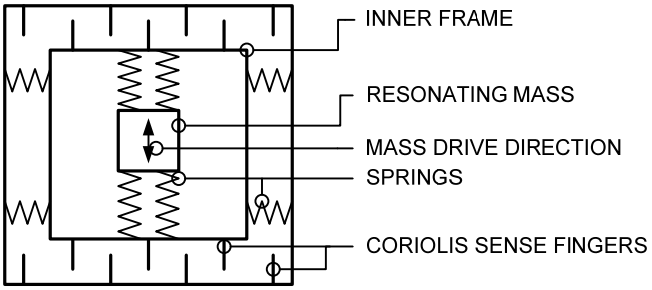

Fig. 6.7: Physical model of the core angular rate sensor [10]

The base sensor output signal is sampled using an ADC, and then the digital data is fed into a proprietary digital calibration circuit. This circuit contains calibration coefficients from the factory calibration, along with user-defined calibration registers that can be used to calibrate system-level errors.

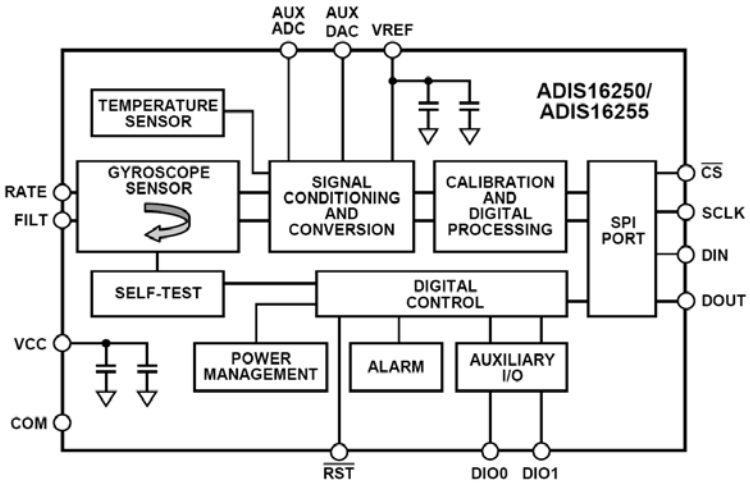

Fig. 6.8: ADIS16255 functional block diagram [11]

The calibrated gyroscope data (GYRO_OUT) is made available through output data registers along with temperature, power supply, auxiliary ADC, and relative angle output calculations. Functional block diagram is in **Fig. 6.8**.

The ADIS16255 are designed for simple integration into industrial system designs, requiring only a 5.0 V power supply and a 4-wire, industry standard serial peripheral interface (SPI). All outputs and user-programmable functions are handled by a simple register structure. Each register is 16 bits in length and has its own unique bit map. The 16 bits in each register consist of an upper (D8 to D15) byte and a lower (D0 to D7) byte, each of which has its own 6-bit address. The ADIS16255 provides access to calibrated rotation measurements, relative angle estimates, power supply measurements, temperature measurements, and an auxiliary 12-bit ADC channel. This output data is continuously updating internally, regardless of user read rates. [10, 11]

6.4 SHT75 digital humidity and temperature sensor

In my design, the probe is equipped with the leak detection system. A very sensitive barometer and a humidity sensor are monitored to ensure that there are no system leaks.

I used excellent humidity and temperature sensor fabricated in one small package. SHT7x (including SHT71 and SHT75) is Sensirion's family of relative humidity and temperature sensors with pins that comes with very short response times (4 seconds at lie), high precision (±2 % to ±5 % according to configuration) and low power consumption (<3 μA standby). The sensors integrate sensor elements plus signal processing in compact format and provide a fully calibrated digital output. A unique capacitive sensor element is used for measuring relative humidity while temperature is measured by a band-gap sensor. The applied CMOSens® technology guarantees excellent reliability and long term stability. Both sensors are seamlessly coupled to a 14bit analog to digital converter and a serial interface circuit. This results in superior signal quality, a fast response time and insensitivity to external disturbances (EMC).

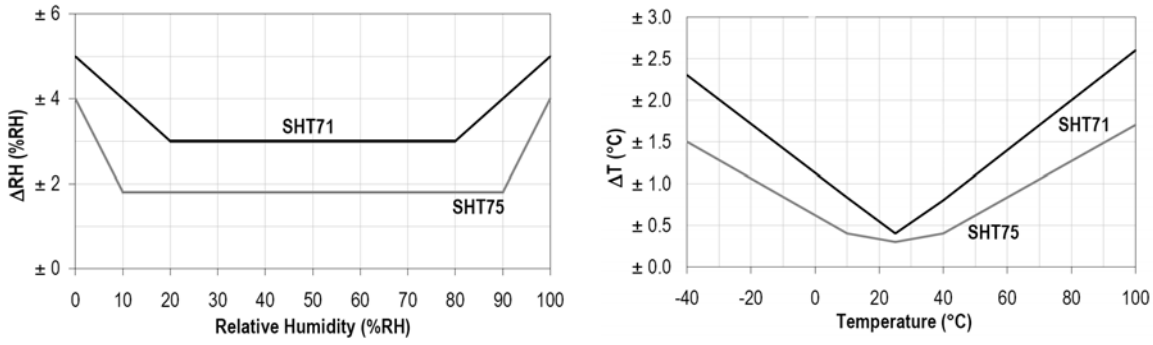

a) b)

Fig. 6.9: SHT75 characteristics: a) Relative humidity, b) Temperature [13]

Each SHT7x is individually calibrated in a precision humidity chamber. The calibration coefficients are programmed into an OTP memory on the chip. These coefficients are used to internally calibrate the signals from the sensors. The 2-wire serial interface and internal voltage regulation allows for easy and fast system integration.

Wiring

A typical connection to the MCU can be seen in **Fig. 6.10**a.

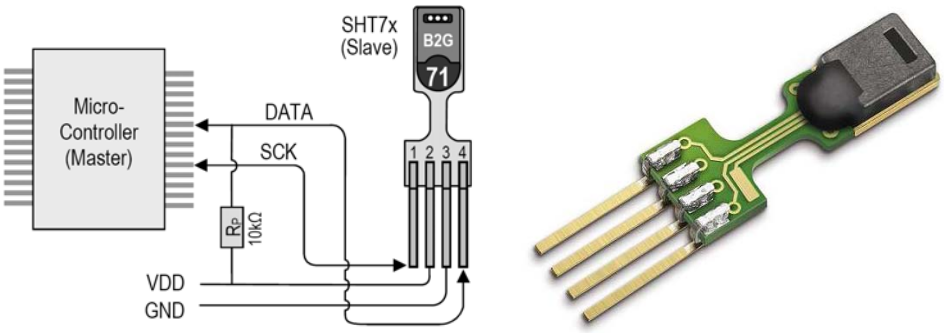

a) b)

Fig. 6.10: SHT75 a) wiring, b) detail [13]

Communication

Serial clock input (SCK) is used to synchronize the communication between microcontroller and SHT7x. Since the interface consists of fully static logic there is no minimum SCK frequency.

Serial data (DATA) tri-state pin is used to transfer data in and out of the sensor. For sending a command to the sensor, DATA is valid on the rising edge of the serial clock (SCK) and must remain stable while SCK is high. After the falling edge of SCK the DATA value may be changed.

Measurement of RH and T

After issuing a measurement command (‘00000101’ for relative humidity, ‘00000011’ for temperature) the controller has to wait for the measurement to complete. This takes a maximum of 20 / 80 / 320 ms for a 8 / 12 / 14 bit measurement. The time varies with the speed of the internal oscillator and can be lower by up to 30 %. To signal the completion of a measurement, the SHT7x pulls data line low and enters Idle Mode. The controller must wait for this Data Ready signal before restarting SCK to readout the data. Measurement data is stored until readout, therefore the controller can continue with other tasks and readout at its convenience. Two bytes of measurement data and one byte of CRC checksum (optional) will then be transmitted. The micro controller must acknowledge each byte by pulling the DATA line low. All values are MSB first, right justified (e.g. the 5th SCK is MSB for a 12-bit value,

for a 8-bit result the first byte is not used). Communication terminates after the acknowledge bit of the CRC data. If CRC-8 checksum is not used the controller may terminate the communication after the measurement data LSB by keeping ACK high. The device automatically returns to Sleep Mode after measurement and communication are completed. **Fig. 6.11** shows an example RH measurement sequence. [13]

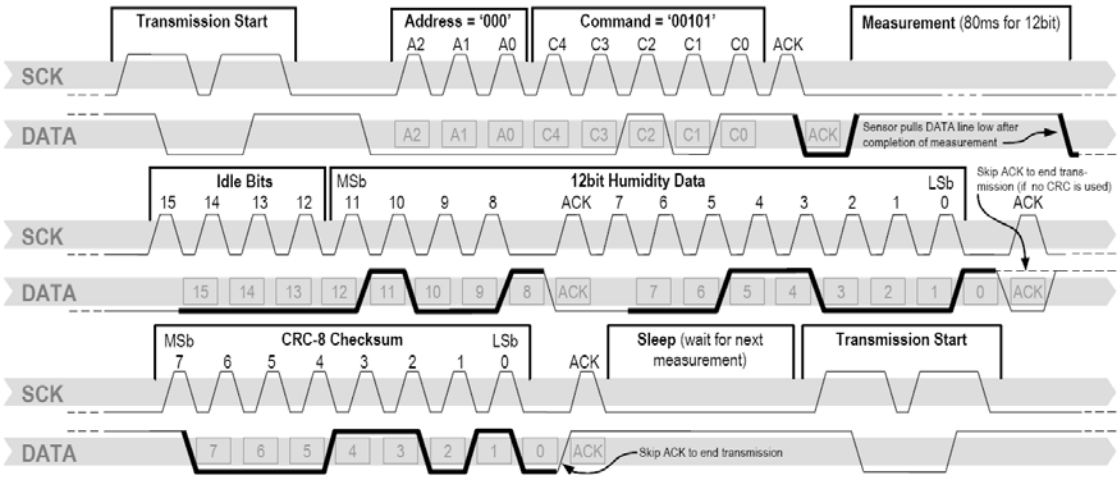

Fig. 6.11: Example RH measurement sequence [13]

Table 6.4: SHT7x list of commands

Command	Code
Reserved	0000x
Measure Temperature	00011
Measure Relative Humidity	00101
Read Status Register	00111
Write Status Register	00110
Reserved	0101x-1110x
Soft reset, resets the interface, clears the status register to default values. Wait minimum 11 ms before next command	11110

6.5 External temperature sensor

External temperature measurement is acquired from very precise DS18B20 sensor produced by Maxim Dallas Semiconductor. The DS18B20 digital thermometer provides 9-bit to 12-bit Celsius temperature measurements and has an alarm function with nonvolatile user-programmable upper and lower trigger points. The DS18B20 communicates over a 1-Wire bus that by definition requires only one data line (and ground) for communication with a central microprocessor. It has an operating temperature range of -55 °C to +125 °C and is accurate to ±0.5 °C over the range of -10 °C to +85 °C. In addition, the DS18B20 can derive

power directly from the data line ("parasite power"), eliminating the need for an external power supply.

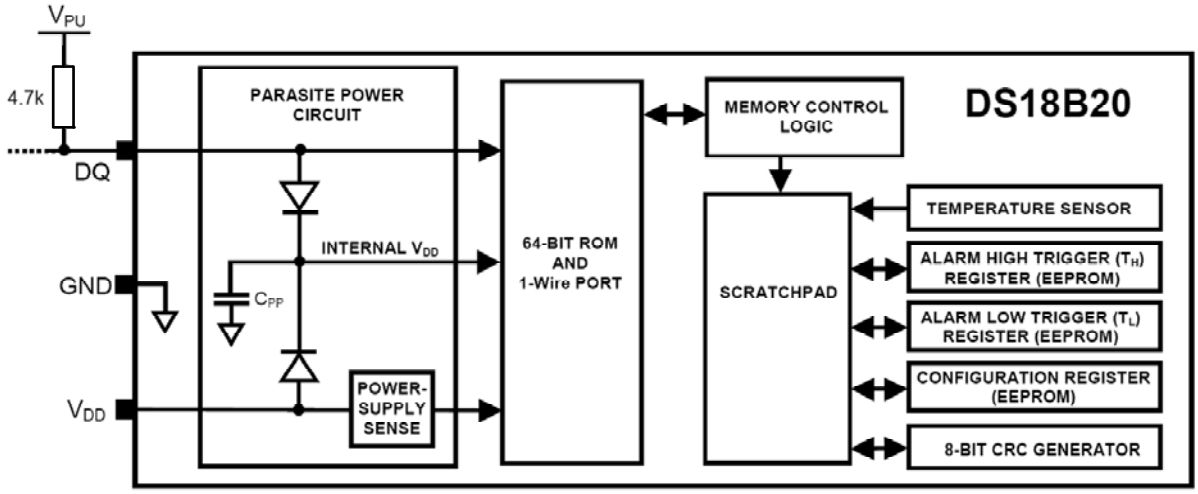

Fig. 6.12: Block diagram of the DS18B20 [14]

Fig. 6.12 shows a block diagram of the DS18B20. The 64-bit ROM stores the device's unique serial code. The scratchpad memory contains the 2-byte temperature register that stores the digital output from the temperature sensor. In addition, the scratchpad provides access to the 1-byte upper and lower alarm trigger registers (T_H and T_L) and the 1-byte configuration register. The configuration register allows the user to set the resolution of the temperature to- digital conversion to 9, 10, 11, or 12 bits. The T_H, T_L, and configuration registers are nonvolatile (EEPROM), so they will retain data when the device is powered down.

The DS18B20 uses Maxim's exclusive 1-Wire bus protocol that implements bus communication using one control signal. The control line requires a weak pull-up resistor since all devices are linked to the bus via a 3-state or open-drain port (the DQ pin in the case of the DS18B20). In this bus system, the microprocessor (the master device) identifies and addresses devices on the bus using each device's unique 64-bit code. Because each device has a unique code, the number of devices that can be addressed on one bus is virtually unlimited.

6.5.1 Measuring temperature principle

The core functionality of the DS18B20 is its direct-to-digital temperature sensor. A block diagram of the temperature measurement circuitry is shown in **Fig. 6.13**. Each temperature sensor measures temperature by counting the number of clock cycles that an oscillator with a low temperature coefficient goes through during a gate period determined by a high temperature coefficient oscillator. The counter is preset with a base count that corresponds to –55 °C. If the counter reaches zero before the gate period is over, the temperature register,

which is also preset to the –55 °C value, is incremented, indicating that the temperature is higher than –55 °C.

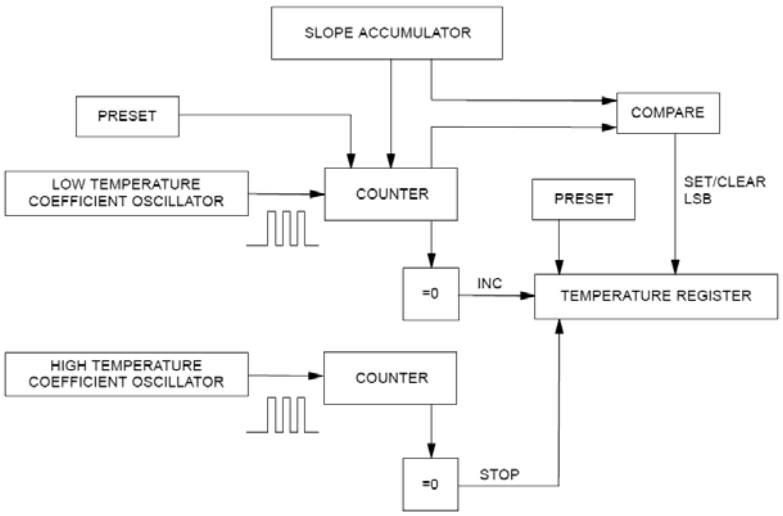

Fig. 6.13: Temperature measurement circuitry [14]

At the same time, the counter is then preset with a value determined by the slope accumulator circuitry. This circuitry is needed to compensate for the parabolic behavior of the oscillators over temperature. The counter is then clocked again until it reaches zero. If the gate period is still not finished, then this process repeats.

The slope accumulator is used to compensate for the nonlinear behavior of the oscillators over temperature, yielding a high resolution temperature measurement (0.5 °C for almost all the products). This is done by changing the number of counts necessary for the counter to go through for each incremental degree in temperature. To obtain the desired resolution, therefore, both the value of the counter and the number of counts per degree C (the value of the slope accumulator) at a given temperature must be known.

6.5.2 Measuring temperature with DS18B20

The resolution of the temperature sensor is user-configurable to 9, 10, 11, or 12 bits, corresponding to increments of 0.5 °C, 0.25 °C, 0.125 °C, and 0.0625 °C, respectively. The default resolution at power-up is 12-bit. The DS18B20 powers up in a low-power idle state. To initiate a temperature measurement and A-to-D conversion, the master must issue a Convert T [44h] command. Following the conversion, the resulting thermal data is stored in the 2-byte temperature register in the scratchpad memory and the DS18B20 returns to its idle state. The DS18B20 output temperature data is calibrated in degrees Celsius. The temperature data is stored as a 16-bit sign-extended two's complement number in the temperature register. The sign bits (S) indicate if the temperature is positive or negative: for positive numbers S = 0 and for negative numbers S = 1. If the DS18B20 is configured for 12-bit resolution, all bits in

the temperature register will contain valid data. For 11-bit resolution, bit 0 is undefined. For 10-bit resolution, bits 1 and 0 are undefined, and for 9-bit resolution bits 2, 1, and 0 are undefined. **Table 6.5** gives examples of digital output data and the corresponding temperature reading for 12-bit resolution conversions. [14]

Table 6.5: Output values of DS18B20

TEMPERATURE (°C)	DIGITAL OUTPUT (BINARY)	DIGITAL OUTPUT (HEX)
+125	0000 0111 1101 0000	07D0h
+85	0000 0101 0101 0000	0550h
+25.0625	0000 0001 1001 0001	0191h
+10.125	0000 0000 1010 0010	00A2h
+0.5	0000 0000 0000 1000	0008h
0	0000 0000 0000 0000	0000h
-0.5	1111 1111 1111 1000	FFF8h
-10.125	1111 1111 0101 1110	FF5Eh
-25.0625	1111 1110 0110 1111	FE6Fh
-55	1111 1100 1001 0000	FC90h

6.6 Inside pressure measurement

A very sensitive barometer is a part of the leak detection system. The barometer is an instrument used to measure atmospheric pressure. Since the probe is completely sealed, inside pressure equals to the atmospheric pressure. Significant increase of inside pressure during deep-water exploring can imply the internal system leakage.

6.6.1 MPXAZ6115A integrated silicon pressure sensor

MPXAZ6115A is media resistant and high temperature accuracy integrated silicon pressure sensor for measuring absolute pressure. The MPXAZ6115A series sensor integrates on-chip, bipolar op amp circuitry and thin film resistor networks to provide a high output signal and temperature compensation. The sensor's packaging has been designed to provide resistance to high humidity conditions as well as common automotive media.

The series piezoresistive transducer is a state-of-the-art, monolithic, signal conditioned, silicon pressure sensor. **Fig. 6.14a** shows a block diagram of the internal circuitry integrated on a pressure sensor chip. The sensor combines advanced micromachining techniques, thin film metallization, and bipolar semiconductor processing to provide an accurate, high level analog output signal that is proportional to applied pressure (**Fig. 6.14b**).

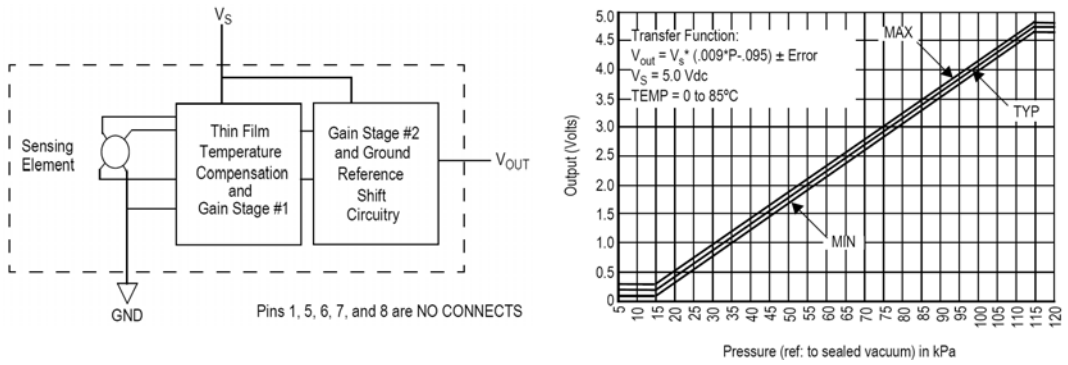

a) b)

Fig. 6.14: MPXAZ6115A a) block diagram, b) output versus absolute pressure [19]

Internal chip structure can be seen in **Fig. 6.15a**. A gel die coat isolates the die surface and wire bonds from the environment, while allowing the pressure signal to be transmitted to the sensor diaphragm. The gel die coat and durable polymer package provide a media resistant barrier that allows the sensor to operate reliably in high humidity conditions as well as environments containing common automotive media. Typical wiring is shown in **Fig. 6.15b**. [19]

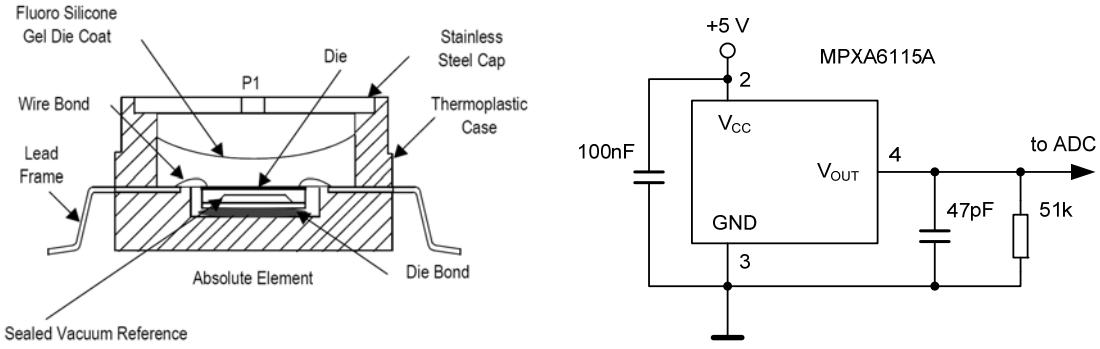

a) b)

Fig. 6.15: MPXAZ6115A a) internal structure, b) typical wiring [19]

6.7 NPI-15 high pressure sensor

Choosing a proper pressure sensor for the depth measurement was extremely important for the whole project. Since pressure sensor is exposed to the harsh environment, I had to select the sensor that fulfills my requirements. Solid state, high reliability, high sensitivity, linearity over the full scale range, thermal compensation and non-corroding casing were desired.

The NovaSensor® NPI-15 is current driven high pressure, media isolated pressure sensor designed to operate in hostile environments that has the outstanding sensitivity, linearity, and hysteresis of a silicon sensor. The piezoresistive sensor chip (**Fig. 6.16a**) is housed in a fluid-

filled cylindrical cavity and isolated from measured media by a stainless steel diaphragm and body. NPI-15 employs SenStable® processing technology, providing excellent stability. The modular design allows for a variety of pressure port modules which are hermetically welded to the sensor header module (**Fig. 6.16b**). For compensation of temperature effects, a complete resistor network is supplied on a hybrid ceramic substrate. The IsoSensor design minimizes temperature errors to provide maximum offset errors of 0.75 % full scale output (FSO) over the 0 to 70 °C compensated range. [17]

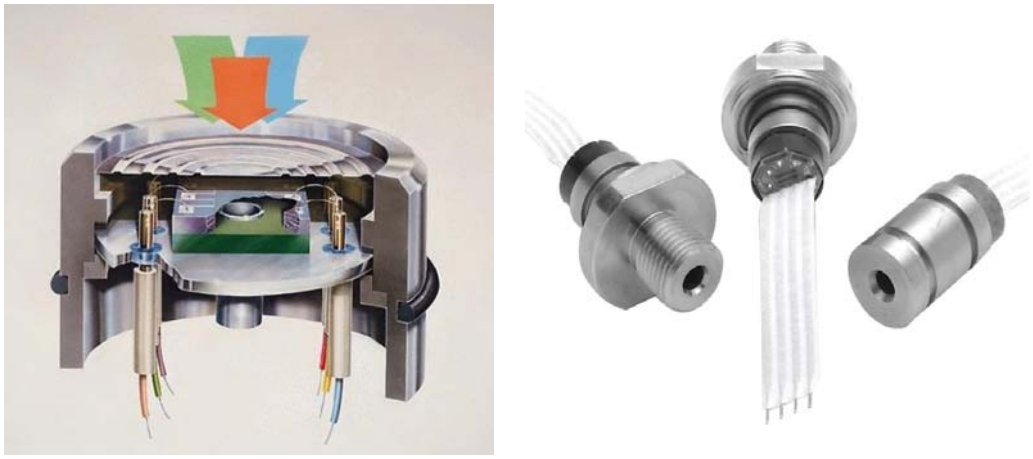

a) b)

Fig. 6.16: NPI-15: a) Piezoresistive sensor chip, b) Pressure port modules [17]

6.7.1 Signal conditioning

The NPI-15 sensor has 200 mV full scale output (FSO) with 1.0 mA excitation and therefore needs to be amplified before entering data acquisition system (AD converter on the MCU board). In order to amplify signal with minimum errors, I chose the three op amp instrumentation amplifier. The INA326 amplifier produced by Burr-Brown amplifies the differential input voltage and rejects the common mode input voltage. It is well-suited for use with Wheatstone bridge sensors integrated in the NPI-15 sensor (**Fig. 6.17a**). The INA326 is high-performance, low-cost, precision instrumentation amplifier with rail-to-rail input and output. It is the true single-supply instrumentation amplifier with very low DC errors and input common-mode ranges that extends beyond the positive and negative rails. Excellent long-term stability and very low 1/f noise assure low offset voltage (max 100 μV) and drift (max 0.4 μV/°C).

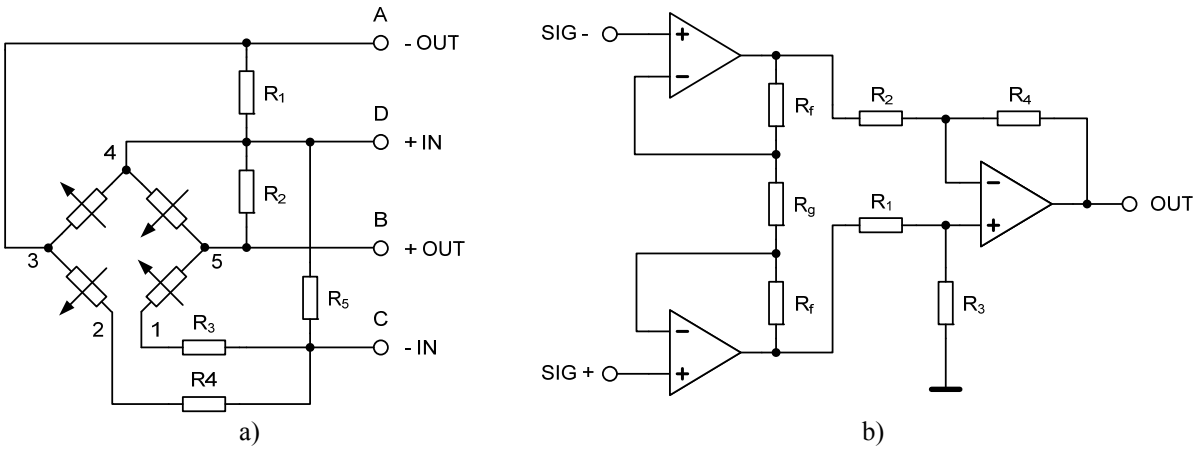

Fig. 6.17: a) NPI-15 Wheatstone bridge with the compensation, b) Three op amp instrumentation amplifier

Unlike single op amp differential amplifier, the three op amp instrumentation amplifier uses three op amps and therefore has high input impedance (**Fig. 6.17b**). The source impedance does not play a role in calculation of gain then. Total gain can be calculated using following equation:

$$V_{OUT} = [(Sig+)-(Sig-)]\cdot\left[\frac{R_4}{R_2}\left(\frac{2R_f}{R_g}+1\right)\right] \tag{4.4}$$

The NPI-15 sensor is driven by 1 mA high-side constant current source (**Fig. 6.18**). LM334 is 3-terminal adjustable current sources featuring 10 000:1 range in operating current and a wide dynamic voltage range of 1 V to 40 V. Current is established with one external resistor or trimmer. The simplest one external resistor connection, then, generates a current with approximate +0.33 %/°C temperature dependence. Zero drift operation is obtained by adding one extra resistor and a diode. This circuit balances the positive temperature coefficient (tempco) of the LM334 (about +0.23 mV/°C) with the negative tempco of a forward-biased silicon diode (about −2.5 mV/°C). [18]

A signal from the sensor is twelve times amplified and filtered. Output is connected (through the DATA connector) to the AD converter integrated in the MCU.

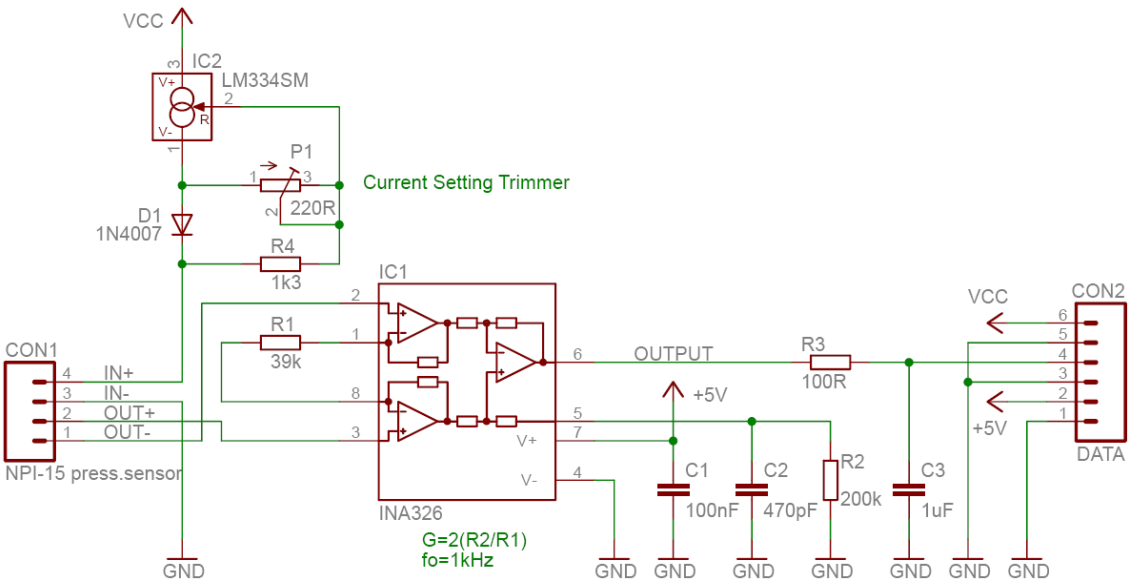

Fig. 6.18: Signal conditioning for NPI-15 pressure sensor

6.7.2 ACS714 Hall effect-based linear current sensor

The Allegro® ACS714 provides economical and precise solutions for AC or DC current sensing in automotive systems. The device consists of a precise, low-offset, linear Hall sensor circuit with a copper conduction path located near the surface of the die. Applied current flowing through this copper conduction path generates a magnetic field which is sensed by the integrated Hall IC and converted into a proportional voltage. Device accuracy is optimized through the close proximity of the magnetic signal to the Hall transducer. A precise, proportional voltage is provided by the low-offset, chopper-stabilized BiCMOS Hall IC, which is programmed for accuracy after packaging. The output of the device has a positive slope when an increasing current flows through the primary copper conduction path (from pins 1 and 2, to pins 3 and 4), which is the path used for current sensing. The internal resistance of this conductive path is 1.2 mΩ typical, providing low power losses. The thickness of the copper conductor allows survival of the device at up to five times overcurrent conditions. The terminals of the conductive path are electrically isolated from the sensor leads (pins 5 through 8). This allows the ACS714 current sensor to be used in applications requiring electrical isolation without the use of opto-isolators or other costly isolation techniques. ACS714 functional block diagram is in **Fig. 6.19**. [22]

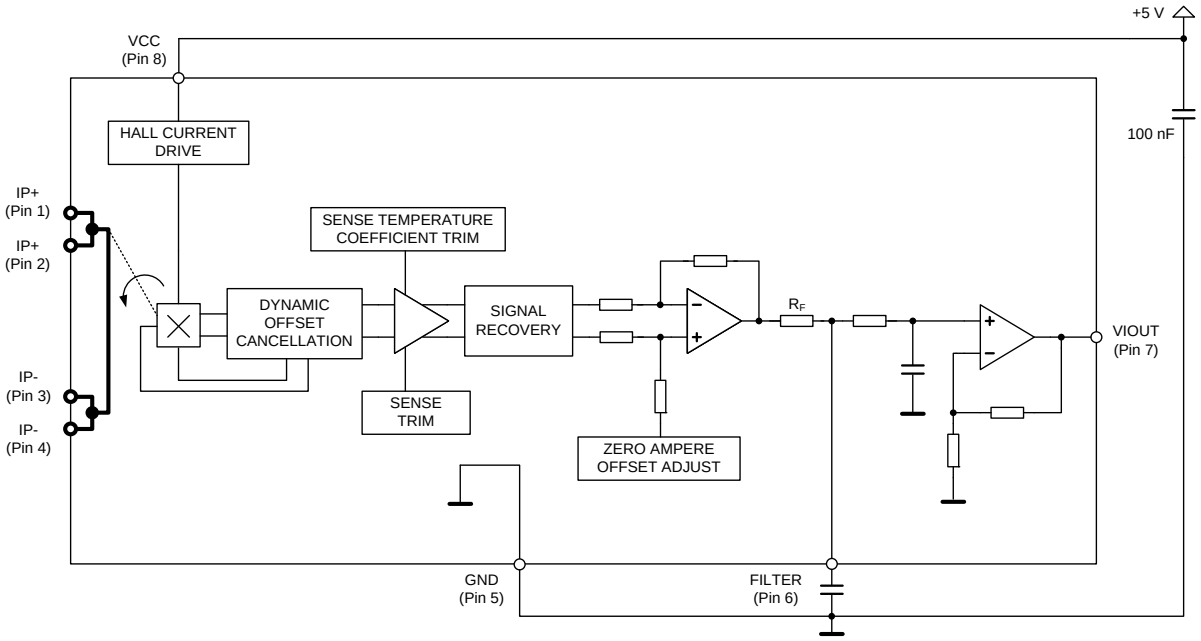

Fig. 6.19: ACS714 functional block diagram [22]

Since I have chosen ACS714-05 with typical sensitivity 168 mV/A, I have decided to amplify the output signal in order to obtain better current resolution with AD converter in MCU. To gain the signal three times, precision, CMOS input, rail-to-rail, wide supply range amplifier was used. Complete signal conditioning is shown in **Fig. 6.20**.

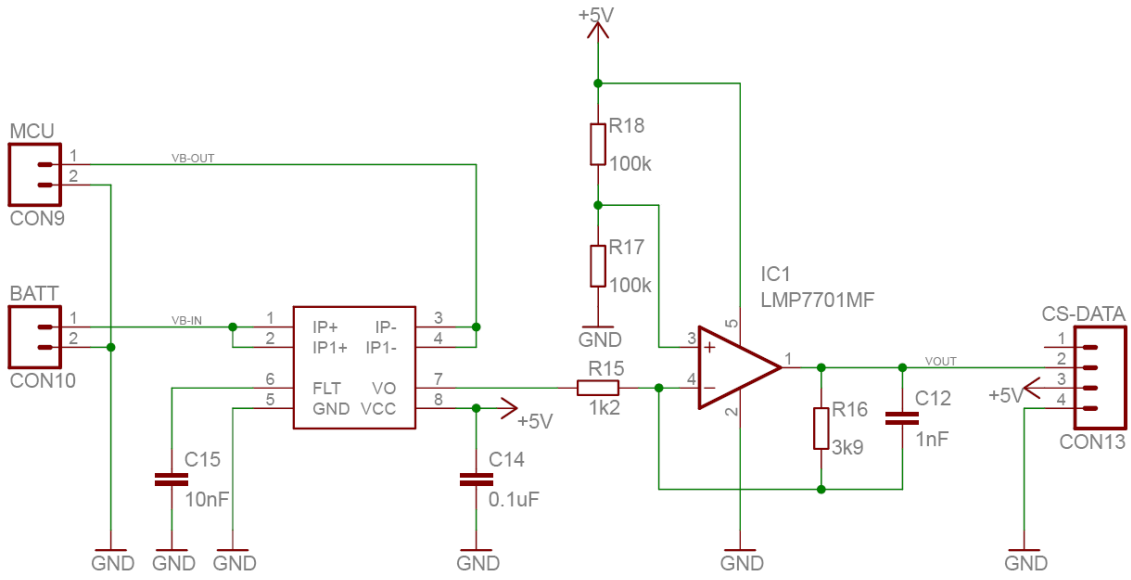

Fig. 6.20: Signal conditioning for ACS714 current sensor

7 Viewing system

Choosing a proper camera for my system was the key element and had to fulfill my requirements. I searched for the camera that supports a digital communication between the camera and the remote PC, a remote controlling and image recording and can work even in very low light conditions. The camera should also provide good quality pictures and video resolution and last but not least should be available for a reasonable price.

Finally, I chose Gembird® LAN-controlled IP camera, which is the best solution for a monitoring, that comes with MJPEG recording, motion detection, flash-card and night-vision support. An internal web server can be accessed any time by the remote PC. CAM77IP is capable of a direct connection to a local and a broadband network. Using Internet explorer such as IE, user can perform remote image surveillance and a management task, allowing an instant capture of the surveillance site. CAM77IP also combines the hardware-accelerated motion detection and the night-vision function [5].

Specification

- Resolution: 160 x 120, 320 x 240 and 640 x 480 pixels
- Image quality: Fine, Normal and Basic
- Stores captured image on PC or SD flash-card
- Supports HTTP, FTP, SMTP, static IP, DHCP, PPPoE, DDNS, NTP protocols
- Supply: input 5 V DC, 400 mA
- Dimensions of camera (L x W x H): 102 x 70 x 65 mm
- Net weight of camera: 168 g

7.1 Camera modification

Since I have bought the camera and since the camera is sold in the original plastic chassis I had to figure how to provide the required camera lens movement.

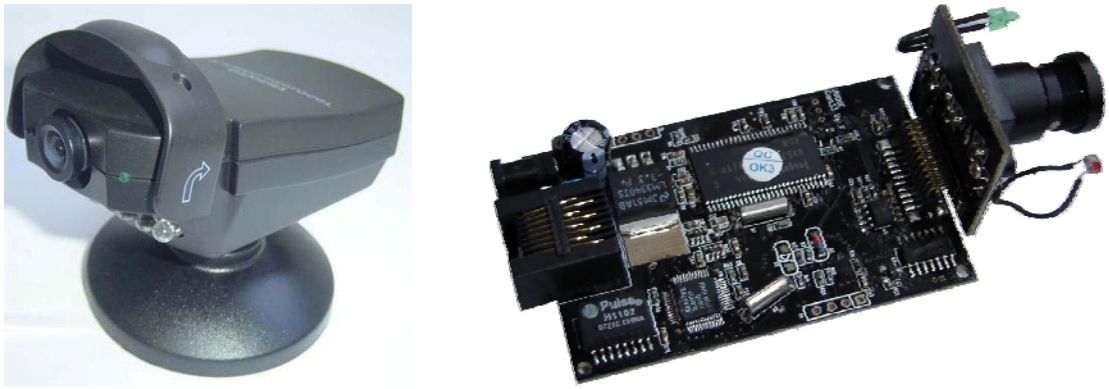

a) b)

Fig. 7.1: Camera modification: a) Original plastic chassis, b) Dismantle camera (without plastic covers)

The solution is to dismantle the camera (**Fig. 7.1a**) and to remove the original plastic chassis (**Fig. 7.1b**). The camera lens is connected to the camera electronic board via 2 x 12 pin connector with 1.27 mm pitch. I unplugged the camera lens but there was problem how to connect the loose camera lens with the camera electronic board. To solve this I ordered a special cable from Samtec production. The Samtec TFSD-15-30-H-09.84-T-NDX cable also needed modification, because there was straight version only and not the required crossed one. Also six unused wires were removed to provide lower cable tensile resistance. The complete solution is shown in **Fig. 7.2**.

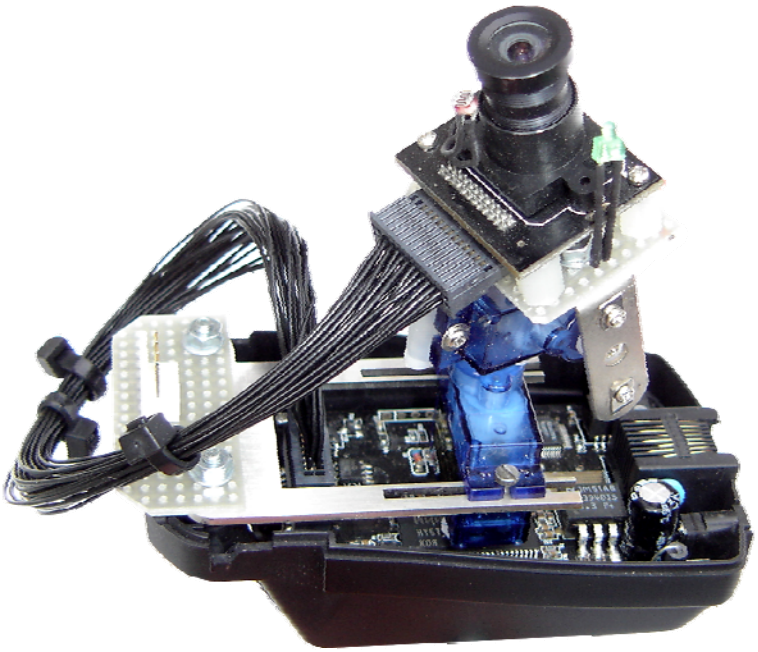

Fig. 7.2: Camera lens mounted on the servo mechanism and connected via modified Samtec cable

7.2 Servo system

The camera lens is mounted on two-axis servo mechanism which provides 200-degree rotation from left to right (horizontal plane) and 180-degree rotation in the vertical direction and allows the camera to view up, down, left or right through a bottom transparent cover. So the camera lens has two degrees of freedom. Two HXT900 servos made by Hextronik were used to build the desired servo mechanism. Each HXT900 weights only 9 g and with its dimensions (21 x 12 x 22 mm) is one of the smallest analog servo in the current production.

HXT900 is driven by a PWM signal from the microcontroller and is powered from the power-supply board.

8 Communication

There are two options how to connect the probe and the remote surface PC. The entire block scheme is shown in **Fig. 4.1** in **Chapter 4**.

8.1 Umbilical cable

If the cable length is kept below 100 meters (100baseTX Ethernet limit) than the cheapest standard UTP cat 5E cable could be used. In a harsh environment a durable armored metal cable or double-layered cable with a twisted pair is recommended. The main advantage of using metal cable is the lifespan and the mechanical resistance. In some cases, unused wires could be used as a back-up power-supply source.

Using optical cable, the probe is capable to transfer data up to 100 Mbit within 2 km distance (100baseFX limit). Therefore the probe is ready to be fitted with a high-resolution camera if necessary.

A special attention must be paid to the optical cable selection. The cable must be a tight buffered construction. A center Aramid strength member provides a higher tension resistance. An additional dielectric or metal armour or a second coating (double-layered cable) is necessary in a harsh environment. I have chosen two types available on the Czech market. The first type, an optical cable with supporting central dielectric fiber, is shown in **Fig. 8.1**. The second type, a dielectric armoured breakout cable, is in **Fig. 8.2**.

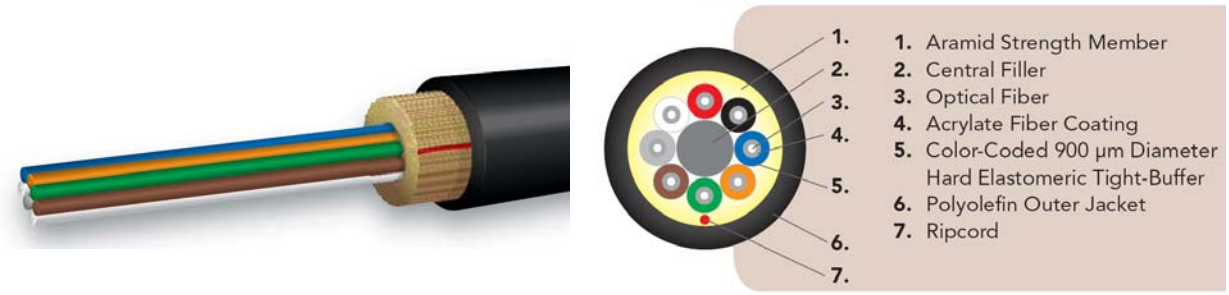

a) b)

Fig. 8.1: Optical cable with supporting central dielectric fiber: a) Overview, b) Internal structure description [29]

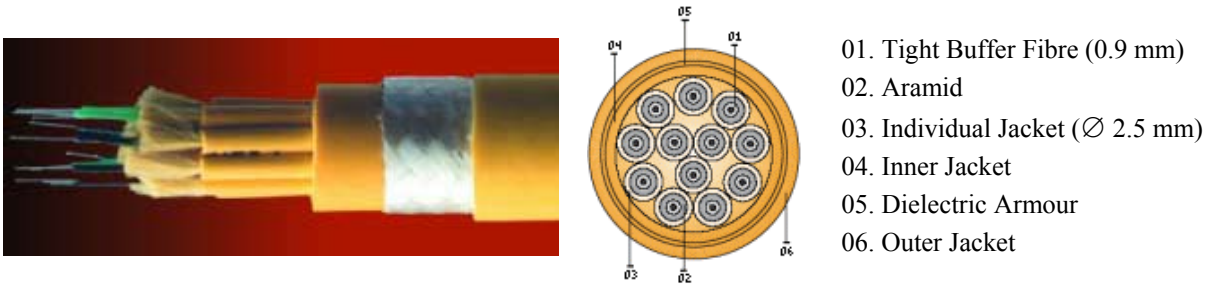

a) b)

Fig. 8.2: Dielectric armoured breakout cable: a) Overview, b) Internal structure description [30]

8.2 Terminal server

For RS232 signal conversion, the Lantronics XPort terminal server was used. The XPort is a complete solution packed into an RJ45 connector. This device server provides a 10BASE-T/100BASE-TX Ethernet connection. An operating system is stored in flash memory together with an embedded web server, a full TCP/IP protocol stack, and standards-based (AES) encryption. The XPort software runs on a DSTni-EX controller which has 256 kB of SRAM, 16 kB of boot ROM, and a MAC with integrated 10/100BASE-TX PHY. The XPort communicates to the edge device through a 3.3 V serial interface and three general-purpose programmable I/O pins. 512 kB of Flash memory is included for storing firmware and web pages. The XPort runs on 3.3 V, and has a built-in voltage supervisory circuit that will trigger a reset if the supply voltage drops to unreliable levels (2.7 V). A built-in 1.8 V regulator drives the processing core of the EX controller. An RJ45 Ethernet cable connects directly into an XPort. Ethernet magnetics, status LEDs, and shielding are built in (**Fig. 8.3**). [26]

The XPort is placed on the Terminal server board (PCB documentation is enclosed in the Appendix). The Terminal server board is connected with MCU board to provide RS232 to Ethernet conversion.

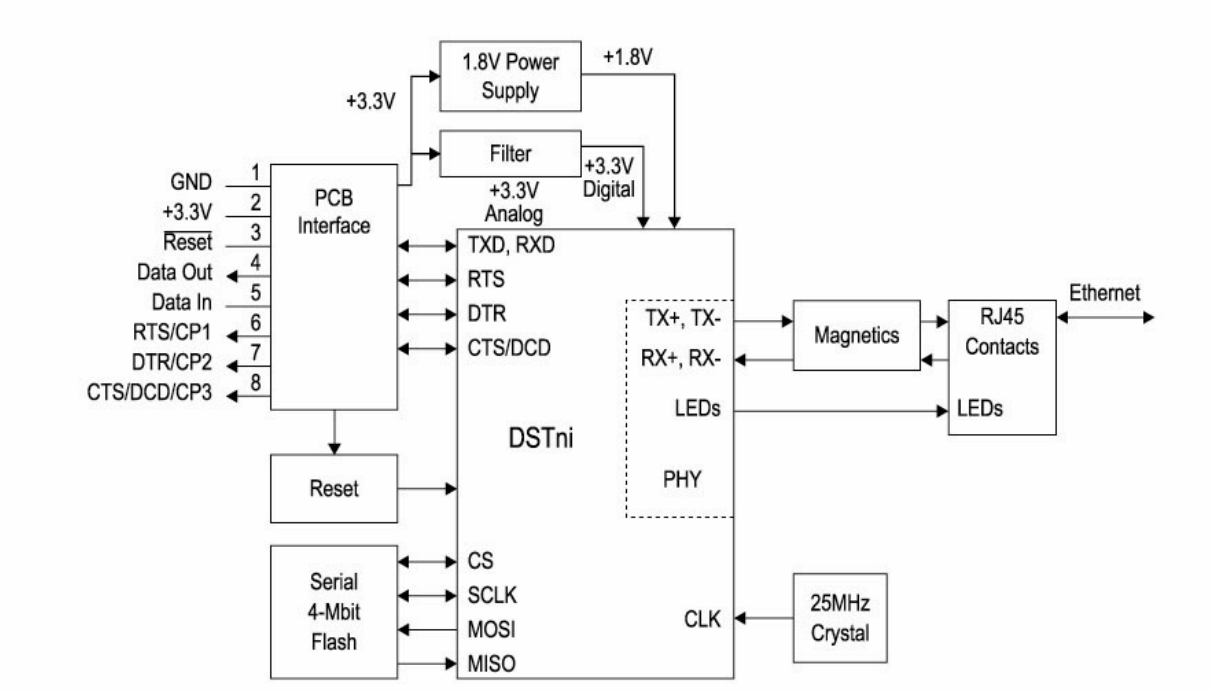

Fig. 8.3: XPort internal block diagram [26]

8.3 Switch

An on-board Ethernet switch gathers output signals from the XPort terminal server and from the IP camera and sends data to the TP-LINK MC100C media converter. For that purposes, 5-port AirLive Live FSH5PS mini Ethernet switch was used. A plastic switch case

was removed to reduce size. The two remaining unused ports allow connection of more than one IP camera (up to three cameras).

8.4 Media converter

The MC100CM is a media converter designed to convert 100BASE-FX fiber to 100Base-TX copper media or vice versa. The MC100CM uses multi-mode fiber cable utilizing the SC-Type connector. The MC100CM supports shortwave (SX) laser specification at a full wire speed forwarding rate. It works at 1310 nm on both transmitting and receiving data.

Other features of this module include Auto MDI/MDI-X for TX port, Auto negotiation of duplex mode on TX port and front panel status LEDs. The MC100CM transmits at extended fiber optic distances utilizing multi-mode fiber up to 2 kilometers. [27]

9 High-power LED module

The probe can be equipped with two external 5-watt high-power LED modules mounted on the probe chassis. Modules are easily replaceable in the field. Each light is individually controlled and the light intensity is adjustable from the surface PC. The high-power LED module uses 5W LED Luxeon K2 distributed by Philips. Luxeon K2 from Lumileds Lighting production is driven by LT3474 drive from Linear Technology production.

9.1 5W LED Luxeon K2

Using high-power LED helps increase power efficiency. The main advantage of LEDs is their facile luminous flux control possibility. Unlike high intensity discharge (HID) bulbs, LEDs output power can be driven with a current. The 5W LED Luxeon (type K2LXK2-PWW4-U00) provides 130 lm (Luminous Flux) at 1500 mA. A high operating temperature (185 °C) and a low thermal resistance (9 °C/W) reduce heat sink area requirements. The Luxeon K2 internal structure is shown in **Fig. 9.1a**. The forward current vs. forward voltage characteristic can be seen in **Fig. 9.1b**.

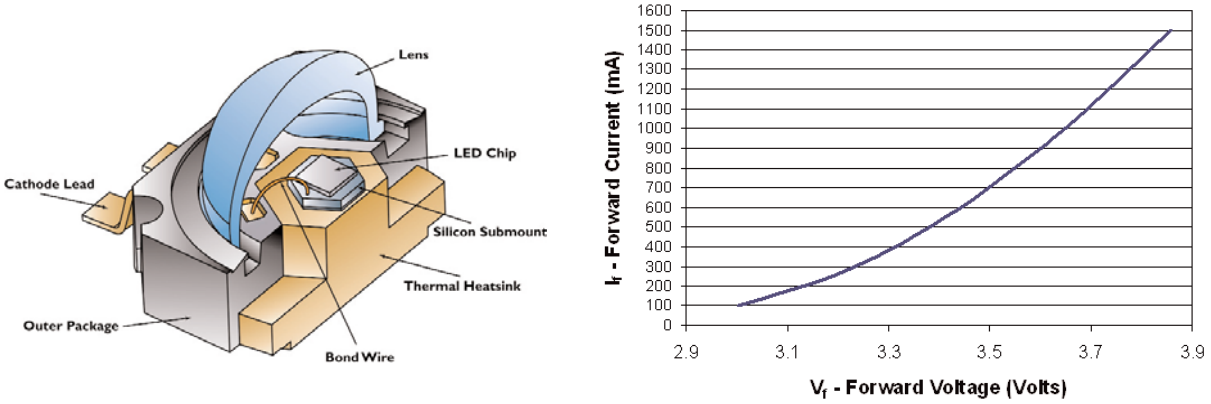

a) b)

Fig. 9.1: Luxeon K2: a) Internal structure, b) Forward current vs. forward voltage [31]

9.2 LED driver

The LT3474 is a fixed frequency step-down DC/DC converter designed to operate as constant-current source. An internal sense resistor monitors the output current allowing accurate current regulation. High output current accuracy is maintained over a wide current range, from 35 mA to 1 A, allowing a wide dimming range. PWM circuitry allows a dimming range of 400:1, avoiding the color shift normally associated with LED current dimming. The high switching frequency offers several advantages, permitting the use of small inductors and ceramic capacitors. The constant switching frequency combined with low-impedance ceramic capacitors result in a low, predictable output ripple. Frequency foldback and thermal shutdown provide additional protection. [32]

10 Power-supply system

A power-supply system is carefully designed to provide the maximal battery efficiency. Using DC-DC modules helps reduce power losses. The power-supply board contains two DC-DC modules set to 5 V, one DC-DC module set to 3,3 V, a LDO adjustable regulator, a switched battery charger with a high efficiency and a hall-based sensor for a current sensing. Each device can be switched off to save the battery energy. This feature contributes to longer operating time. The power-supply board is controlled by MCU.

10.1 DC-DC module

The best and the cheapest solution for the probe are PTN78000W plug-in power modules made by Texas Instruments. The PTN78000 is a series of high-efficiency, step-down Integrated Switching Regulators (ISR) that represent the third generation in the evolution of the popular 78ST100 series of products. The PTN78000 has improved electrical performance characteristics and the case-less, double-sided package also exhibits improved thermal characteristics. Operating from a wide-input voltage range, the PTN78000 provides high-efficiency, step-down voltage conversion for loads of up to 1.5 A. The output voltage is set using a single external resistor. The PTN78000W may be set to any value within the range, 2.5 V to 12.6 V. The output voltage of the PTN78000W can be as little as 2 V lower than the input, allowing operation down to 7 V, with an output voltage of 5 V. The PTN78000 has undervoltage lockout and an integral on/off inhibit. Additional features are described below.

Undervoltage Lockout

The undervoltage lockout (UVLO) circuit prevents the module from attempting to power up until the input voltage is above the UVLO threshold. This prevents the module from drawing excessive current from the input source at power up. Below the UVLO threshold, the module is held off.

Current Limit Protection

The PTN78000 modules protect against load faults with a continuous current limit characteristic. Under a load fault condition, the output current cannot exceed the current limit value. Attempting to draw current that exceeds the current limit value causes the module to progressively reduce its output voltage. Current is continuously supplied to the fault until it is removed. On removal of the fault, the output voltage promptly recovers. When limiting output current, the regulator experiences higher power dissipation, which increases its temperature. If the temperature increase is excessive, the module's overtemperature protection begins to periodically turn the output voltage completely off.

Overtemperature Protection

A thermal shutdown mechanism protects the module's internal circuitry against excessively high temperatures. A rise in temperature may be the result of a drop in airflow, a high ambient temperature, or a sustained current-limit condition. If the junction temperature of the internal control IC rises excessively, the module turns off, reducing the output voltage to zero. The module instantly restarts when the sensed temperature decreases by a few degrees. [28]

Efficiency and output voltage ripple characteristics can be seen in **Fig. 10.1**

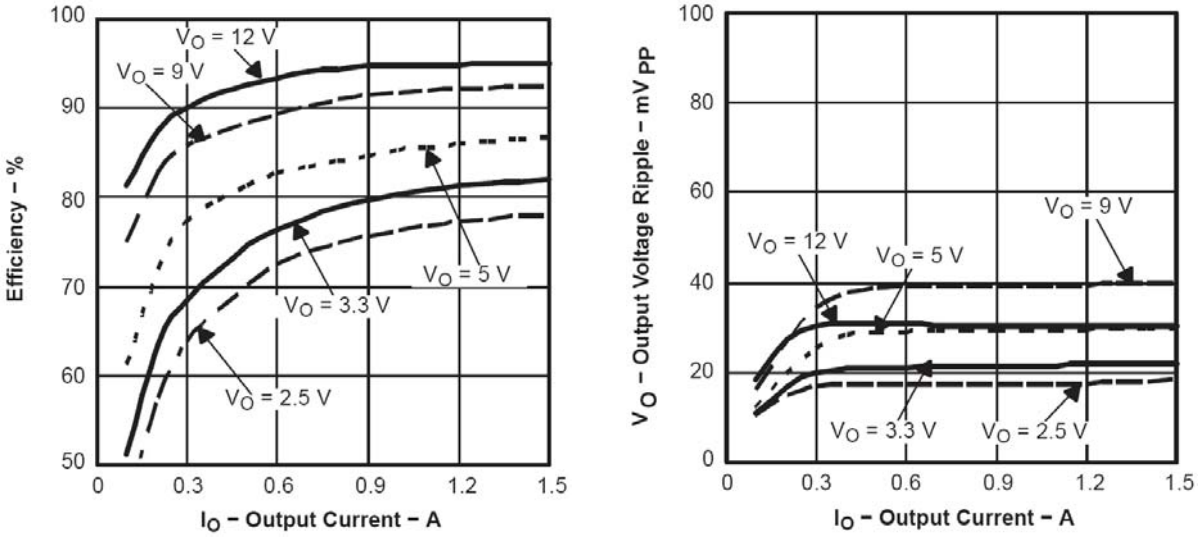

Fig. 10.1: PTN78000W: a) Efficiency vs. output current, b) Output voltage ripple vs. current (15V input) [28]

10.2 Low dropout regulator

An adjustable low dropout voltage regulator is designed as an additional power-supply reserved for the future electronic probe systems. The LT1763 regulator made by Linear Technology is chosen in the current probe design. The LT1763 is the micropower, low noise, low dropout (LDO) regulator capable of supplying 500 mA of output current with a dropout voltage of 300 mV. The low 30 μA quiescent current makes LT1763 an ideal choice in battery-powered systems. A key feature of the LT1763 regulators is low output noise. With the addition of an external 0.01 μF bypass capacitor, the output noise drops to 20 μVRMS over a 10 Hz to 100 kHz bandwidth. Therefore, LDO could be used as a low-noise power-supply for additional sensors. An internal protection circuitry includes a reverse battery protection, a current limiting, a thermal limiting and a reverse current protection.

LDO output is adjusted to 7 V using resistor network with a 1.22 V reference voltage. The output can be set from 1.22 V to 20 V.

10.3 Sealed lead-acid battery charger

A 12 V sealed lead-acid (SLA) battery is used to power the whole probe. Together with 5 Ah battery capacity, the probe is capable to work at least 5 hours with all systems switched on. I order to achieve the highest possible efficiency, switching charger regulator is used. I have chosen the LT1513 device produced by Linear Technology that could be used for charging all sort of batteries (Li-Ion, SLA, Ni-Mh, Li-Pol).

The LT1513 is a 500 kHz current mode switching regulator specially configured to create a constant- or programmable-current/constant-voltage battery charger. In addition to the usual voltage feedback node, it has a current sense feedback circuit for accurately controlling output current of a flyback or SEPIC (Single-Ended Primary Inductance Converter) topology charger. These topologies allow the current sense circuit to be ground referred and completely separated from the battery itself, simplifying battery switching and system grounding problems. In addition, these topologies allow charging even when the input voltage is lower than the battery voltage. Maximum switch current on the LT1513 is 3 A. This allows battery charging currents up to 2 A for a single lithium-ion cell. Charging current can be easily programmed for all battery types.

The charge algorithm for lead-acid batteries is similar to lithium-ion but differs from nickel-based chemistries in that voltage rather than current limiting is used. The charge time of a sealed lead-acid battery is 12-16 hours. With higher charge currents and multi-stage charge methods, the charge time can be reduced to 10 hours or less. Lead-acid cannot be fully charged as quickly as nickel or lithium-based systems.

Concerning all of the factors mentioned above, I have set the battery charging voltage to 14.28 V which is 2.38 V per cell. The charging current is limited to 550 mA. I performed a brief test measurement during battery charging in order to obtain a battery charging profile (**Table 6.2**). The performance graphs are shown in **Fig. 10.2** and **Fig. 10.3**.

Table 10.1: Battery charging profile

Time [min]	Battery voltage [V]	Charging current [mA]	Note
0	12.60	550	Start of charging process
5	12.85	540	
28	13.06	528	
73	13.15	481	
118	13.30	480	
163	13.49	480	
203	13.70	470	90% of full charge capacity
228	14.28	368	
273	14.29	277	
360	14.32	4	Maintenance current

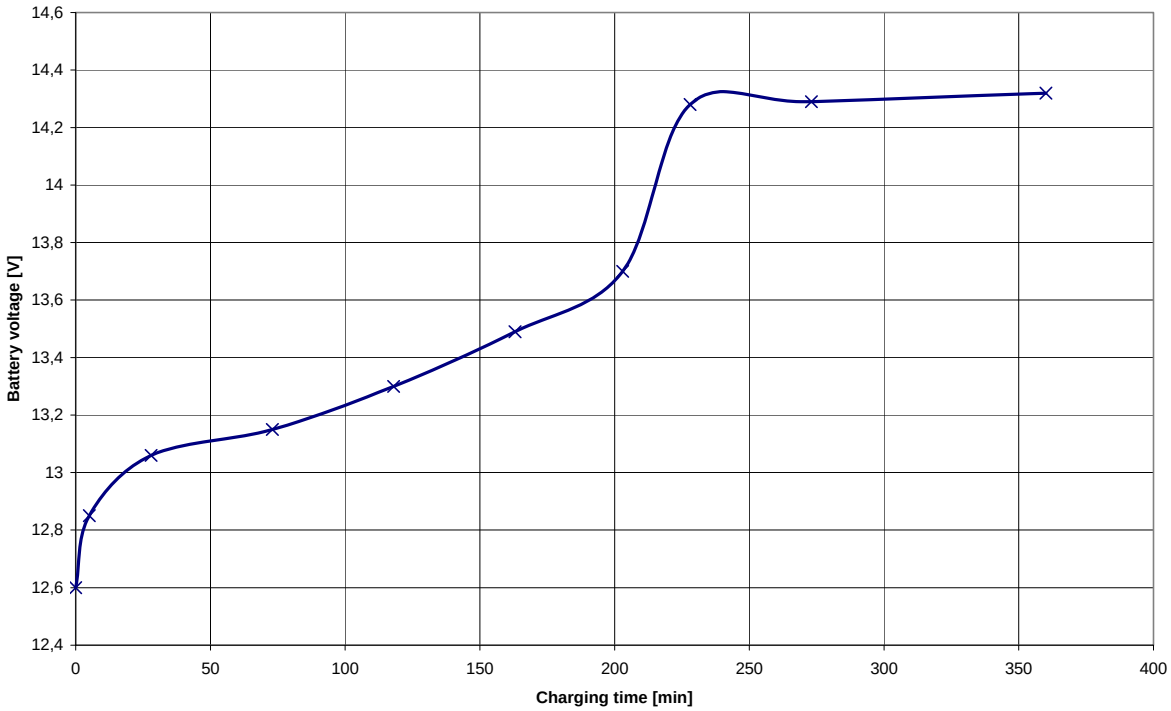

Fig. 10.2: Battery charging profile: Battery voltage vs. charging time

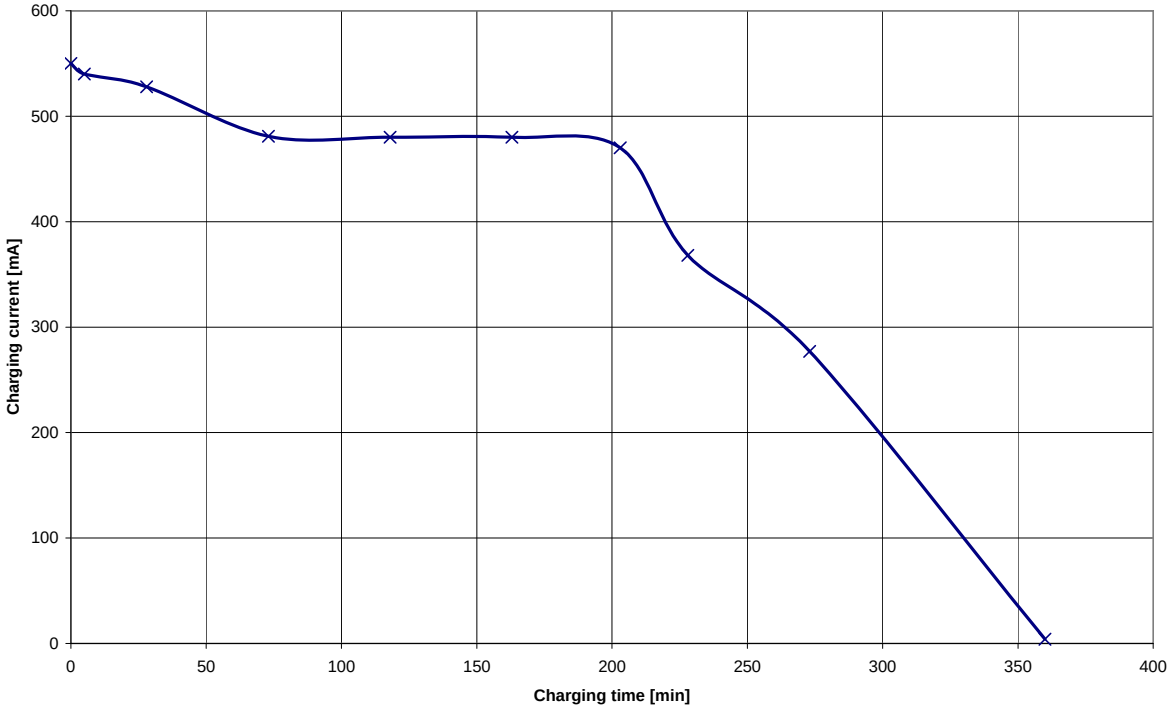

Fig. 10.3: Battery charging profile: Charging current vs. charging time

11 Software solution

As for software, both MCU and PC interface had to be programmed. A PC interface software provides all probe system function controlling and telemetry data displaying.

For MCU programming, AVR Studio 4.16 together with AVR Wizard was used. AVR Wizard enables fast programming using C language rather than assembler. Standard libraries and routines for communication with external devices via SPI and I^2C are used. USART communication speed is set to 19200 bauds.

For PC control software programming, Borland C++ Builder 6.0 was used. Deep-water probe control interface can be seen in **Fig. 11.1**.

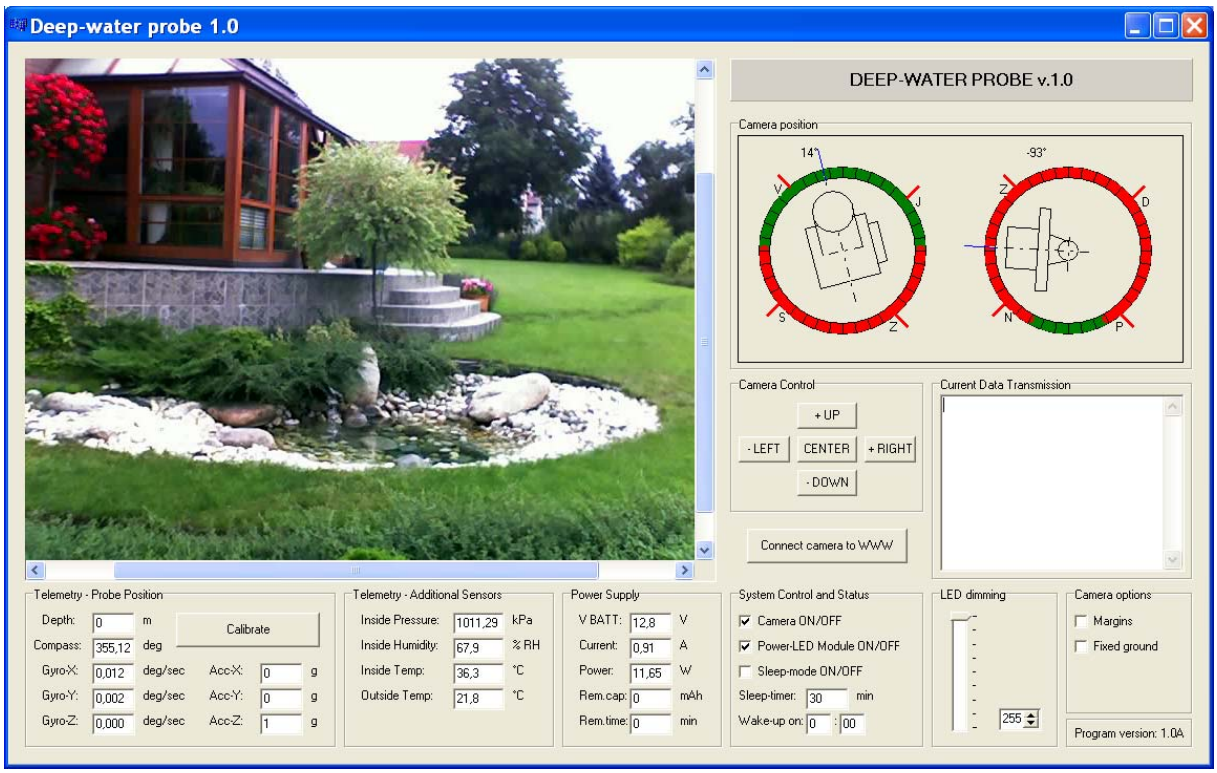

Fig. 11.1: Deep-water probe control interface

In order to be familiar with each control component, I have described deep-water probe control interface.

11.1 Camera interface

Camera screen – The video data is displayed in the top-left window corner. Use '*Connect camera to the WWW*' button to connect to the IP camera internal webserver.

Camera control – The camera lens mounted on the camera servo mechanism can be controlled either using keyboard arrows or clicking on the buttons.

Camera position – A vector graphic is used to draw the current camera lens position. The angle is counted as a difference between the electronic compass heading course and the camera servo position.

11.2 Camera options

Margins – Servo mechanism margins can be set to define minimal and maximal possible camera lens position limits.

Fixed ground – A fixed ground option is reserved for the future use with inertial navigation system.

11.3 System control and status

V BATT – The battery voltage. A typical battery voltage ranges from 12 V to 14.4 V.

Current – The total current that is drained from the battery. The current sensor is bi-directional which means that a user can see a battery charging current also.

Power – The total power drained from the battery (V BATT multiplied by Current).

Rem.cap. – The estimated remaining battery capacity (The initial capacity is 5000 mAh).

Rem.time – The estimated remaining capacity derived from the current and the remaining capacity.

Camera ON/OFF – The camera and the servo mechanism can be switched off to save the energy.

Power LED module ON/OFF – The additional lighting can be switched on.

Sleep mode ON/OFF – This feature is implemented to provide the maximum battery energy saving.

LED dimming – The LED output power can be controlled with a slider that represents PWM signal.

11.4 Telemetry data – probe position

Depth – The data from the high-pressure sensor interprets a real depth.

Compass – The electronic compass informs user about a heading position.

Gyro X, Y, Z – The gyroscopic data gives information about probe rotations and can be used to correct the electronic compass data.

Acc X, Y, Z – The data from the 3-axis accelerometer provide two types of information. In a static mode (the probe is still and without moving), values represent a till of the probe. In a dynamic mode (the probe is in an ascent or descent phase and is going up or down), values represent an acceleration of the probe.

11.5 Telemetry data – additional sensors

Inside pressure – The inside pressure sensor can show possible internal leak. A typical inside pressure value is about 101 kPa. A rapid increase in pressure can signal possible system leaks.

Inside humidity – The inside humidity monitoring provides an on-board RH humidity measurement. Since the whole probe is completely sealed, a rapid increase in humidity signals system leaks. If the humidity value is over 95 %, the MCU board can shutdown all electronic systems in the probe in order to protect very expensive electronics to be destroyed by mineral water.

Inside temp – The inside temperature is read from a very precise humidity sensor.

Outside temp – The outside temperature is read from a sensor placed in the sensor dome on the top of the probe

12 Conclusion

In this diploma thesis, I focused on submersible probes and deep-water devices. The main purpose of this diploma thesis was to show whether it is possible to build an operating deep-water probe that has also practical uses and has a reasonable price.

Firstly, an electrical design of a deep-water probe capable of diving into depth over 200 meters was done. I proposed an entire functional and block diagram of the device. Each part of the probe is described in detail, its principle and function are also thoroughly explained.

Secondly, I created printed circuit board (PCB) layouts for the microcontroller unit board, the sensor board, the power-supply board, the power LED module and for supporting electronic systems. Each PCB was made, assembled and tested electrically.

Thirdly, I had to modify an on-board camera and mount the camera lens on top of the two-axis servo mechanism. The whole probe electronic system parts were put together, fixed to the internal probe self-supporting structure and fit into the custom-made chassis that I also designed and built. The probe chassis is designed to sustain pressure of up to 350 m (35 bars) using appropriate materials. The entire technical documentations and drawings are enclosed in Appendix (Chapter 15).

Finally, the MCU was programmed and I have made a program for communication between the probe and the surface PC. The program is able to display acquired data on the surface PC screen. Video signals and telemetry data can be recorded for further scientific analysis.

Considering the manufacturing costs, we are getting the state-of-art probe that has many innovations like the optical high-density data transmission and the digital camera. Together with the external additional systems, this probe is one of the best in its class.

Special attention is paid to an optical cable selection. I put stress on a cable quality and mechanical resistance. The optical cable with these parameters needed to be ordered as a custom-made cable and that takes time. Therefore, the whole probe has not been tested in the application area. Nevertheless, the probe chassis has been already tested in the high-pressure chamber under pressure of 3500 kPa (35 bars) and everything went fine without any leaks.

In the future, I would like to add external thrusters to provide three-dimensional probe movement capability. I have already designed an improved chassis that enables to use at least two high-resolution cameras placed in the spherical transparent dome and it will still be using the current electrical systems that I have built and described in this thesis. Additional cost reduction is also intended.

13 References

[1] CHRIST, Robert D., WERNLI, Robert L. *The ROV Manual : A User Guide for Observation Class Remotely Operated Vehicles*. [v.l.] : Butterworth-Heinemann Ltd , 2007. 320 p. ISBN 978-0750681483.

[2] Electronic Compass Design. *Application notes for KMZ51 and KMZ52.* [cit. 2009-01-11]. Available on WWW: www.nxp.com/acrobat_download/applicationnotes/AN00022_COMPASS.pdf

[3] HMC1052 - High performance magnetoresistive sensor. *1, 2 and 3 Axis Magnetic Sensors HMC1051/HMC1052/HMC1053 datasheet.* [cit. 2009-01-11]. Available on WWW: www.nxp.com/acrobat_download/applicationnotes/AN00022_COMPASS.pdf

[4] Gembird® LAN-controlled IP camera. *CAM77IP datasheet.* [cit. 2009-02-08]. Available on WWW: http://www.gmb.nl/eGMB/repository/4261/CAM77IP_manual---2dae6ce8-9c3c-41f2-9376-0c2544a031b1.pdf

[5] Practical guide to Accelerometers. *SENSR accelerometers overview.* [cit. 2009-03-01]. Available on WWW: http://www.sensr.com/pdf/practical-guide-to-accelerometers.pdf

[6] MMA7455L - Three Axis Low-g Accelerometer. *MMA7455L Freescale datasheet.* [cit. 2009-03-01]. Available on WWW: http://www.freescale.com/files/sensors/doc/data_sheet/MMA7455L.pdf?fpsp=1

[7] MEMS Gyroscopes and Their Applications. *A study of the advancements in the form, function, and use of MEMS gyroscopes.* [cit. 2009-04-25]. Available on WWW: http://clifton.mech.northwestern.edu/~me381/project/done/Gyroscope.pdf

[8] Steven Nasiri. *A Critical Review of MEMS Gyroscopes Technology and Commercialization Status* [cit. 2009-04-25]. Available on WWW: http://www.rgrace.com/Conferences/AnaheimExtra/paper/nasiri.doc

[9] David Krakauer, Analog Devices Inc. *A Unique Angular-Rate-Sensing Gyro* [cit. 2009-04-25]. Available on WWW: http://archives.sensorsmag.com/articles/0903/53/main.shtml

[10] ADIS16255 – Programmable Low Power Gyroscope. *ADIS16255 Analog Devices Datasheet.* [cit. 2009-04-25]. Available on WWW: http://www.analog.com/static/imported-files/data_sheets/ADIS16250_16255.pdf

[11] Denes K. Roveti. *Choosing a Humidity Sensor: A Review of Three Technologies* [cit. 2009-04-28]. Available on WWW: http://www.sensorsmag.com/sensors/Technology+Tutorials%2FSensors%2FHumidity%2FMoisture/Choosing-a-Humidity-Sensor-A-Review-of-Three-Techn/ArticleStandard/Article/detail/322590

[12] SHT75 – Humidity and Temperature Sensor. *SHT75 Sensirion Datasheet.* [cit. 2009-04-25]. Available on WWW: http://www.sensirion.ch/en/pdf/product_information/Datasheet-humidity-sensor-SHT7x.pdf

[13] DS18B20 – Programmable Resolution 1-Wire Digital Thermometer. *DS18B20 Maxim Dallas Semiconductor Datasheet.*
[cit. 2009-04-25]. Available on WWW:
http://datasheets.maxim-ic.com/en/ds/DS18B20.pdf

[14] David Heeley. *Understanding Pressure and Pressure Measurement*
[cit. 2009-04-28]. Available on WWW:
http://www.freescale.com/files/sensors/doc/app_note/AN1573.pdf

[15] Robert E. Bicking. *Fundamentals of Pressure Sensor Technology*
[cit. 2009-04-28]. Available on WWW:
http://www.sensorsmag.com/articles/1198/fun1198/main.shtml

[16] NPI-15 Series Current Driven High Pressure, Media Isolated Pressure Sensor. *GE NovaSensorDatasheet.*
[cit. 2009-04-28]. Available on WWW:
http://www.gesensing.com/products/resources/datasheets/NPI_15_04_03c.pdf

[17] LM334 – 3-Terminal Adjustable Current Sources. *National Semiconductor Datasheet.*
[cit. 2009-04-25]. Available on WWW:
http://www.national.com/pf/LM/LM334.html

[18] MPXAZ6115A integrated silicon pressure sensor. *Freescale Datasheet.*
[cit. 2009-04-25]. Available on WWW:
http://www.freescale.com/files/sensors/doc/data_sheet/MPXAZ6115A.pdf

[19] Low side and high side current sensing. *Texas Instruments Current Sensing Application Notes.*
[cit. 2009-04-25]. Available on WWW:
http://focus.ti.com/analog/docs/microsite.tsp?sectionId=560&tabId=2180&micrositeId=7

[20] Richard Dickinson. *Isolated Open Loop Current Sensing Using Hall Effect Technology in an Optimized Magnetic Circuit.*
[cit. 2009-04-25]. Available on WWW:
http://www.allegromicro.com/en/Products/Design/current_sensing/bsp_v1_52.pdf

[21] Richard Dickinson. *Isolated Open Loop Current Sensing Using Hall Effect Technology in an Optimized Magnetic Circuit.*
[cit. 2009-04-25]. Available on WWW:
www.allegromicro.com/en/Products/Part_Numbers/0714/0714.pdf

[22] Atmel ATmega128 – 8-bit AVR microcontroller. *Atmel ATmega128 Datasheet.*
[cit. 2009-04-25]. Available on WWW:
http://www.atmel.com/atmel/acrobat/doc2467.pdf

[23] 1 Mbit SPI Bus Serial EEPROM. *Microchip Technology Inc. 25AA1024 Datasheet.*
[cit. 2009-04-25]. Available on WWW:
http://ww1.microchip.com/downloads/en/DeviceDoc/21836F.pdf

[24] DS1307 - Serial I^2C Real-Time Clock. *DS1307 Maxim Dallas Semiconductor Datasheet.*
[cit. 2009-04-25]. Available on WWW:
http://www.atmel.com/atmel/acrobat/doc2467.pdf

[25] XPort - Embedded Ethernet Device Server. *Lantronics XPort Datasheet.*
[cit. 2009-04-25]. Available on WWW:
http://www.lantronix.com/device-networking/embedded-device-servers/xport.html

[26] MC100CM – Media converter. *TP-link MC100CM Datasheet.* [cit. 2009-04-25]. Available on WWW: http://www.tp-link.com/products/product_des.asp?id=117

[27] PTN78000W – Plug-in Power Module. *PTN78000W Texas Instruments Datasheet.* [cit. 2009-04-25]. Available on WWW: http://www.ti.com/lit/gpn/ptn78000w

[28] RM optical cable. *Datasheet.* [cit. 2009-04-25]. Available on WWW: http://www.occfiber.com/media/library_documents/1236713834_4c_OCC-FOC_Outdoor.pdf

[29] CDAD – Optical cable. *Optral Datasheet.* [cit. 2009-04-25]. Available on WWW: http://www.optral.es/ficheros/catalogo/pdf/ETW55001i.pdf

[30] Luxeon K2. *Lumileds – Philips Datasheet.* [cit. 2009-04-25]. Available on WWW: http://www.philipslumileds.com/pdfs/DS51.pdf

[31] LT3474 – Led Driver. *Linear Lechnology Datasheet.* [cit. 2009-04-25]. Available on WWW: http://cds.linear.com/docs/Datasheet/3474fd.pdf

[32] ROBERTS, Geoff. *Guidance and Control of Underwater Vehicles 2003*. [v.l.] : Pergamon, 2003. 256 p. 4. ISBN 978-0080442020.

[33] GRIFFITHS, Gwyn. *Technology and Applications of Autonomous Underwater Vehicles*. [v.l.] : CRC Press, 2002. 368 p. 1. ISBN 978-0415301541.

[34] BRÄUNL, Thomas. *Embedded Robotics: Mobile Robot Design and Applications with Embedded Systems*. 2nd edition. [v.l.] : Springer, 2006. 458 p. ISBN 978-3540343189.

[35] ROBERTS, Geoff. *Advances in Unmanned Marine Vehicles*. [v.l.] : Institution of Engineering and Technology, 2005. 441 p. ISBN 978-0863414503.

[36] SEDRA, Adel S., SMITH, K. C. *Microelectronic Circuits*. 5th edition. USA : Oxford University Press, 2004. 1392 p. 5. ISBN 978-0195142518.

14 List of abbreviations

ADC	Analog-to-digital conversion
ASIC	Application-specific integrated circuit
CRC	Cyclic redundancy check
DAC	Digital-to-analog conversion
EMC	Electromagnetic compatibility
GPS	Global positioning system
I2C	Inter-integrated circuit
IC	Integrated circuit
IMU	Inertial measurement unit
LDO	Low-dropout linear regulator
LSB	Least significant bit
MC	Magnetic compass
MCU	Microcontroller unit
MEMS	Microelectromechanical systems
MR	Magnetoresistive
MSB	Most significant bit
PCB	Printed circuit board
RF	Radio frequency
RH	Relative humidity
ROV	Remotely operated vehicle
RTC	Real time clock
SPI	Serial peripheral interface
UTP	Unshielded twisted pair

15 Appendix

List of appendices:

i. MCU board – PCB top layer (150 % scale)

ii. MCU board – PCB bottom layer (150 % scale)

iii. MCU board – Parts layout in top layer (150 % scale)

iv. MCU board – Parts layout in bottom layer (150 % scale)

v. Sensor board – PCB top layer (140 % scale)

vi. Sensor board – PCB top layer (140 % scale)

vii. Sensor board – Parts layout in top layer (140 % scale)

viii. Power-supply board – PCB top layer (150 % scale)

ix. Power-supply board – PCB bottom layer (150 % scale)

x. Power-supply board – Parts layout in top layer (150 % scale)

xi. Power-supply board – Parts layout in bottom layer (150 % scale)

xii. Power LED module – PCB top layer (200 % scale)

xiii. Power LED module – PCB bottom layer (200 % scale)

xiv. Power LED module – Parts layout in top layer (200 % scale)

xv. Terminal server board – PCB top layer (200 % scale)

xvi. Terminal server board – Parts layout in bottom layer (200 % scale)

xvii. MCU board – electrical diagram

xviii. Sensor board – electrical diagram

xix. Power-supply board – electrical diagram

xx. Power LED module – electrical diagram

xxi. Terminal server – electrical diagram

xxii. Mechanical design – top panel

xxiii. Mechanical design – bottom panel

xxiv. Mechanical design – battery distance-column

xxv. Mechanical design – probe lug

xxvi. Mechanical design – camera holder

i. MCU board – PCB top layer (150 % scale)

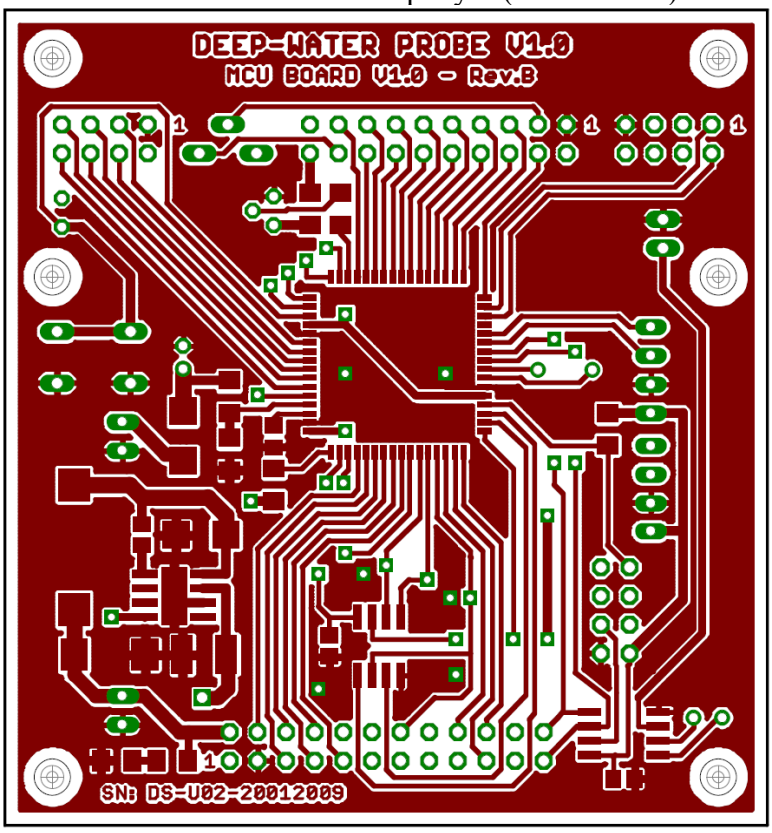

ii. MCU board – PCB bottom layer (150 % scale)

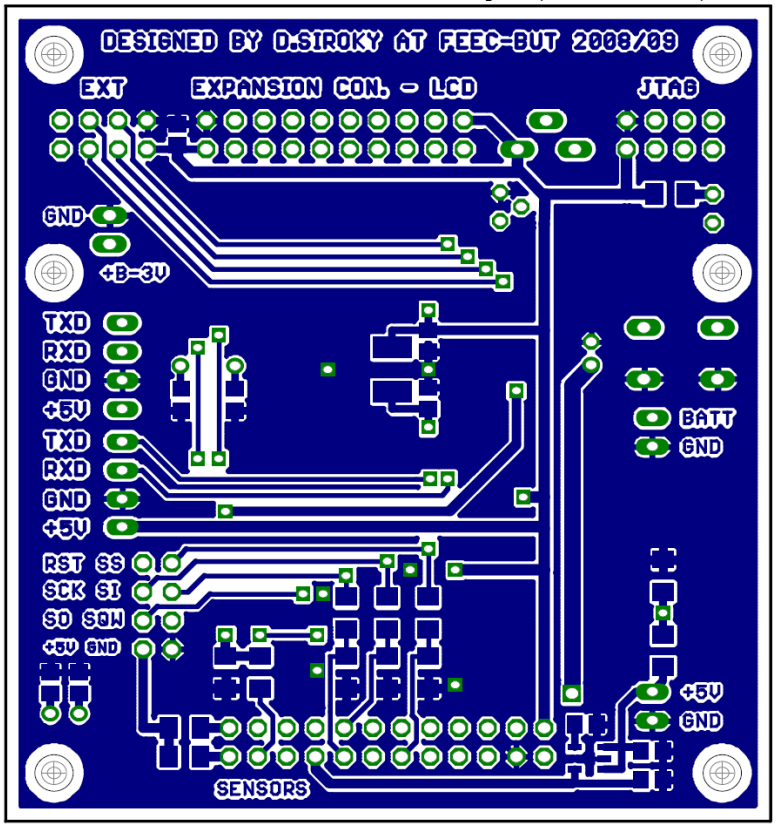

iii. MCU board – Parts layout in top layer (150 % scale)

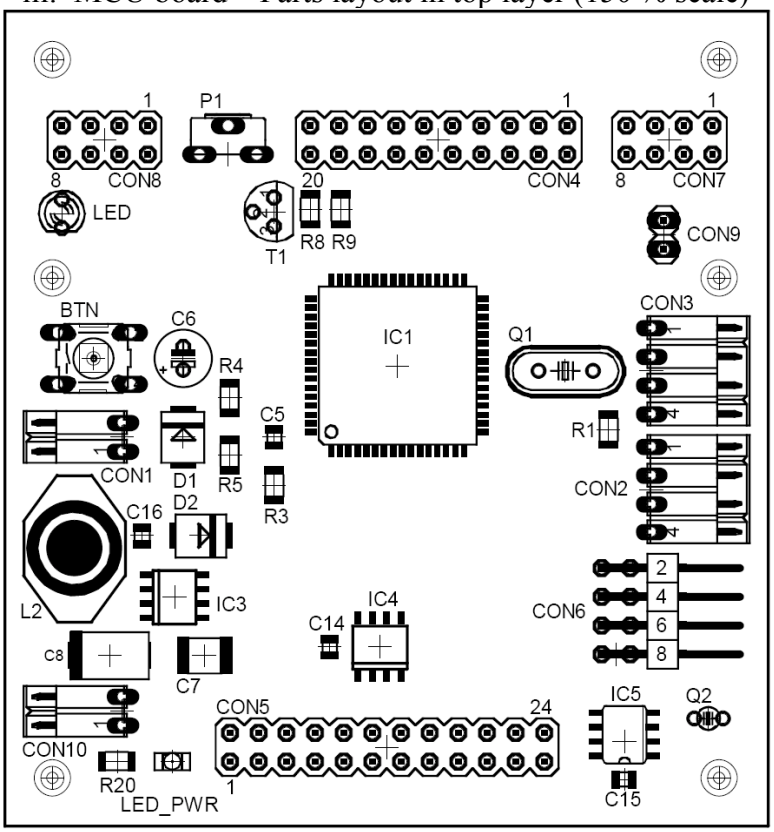

iv. MCU board – Parts layout in bottom layer (150 % scale)

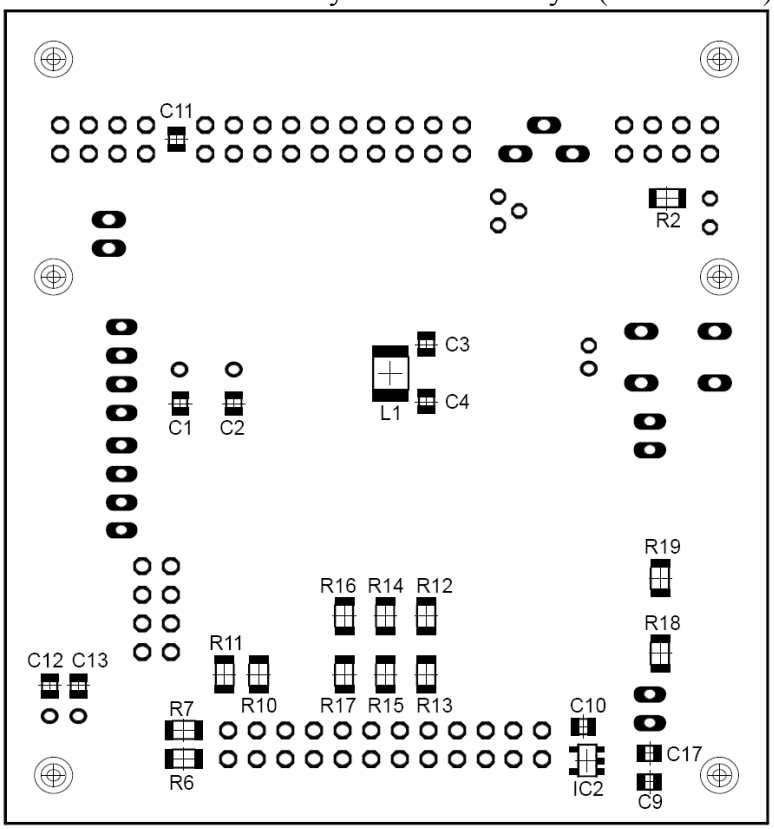

v. Sensor board – PCB top layer (140 % scale)

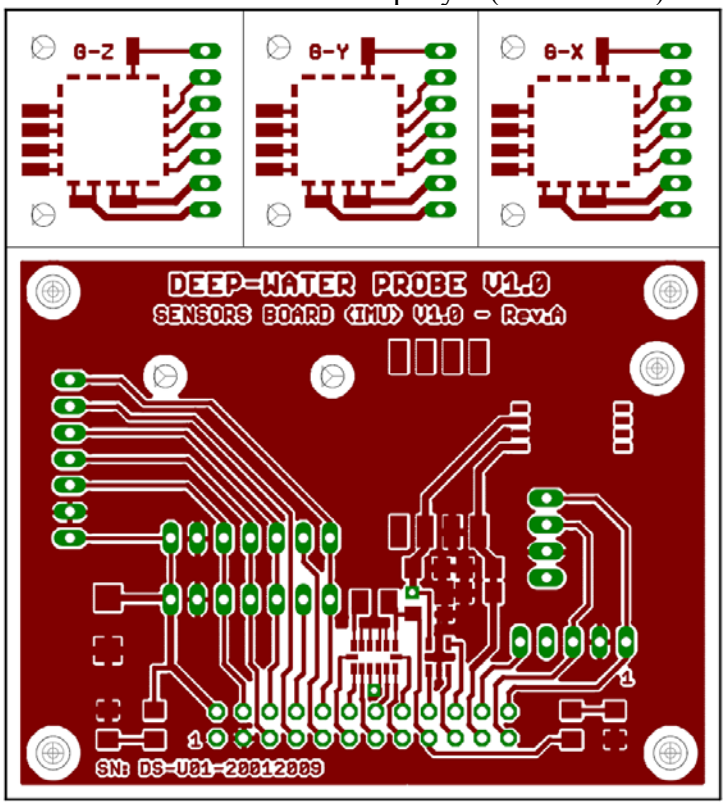

vi. Sensor board – PCB top layer (140 % scale)

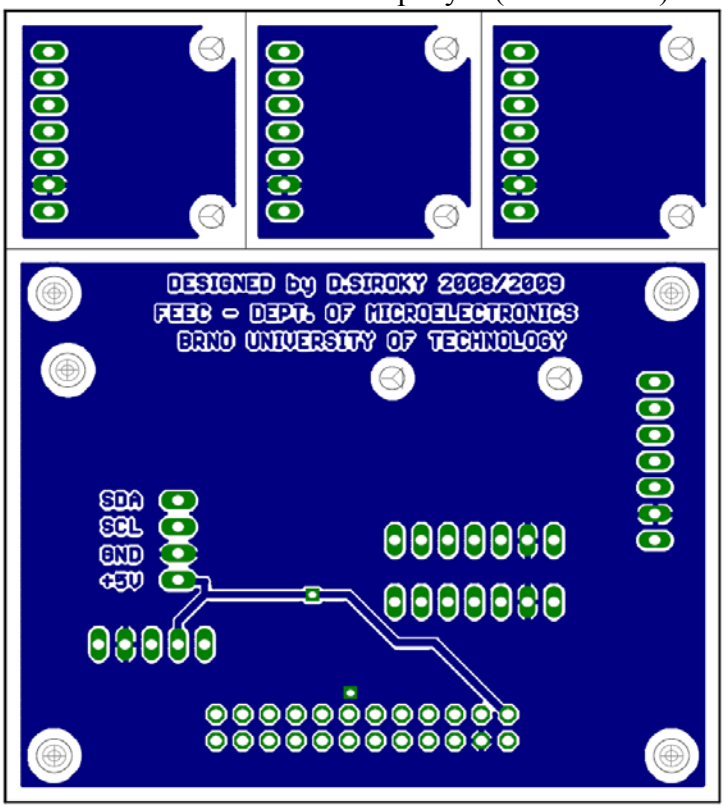

vii. Sensor board – Parts layout in top layer (140 % scale)

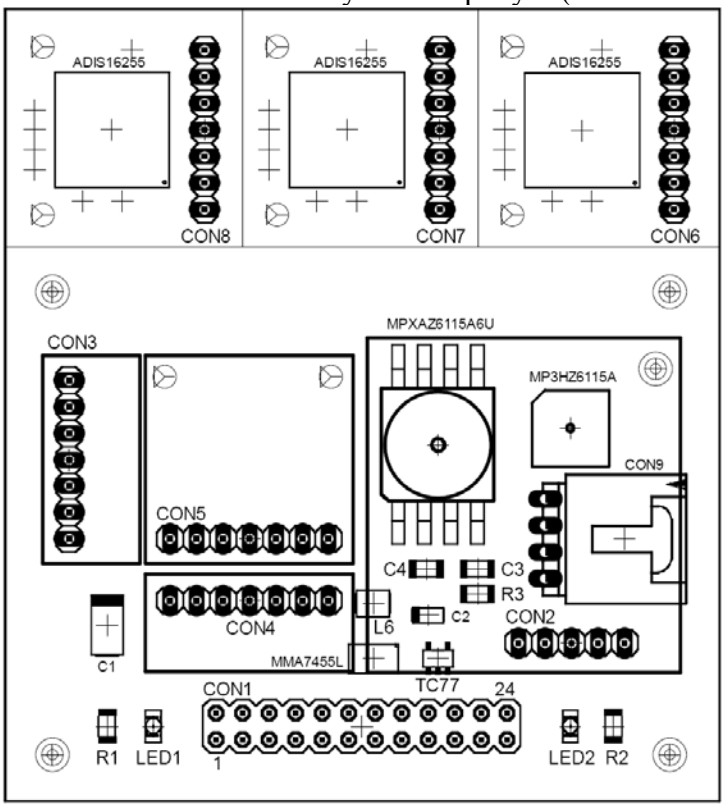

viii. Power-supply board – PCB top layer (150 % scale)

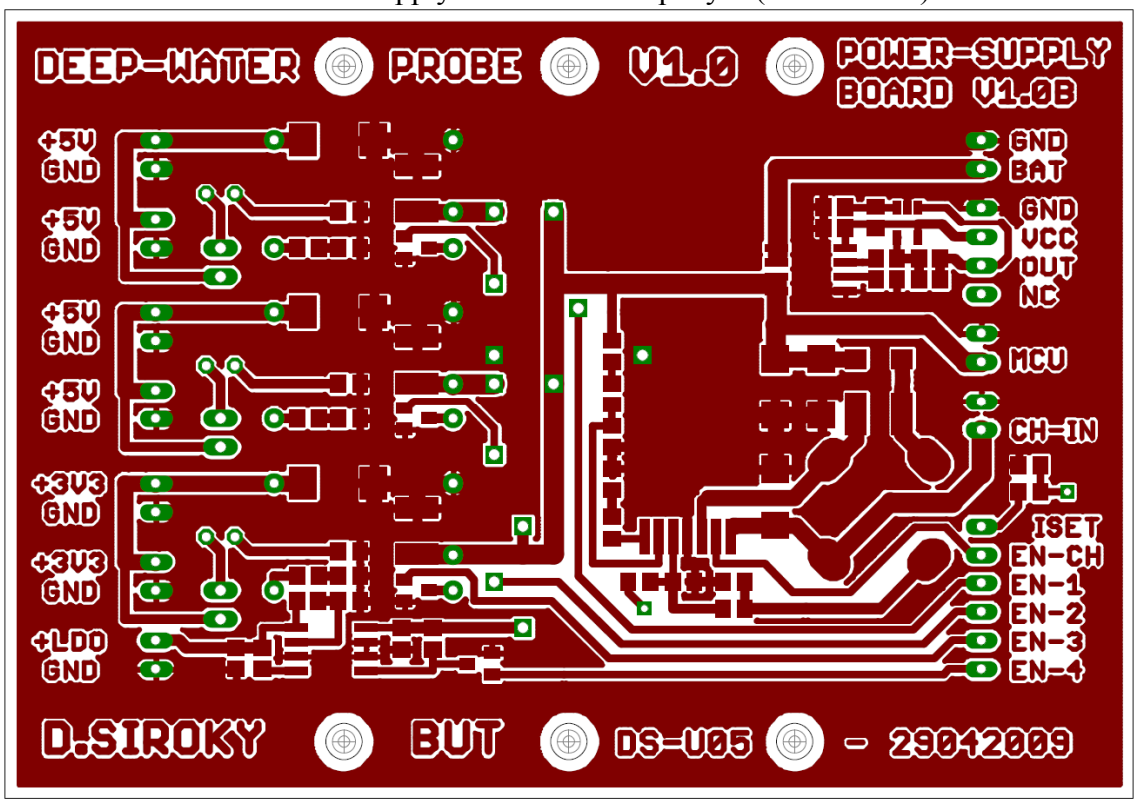

ix. Power-supply board – PCB bottom layer (150 % scale)

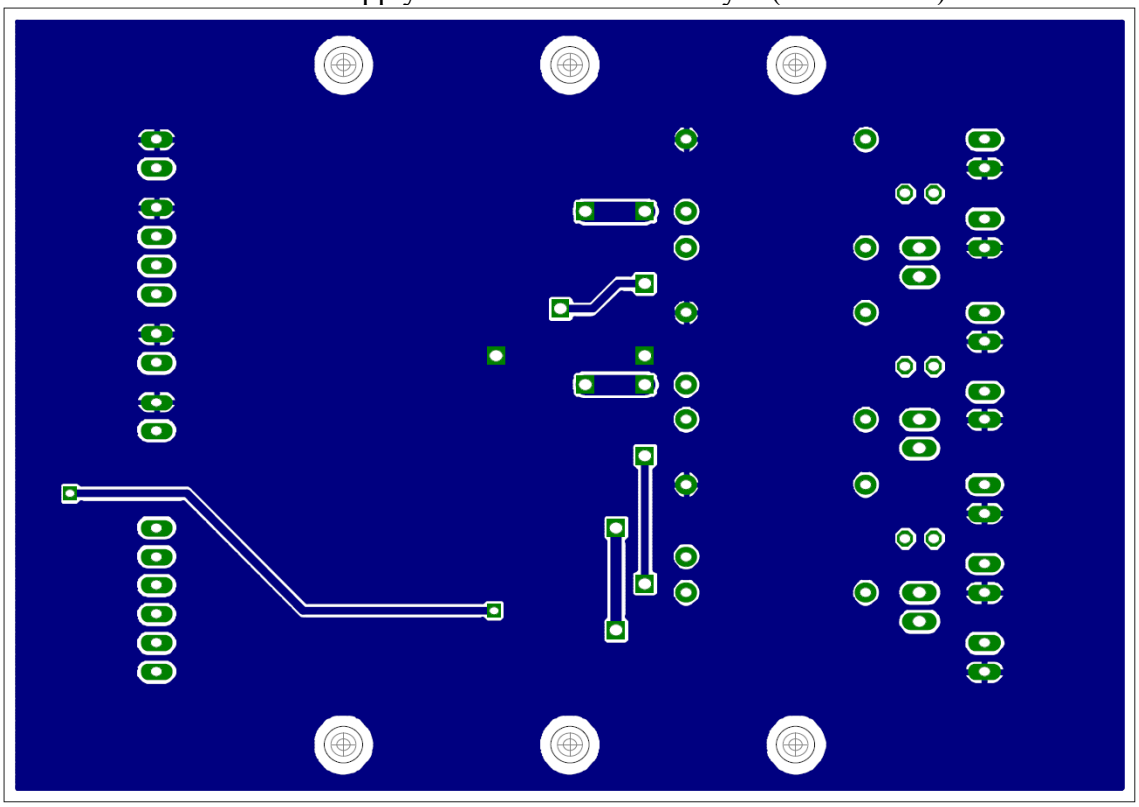

x. Power-supply board – Parts layout in top layer (150 % scale)

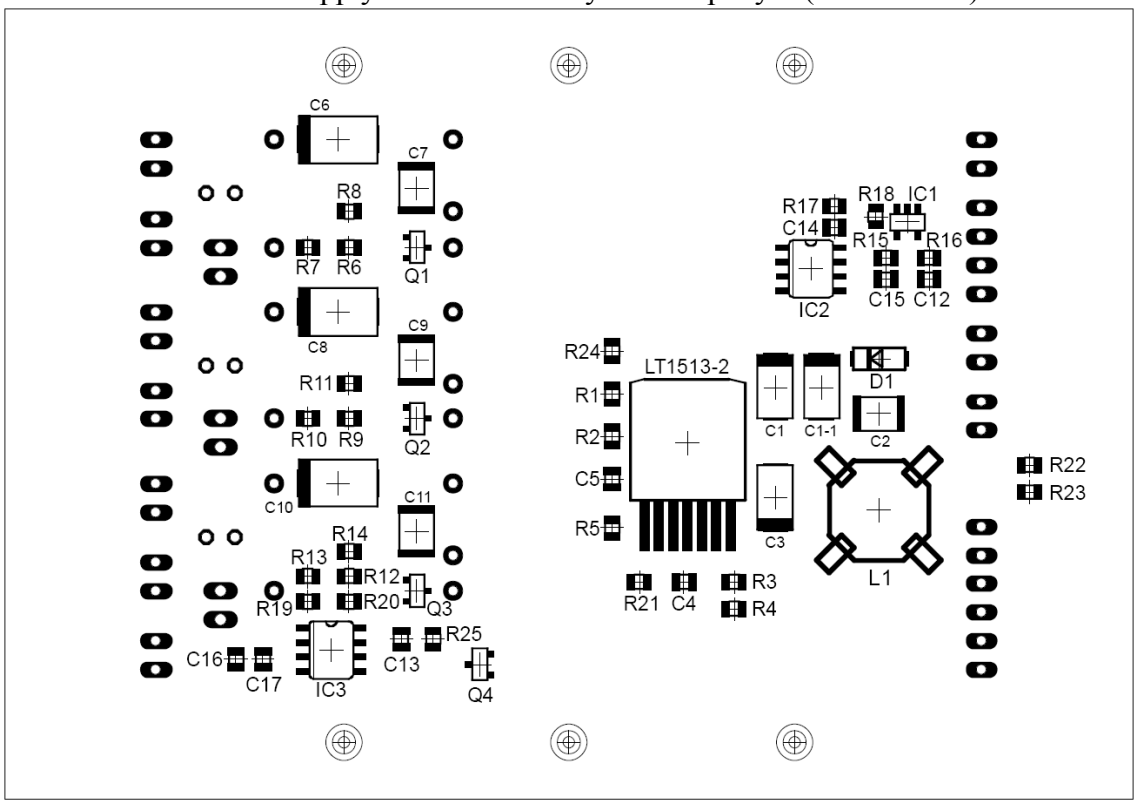

xi. Power-supply board – Parts layout in bottom layer (150 % scale)

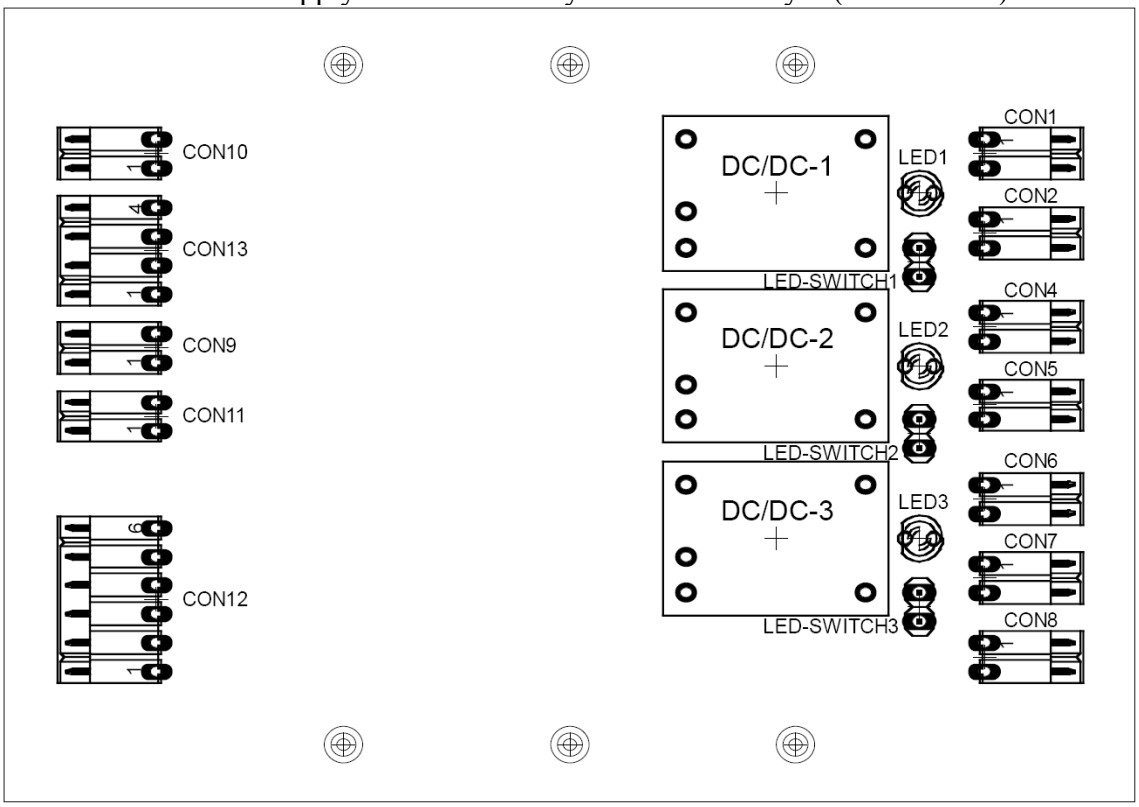

xii. Power LED module – PCB top layer (200 % scale)

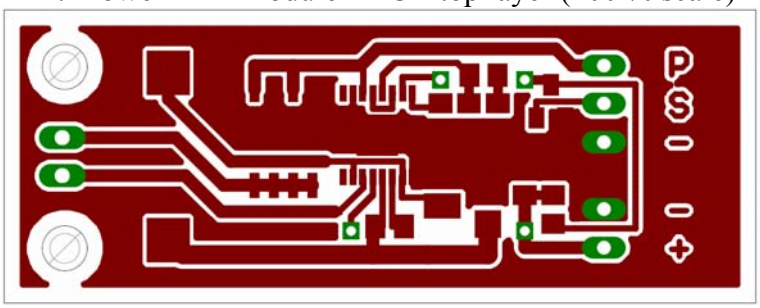

xiii. Power LED module – PCB bottom layer (200 % scale)

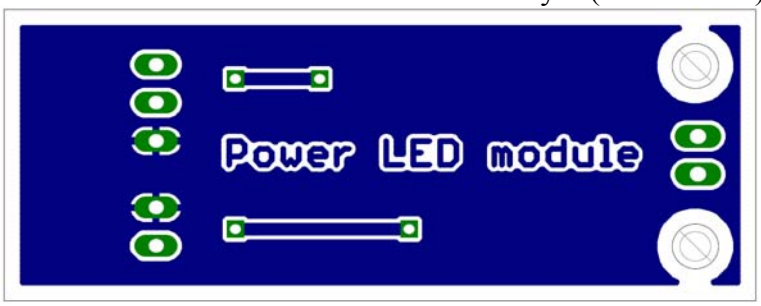

xiv. Power LED module – Parts layout in top layer (200 % scale)

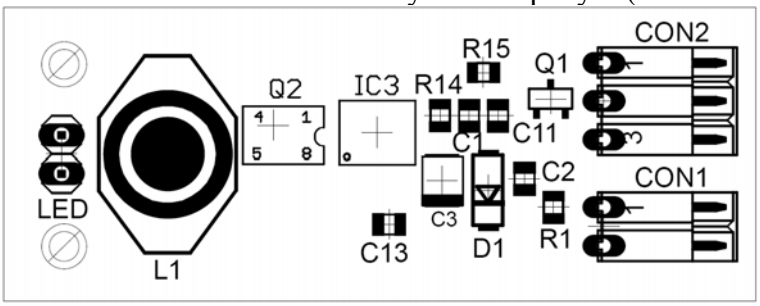

xv. Terminal server board – PCB top layer (200 % scale)

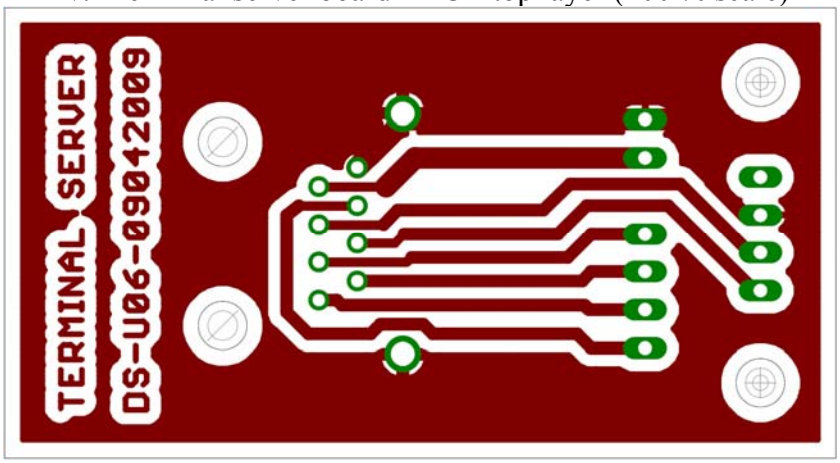

xvi. Terminal server board – Parts layout in bottom layer (200 % scale)

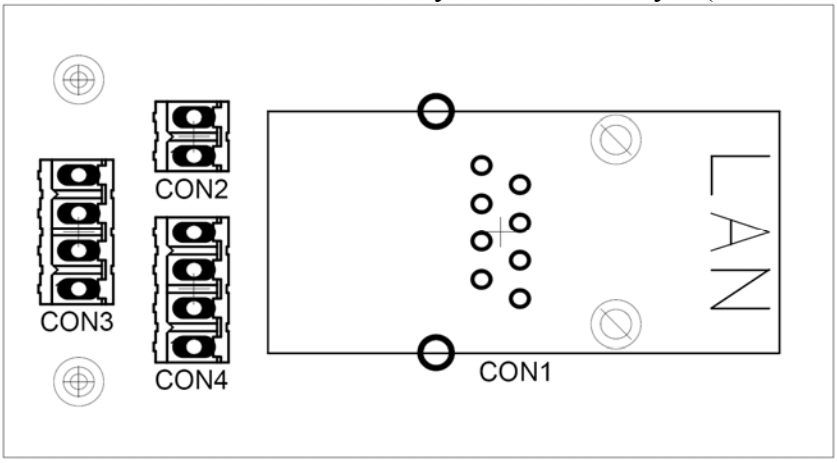

MCU board - electrical diagram

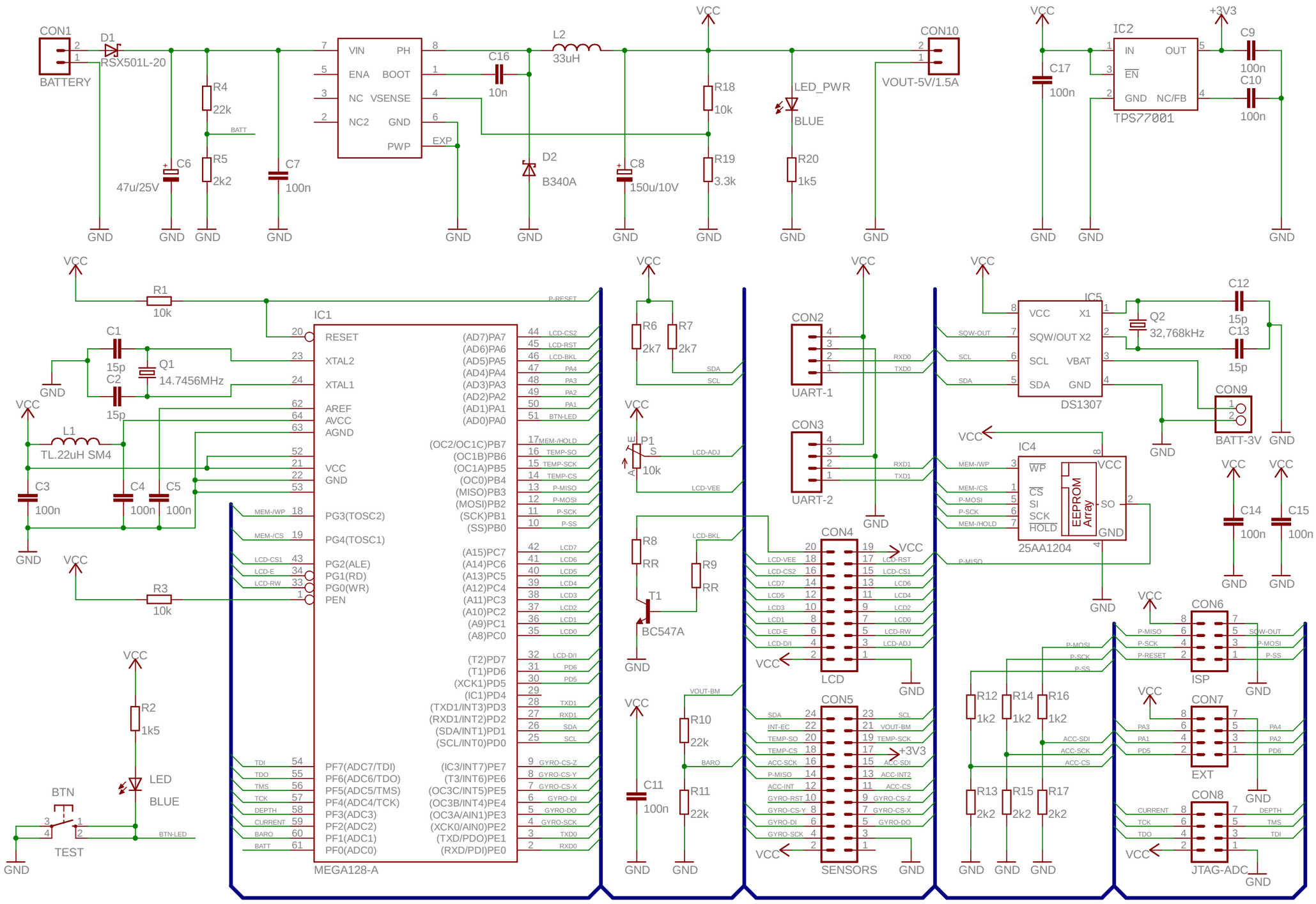

Sensor board - electrical diagram

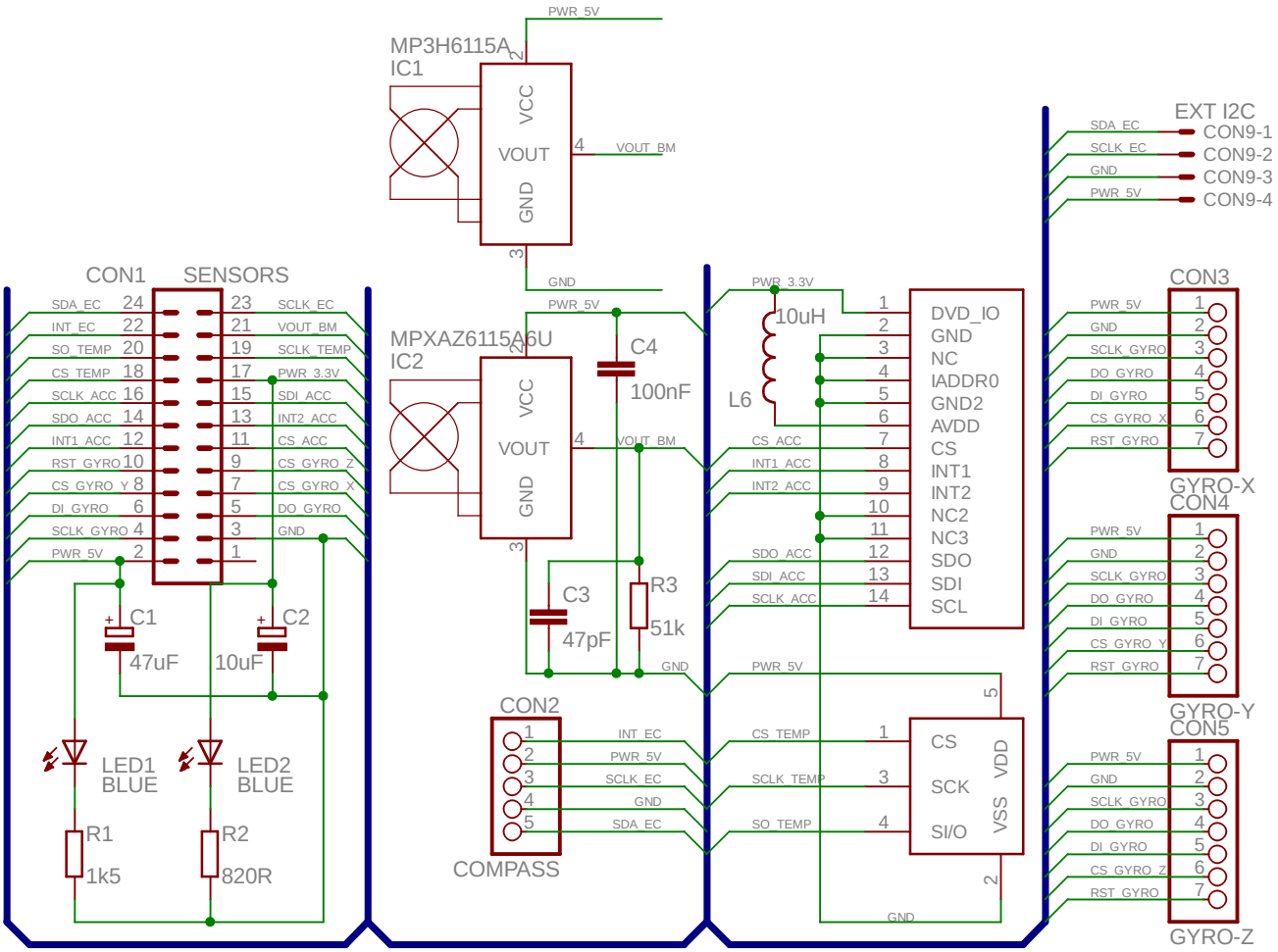

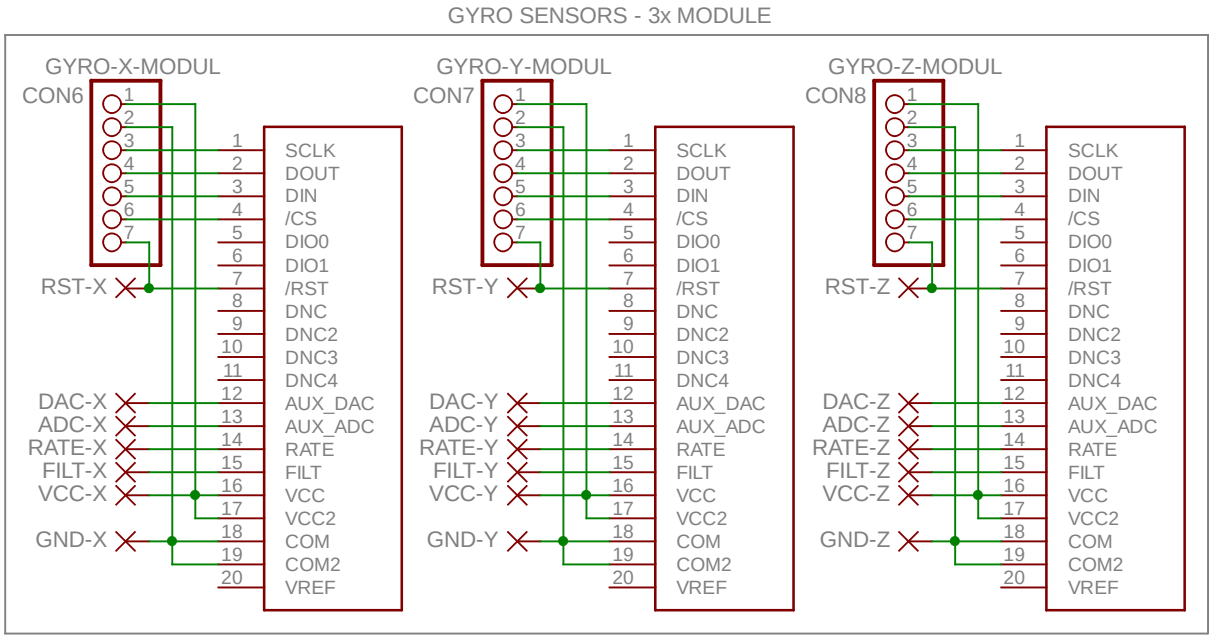

Power-supply board - electrical diagram

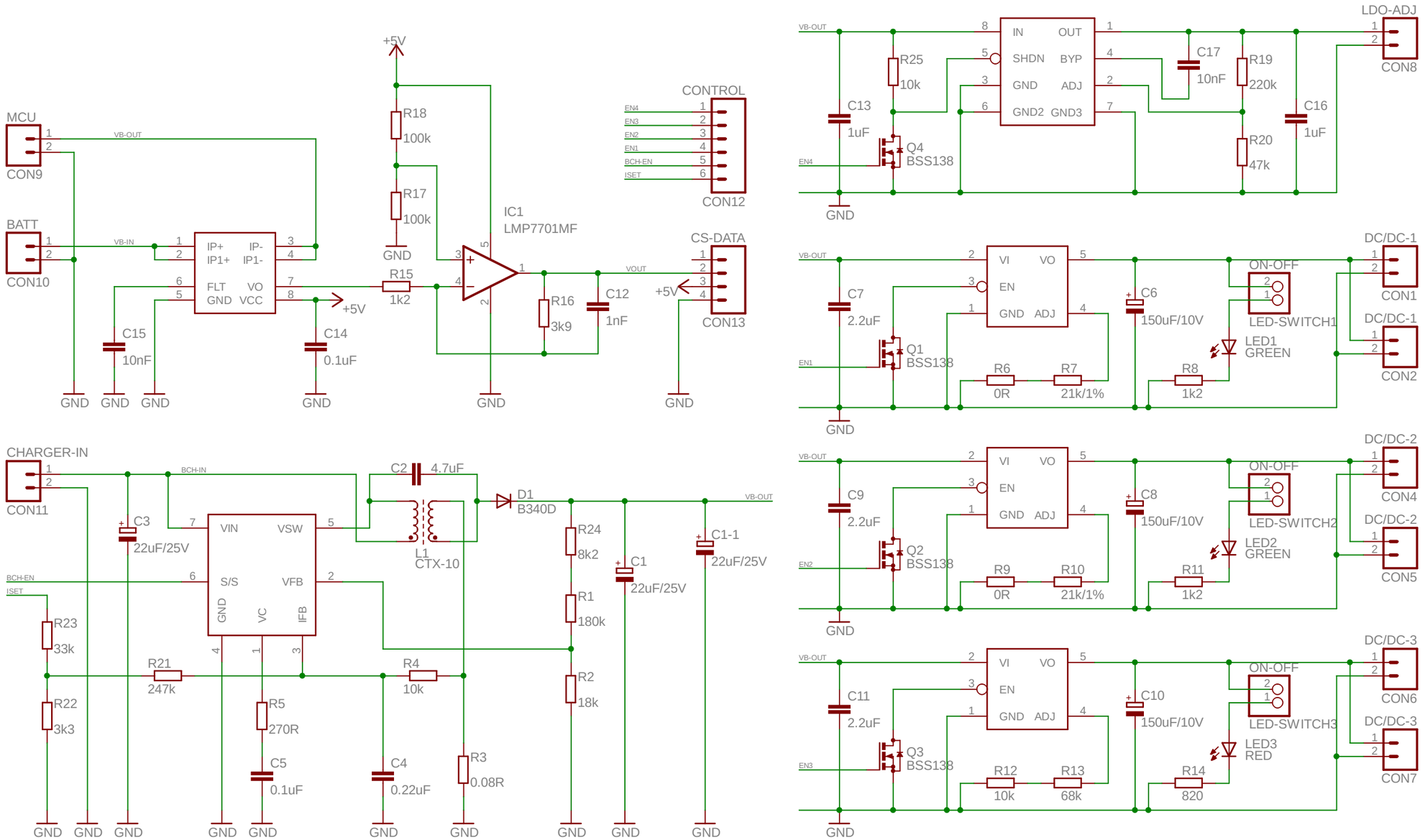

Power LED module - electrical diagram

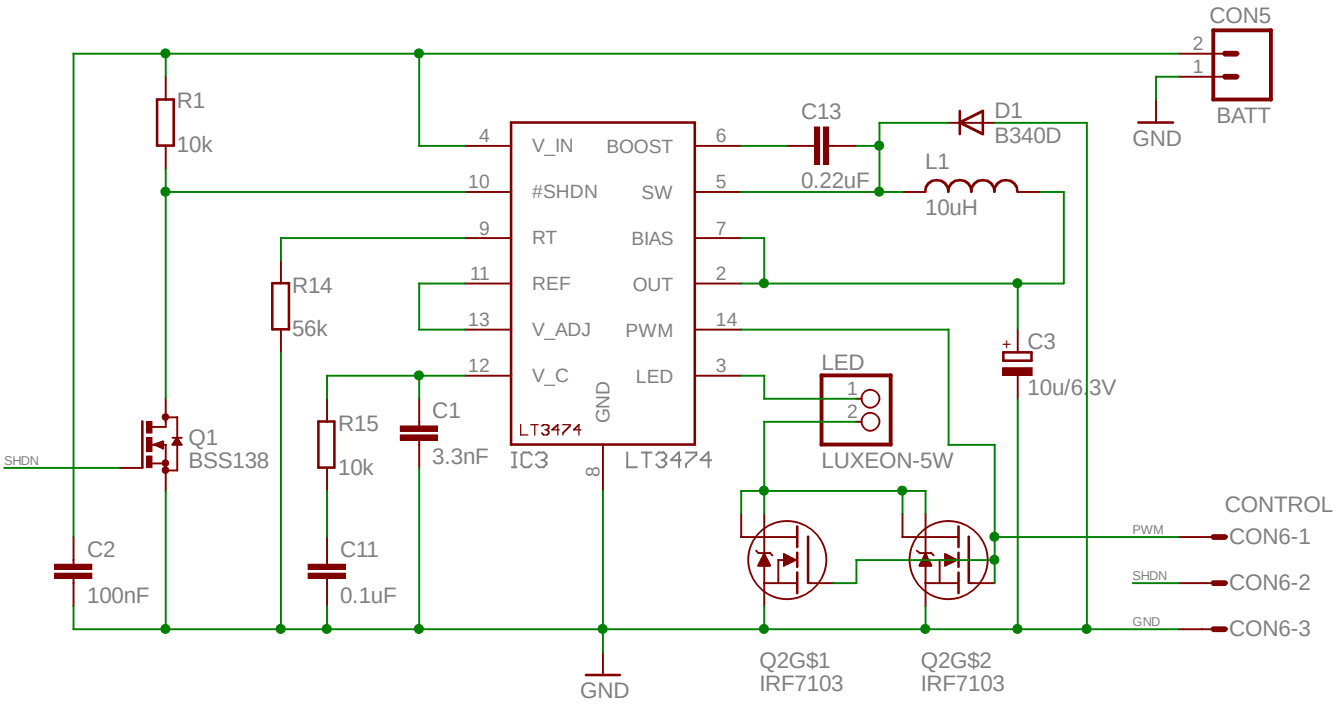

Terminal server - electrical diagram

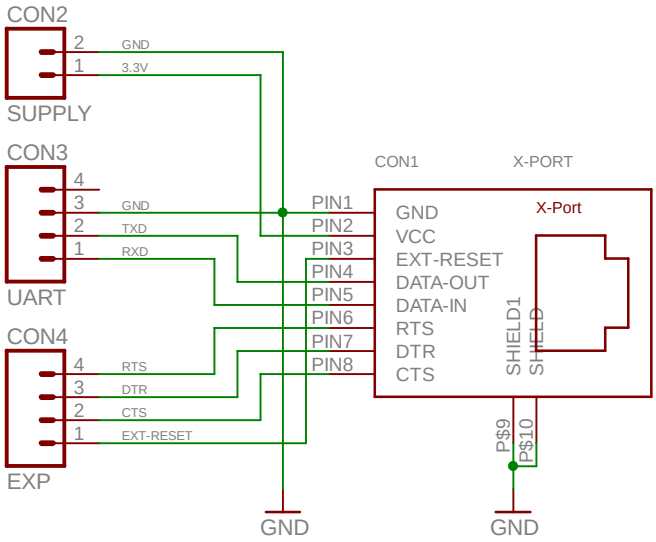

RevN.	Revision note	Date	Sign	Inspec.

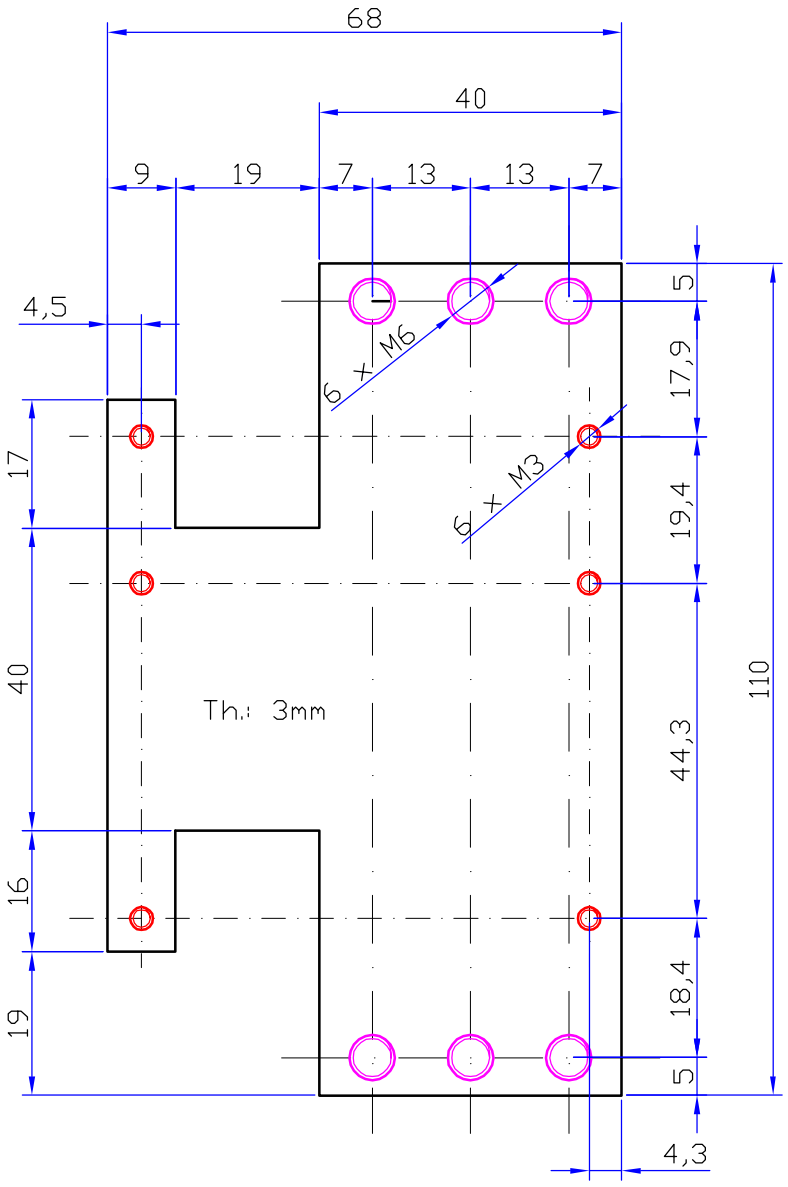

Ref	Pieces	Name, label, material, dimension etc.			Item nmr./Reference	
Drawn Daniel Široký		Checked Daniel Široký	Approved Daniel Široký	File name Top.dwg	Date 15/02/09	Scale 1:1
Brno University of Tech.		Top panel 68 x 110				
		001-01-2009			Version 1.0	Sheet 1/1

RevN.	Revision note	Datum	Sign	Inspec.

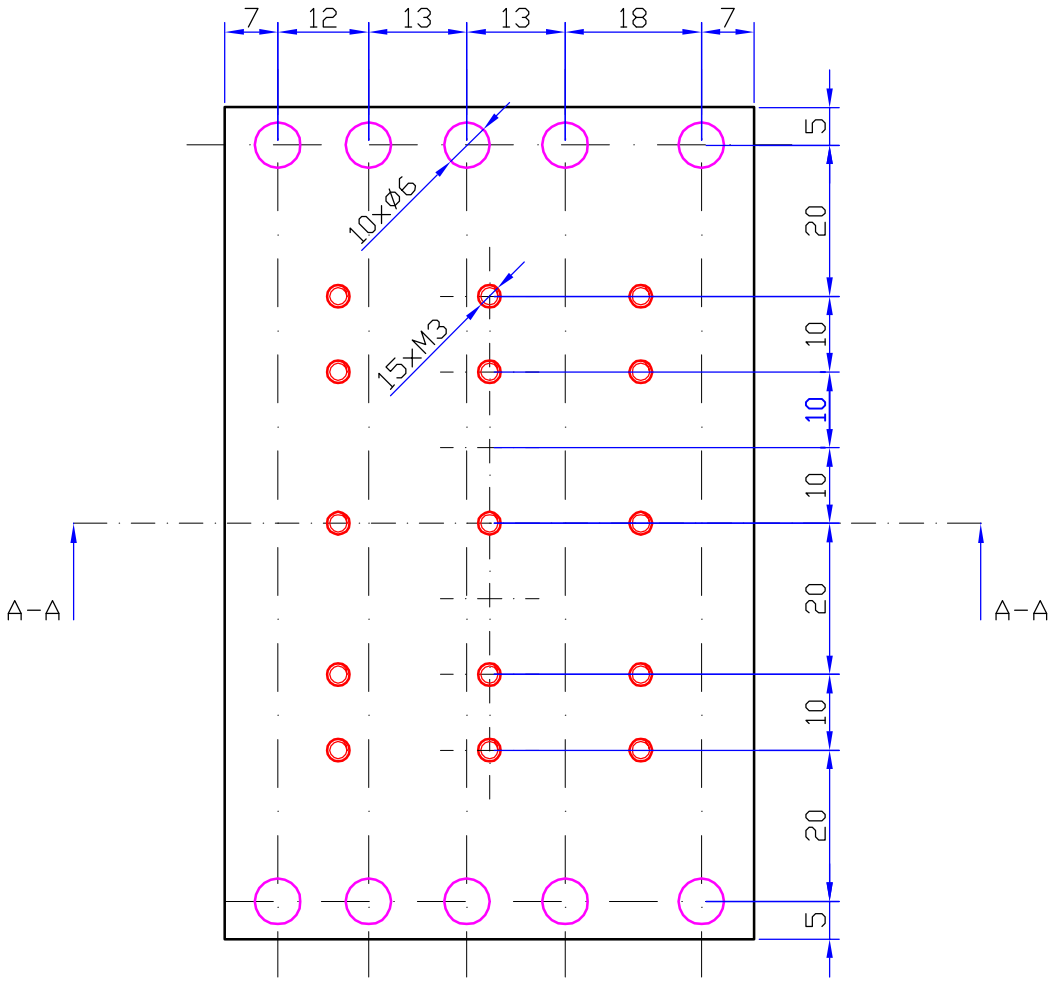

Section A–A

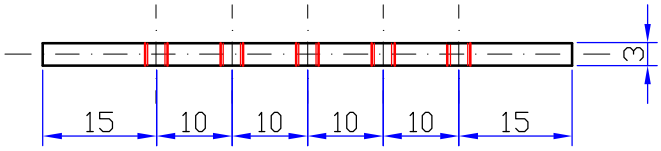

Ref	Pieces	Name, label, material, dimension etc.		Item nmr./Reference	
Drawn Daniel Široký	Checked Daniel Široký	Approved Daniel Široký	File name Bottom.dwg	Date 15/02/09	Scale 1:1
Brno University of Tech.		Bottom panel 70 x 110			
		002-01-2009		Version 1.0	Sheet 1/1

RevN.	Revision note	Date	Sign	Inspec.

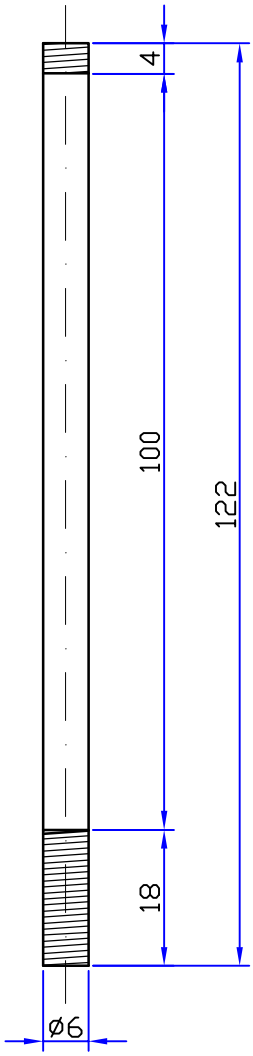

Ref	Pieces	Name, label, material, dimension etc.		Item nmr./Reference	
Drawn Daniel Široký	Checked Daniel Široký	Approved Daniel Široký	File name Bat-DC.dwg	Date 15/02/09	Scale 1:1
Brno University of Tech.	Battery distance-column				
	003-01-2009			Version 1.0	Sheet 1/1

RevN.	Revision note	Date	Sign	Inspec.

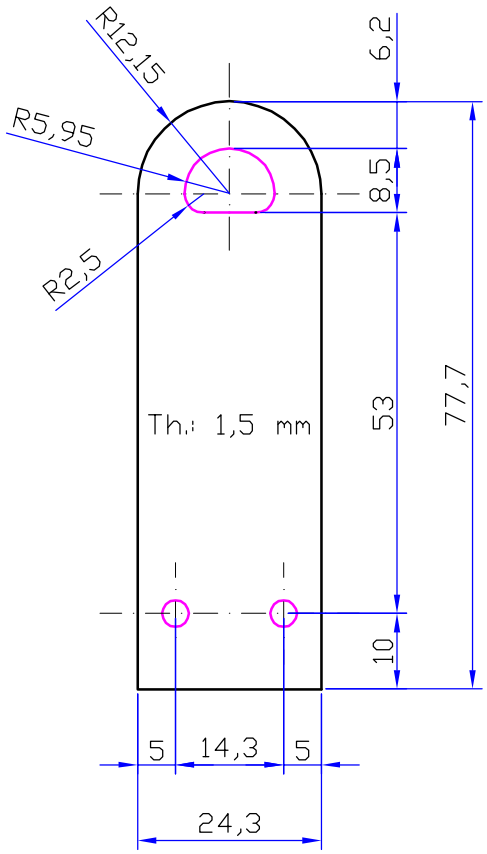

Ref	Pieces	Name, label, material, dimension etc.		Item nmr./Reference	
Drawn Daniel Široký	Checked Daniel Široký	Approved Daniel Široký	File name Lug.dwg	Date 15/02/09	Scale 1:1
Brno University of Tech.		Probe lug			
		005-01-2009		Version 1.0	Sheet 1/1

RevN.	Revision note	Date	Sign	Inspec.

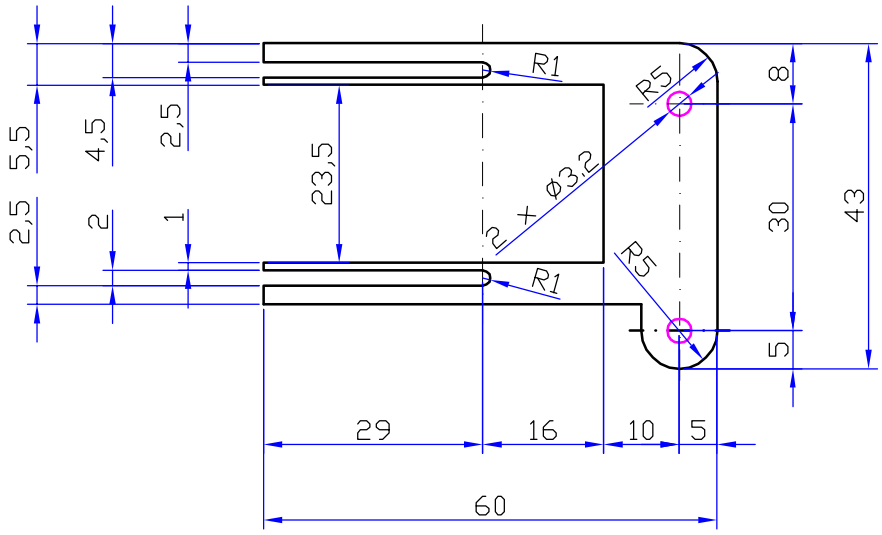

Th.: 1,5 mm

Ref	Pieces	Name, label, material, dimension etc.		Item nmr./Reference	
Drawn Daniel Široký	Checked Daniel Široký	Approved Daniel Široký	File name C-Holder.dwg	Date 15/02/09	Scale 1:1
Brno University of Tech.		Camera holder			
		006-01-2009		Version 1.0	Sheet 1/1